Olav Johannes Kopperud

Corrosion of AISI 316L in Fish Processing Facilities

The Effect of Operational Conditions, Maintenance Procedures, and Biofilm

Master's thesis

NTNU
Norwegian University of
Science and Technology

Olav Johannes Kopperud

Corrosion of AISI 316L in Fish Processing Facilities

The Effect of Operational Conditions, Maintenance Procedures, and Biofilm

Master's thesis in Mechanical Engineering
Supervisor: Roy Johnsen
June 2023

Norwegian University of Science and Technology
Faculty of Engineering
Department of Mechanical and Industrial Engineering

NTNU
Norwegian University of
Science and Technology

Preface

This thesis concludes the work and research done during my Master's Project at the Department of Mechanical and Industrial Engineering of the Norwegian University of Science and Technology (NTNU), as the concluding part of the integrated Master's degree in Mechanical engineering. The work was supervised by Professor Roy Johnsen. The experimental work has been performed at the Department of Mechanical and Industrial Engineering at NTNU, and at SalMar ASA's facilities InnovaMar and InnovaNor. The experimental work has been performed by the author, and the SEM analysis by Dong Wang, in accordance with rules and regulations at NTNU.

Olav Johannes Kopperud

Olav Johannes Kopperud

2023-06-08
Trondheim, Norway

Acknowledgements

First and foremost, I would like to thank my supervisor, Roy Johnsen, for his encouragement, interest and excitement for the project and the results provided. His knowledge, guidance and availability throughout the project have been very much appreciated.

I would like to thank Ole Meland, Morten Dragsnes and other maintenance staff at SalMar for their help with installing the test equipment and being available to fix issues with the equipment during testing, as well as Dong Wang for being available and helping with the setup at the Lab and the SEM testing.

The help from Herlof Øyen at Mowi, Roar Landvaag at Marine Metall, and Martin Olsen from Blått Kompetansesenter during the pre-study for this project, together with feedback from many other facilities on their corrosion-related issues, is highly appreciated and was very helpful in determining the path of the project.

Additionally, I am grateful to the residents of Room 238 for their enthusiasm, valuable feedback, and occasional distractions during the writing of my thesis. The frequent coffee breaks we shared during long workdays were essential in helping me maintain my well-being throughout the semester.

Last but not least, I would like to thank my family for their continuous support and encouragement throughout the semester.

Abstract

Fish processing facilities utilize a lot of process equipment and piping constructed of AISI 316L and AISI 340L stainless steel. The production equipment is intermittently exposed to seawater, which has caused several corrosion-related issues in many facilities.

The objective of this thesis is to investigate how the operating conditions, together with construction and maintenance procedures, in fish processing facilities affect the corrosion resistance of AISI 316L. Furthermore, to design and construct a functional test setup for corrosion testing at remote locations, in corrosive environments, so that experiments can be performed within the facilities.

The work consisted of an initial period where the test setup was designed, prototyped and constructed, before deployment to the processing facilities InnovaMar at Frøya and InnovaNor at Senja, together with the lab at NTNU. The tests performed at these locations were Open Circuit Potential tests on a variety of samples, including AISI 316L samples obtained from piping sections at InnovaNor. This was performed in order to monitor the state of the test samples in the operating conditions of the facility. Potentiostatic tests at different temperatures and potentials were also performed in the lab in order to determine what conditions could trigger the initiation of corrosion on the samples. After potentiostatic testing, SEM imaging and EDS were utilized to analyze some of these samples.

The test setup provided continuous, live, OCP data throughout the test period, allowing for close monitoring of the state of the samples. It was found that crevice corrosion on both AISI 304L and AISI 316L can occur in the facilities during normal operating conditions. AISI 316L piping that was welded without following proper welding routines suffered from pitting corrosion in the same conditions. Several samples did also show signs of pit initiation when the facilities were shut down, exposing the samples to stagnant seawater and temperatures up to 12°C for prolonged periods.

The equipment in the facilities is regularly cleaned, which was not the case for specimens in the test chamber. However, the results from these tests, together with observations of corrosion-related failures in the facilities, indicate that poor weld quality, elevated temperatures during halts in production, and crevices in equipment are critical factors regarding the survivability of AISI 316L in the operating conditions of fish processing facilities.

Sammendrag

Fiskeforedlingsindustrien bruker mye prosessutstyr og rør konstruert av AISI 316L og AISI 340L rustfritt stål. Produksjonsutstyret er jevnlig utsatt for sjøvann, noe som har forårsaket korrosjons-relaterte problemer i flere anlegg. AISI 316L og AISI 304L regnes normalt ikke som sjøvannsbestandig, men til tross for en del problemer har utstyret totalt sett overlevd overraskende bra i disse anleggene. Imidlertid forekommer lokale korrosjons-angrep i form av spalt- og grop-korrosjon, noe som forårsaker lekkasjer og feil på utstyr.

Målet med denne oppgaven er å undersøke hvordan driftsforhold sammen med konstruksjons- og vedlikeholdsprosedyrer i fiskeforedlingsanlegg påvirker korrosjonsmotstanden til AISI 316L. I tillegg er det et mål å designe og konstruere et funksjonelt testoppsett for korrosjonstesting på eksterne lokasjoner i korrosive miljøer, slik at eksperimenter kan utføres i anleggene.

Arbeidet bestod av en innledende periode hvor testoppsettet ble designet, prototypet og konstruert, før de ble utplassert på foredlingsanleggene InnovaMar på Frøya, og InnovaNor på Senja, samt ved laboratoriet på NTNU. Testene utført på disse stedene var åpen kretspotential-tester på forskjellige prøver, inkludert AISI 316L prøver kuttet fra rørseksjoner hos InnovaNor. Potensiostatiske tester ved forskjellige temperaturer og potensialer ble også utført i laboratoriet for å finne ut hvilke forhold som kunne utløse initiering av korrosjon på prøvene. Etter disse testene ble noen av prøvene analysert ved hjelp av SEM og EDS.

Testoppsettet ga kontinuerlig data gjennom hele testperioden, noe som muliggjorde tett overvåking av prøvenes tilstand. Ved å sammenligne temperaturene og potensialene i anleggene med de potensiostatiske testene utført i laboratoriet, ble det funnet at spaltkorrosjon på både AISI 304L og AISI 316L kan oppstå i anleggene under normale driftsforhold. AISI 316L rør som ble sveiset uten korrekte sveiserutiner fikk også påvist gropkorrosjon under de samme forholdene. Mange prøver viste også tegn til initiering av gropkorrosjon når anleggene ble skrudd av, da prøvene ble utsatt for stillestående sjøvann og temperaturer opp mot 12°C i lengre tid.

Utstyret i anleggene rengjøres regelmessig, noe som ikke var tilfelle for prøvene i testkammeret. Resultatene fra disse testene, sammen med observasjoner av korrosjonsrelaterte feil i anleggene, indikerer imidlertid at dårlig sveisekvalitet, forhøyet temperatur ved produksjonsstans, og spalter i utstyr er kritiske faktorer for overlevelsesevnen til AISI 316L under driftsforholdene til fiskeforedlingsanlegg.

Contents

List of Figures

List of Tables

Abbreviations

AC Alternating Current.

AISI 304 UNS S30400.

AISI 316 UNS S31600.

BCC Body Centered Cubic.

CCT Critical Crevice corrosion Temperature.

CPT Critical Pitting Temperature.

DC Direct Current.

EDS Energy Dispersive Spectroscopy.

FCC Face Centered Cubic.

HAZ Heat Affected Zone.

HER Hydrogen Evolution Reaction.

MIC Microbiologically Induced Corrosion.

OCP Open Circuit Potential.

ORR Oxygen Reduction Reaction.

PREn Pitting Resistance Equivalence number.

RSW Refrigerated Seawater.

SDSS Super Duplex Stainless Steel.

SEM Scanning Electron Microscopy.

Chapter 1.

Introduction

This project is a continuation of the pre-study done in the fall of 2022 [1]. Parts of chapter 2 and the relevant literature was structured during the pre-study.

1.1. Background

Fish farming involves a variety of steps in order to produce fish products for consumption. The production process spans the whole life cycle of the fish, from hatching to processing, as seen in Figure 1.1.
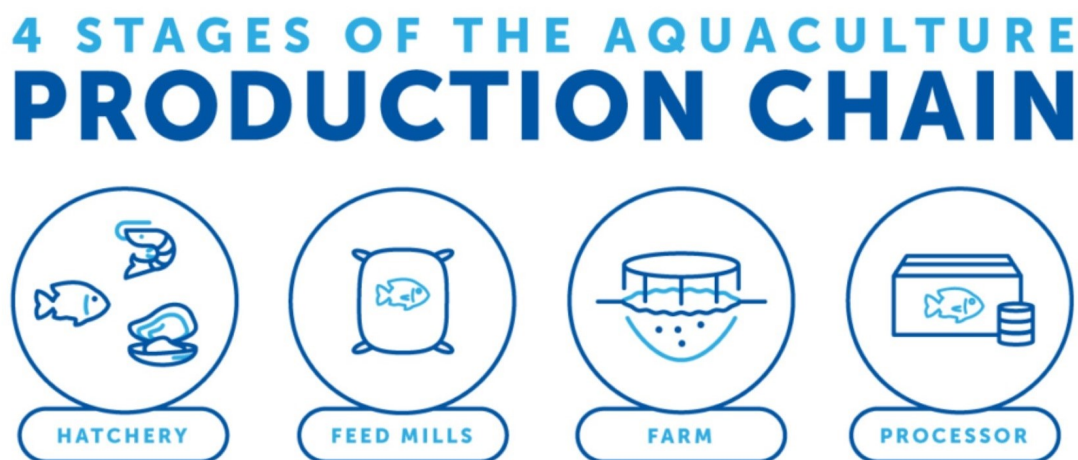
Figure 1.1.: Value chain of the aquaculture industry [2].

The processing facilities are the last stage in this process, where the fish is euthanized, gutted, and filleted. There are strict regulations regarding material choice, cleanliness and chemicals used in the processes, stipulated by the Norwegian Food Safety Authority [3]–[5].

The processing area consists of a series of machines, tanks, conveyors, chutes and piping. The equipment supposed to be in contact with fish products and seawater is mostly made out of AISI 316L, with supporting structures of AISI 304L stainless steel [6]. The different process steps are shown in Figure 1.2. To ensure bacteria are not entering the production, the process water is disinfected through a UV filter, which is supposed to inactivate the microorganisms. One supplier of such systems claims a disinfection efficiency of 99,99% [7]. Daily cleaning of the facility is also done to ensure hygienic production.
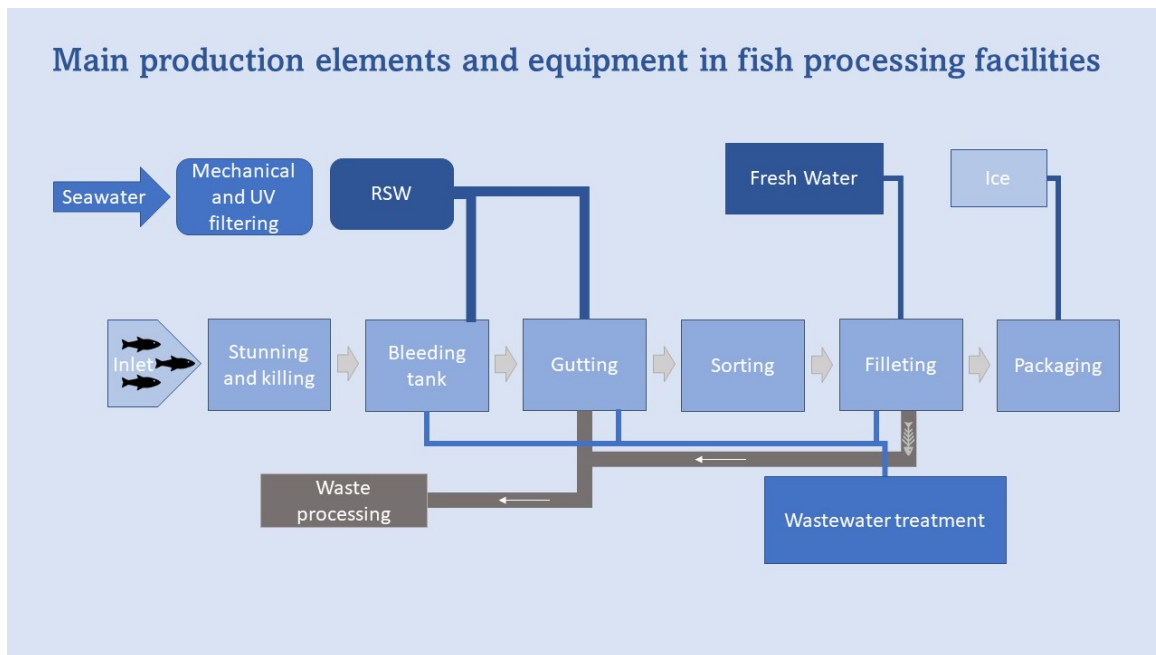
Figure 1.2.: Process schematics of a processing facility.

The equipment is exposed to Refrigerated Seawater (RSW), cleaning agents, marine atmosphere, variations in temperature, and high mechanical loads. This constitutes a harsh environment for stainless steel, necessitating a thorough understanding of what materials are suitable in these conditions, and implementation of effective monitoring processes to mitigate equipment damage.

During the pre-study, contact was established with several fish processing facilities, with help from Roar Landvaag at Marine Metall, and Martin Fredrik Olsen at Blått Kompetansesenter. Interviews were conducted with heads of maintenance at Lerøy, Salmar and Mowi. This survey, together with a visit at Mowi Ulvan, identified many corrosion-related issues at these facilities.

Table 1.1.: Overview of failures in different processing facilities [1].

Failure Mode	Mowi Ulvan	Mowi Herøy	Mowi Eggesbønes	Salmar InnovaNor	Lerøy Jøsnøya
Weld Corrosion	X	X		X	
Crevice corrosion	X			X	
Pitting corrosion	X	X	X	X	
Valves and housing	X			X	
Motors	X				X
Framework	X	X		X	
Fatigue	X	X			
Hot water tanks			X		X
Possible stray current				X	X

(a) Weld pitting at Mowi Ulvan
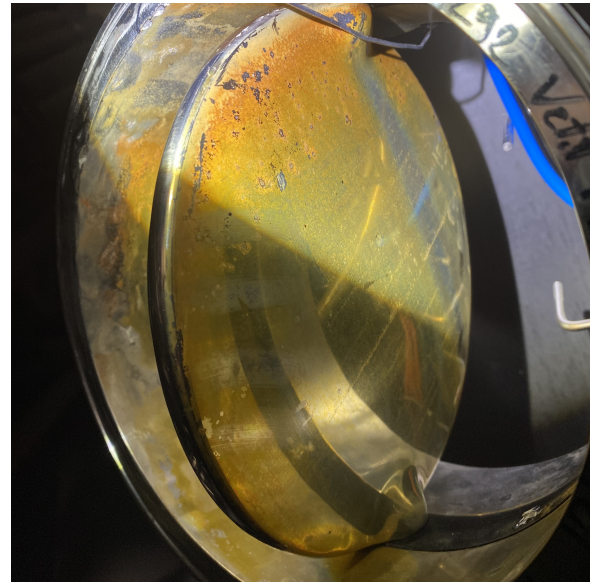
(b) Valve corrosion at InnovaNor

(c) Internal weld corrosion at InnovaNor

(d) Pitting repairs at InnovaNor

Figure 1.3.: Corrosion damages in different facilities.

Table 1.1 shows some of the numerous instances of corrosion-related failures in these facilities discovered during the pre-study to this project [1]. Some of these failures are also shown in Figure 1.3. It's worth noting that since pitting corrosion is prevalent in most of the facilities, it's likely that conditions are also suitable for crevice corrosion, as explained in subsection 2.2.3. Interestingly, findings of crevice corrosion were only uncovered during the survey of visited facilities, implying that there could be an underreporting of this corrosion mechanism by the facilities themselves, and a lack of knowledge about this corrosion mechanism.

InnovaNor experienced substantial corrosion damages quickly after starting production at the facility, requiring the change of a lot of piping. These damages were inspected by Roy Johnsen, and a lot of the pipe sections were brought to NTNU Trondheim to be able to conduct experiments with samples from these pipes.

1.2. Objective

The first objective for this master's project is to document the corrosion resistance of typical construction alloys, mainly AISI 316L together with AISI 304L, in the operating conditions found in fish processing facilities. This includes variations in the alloys' resistance due to changing operating conditions and any changes to their material properties resulting from welding.

The second objective of this project is to design and construct a comprehensive test setup that enables extensive corrosion testing to be conducted remotely in harsh environments, in order to perform tests within the fish processing facilities.

Chapter 2.

Theoretical foundation

Corrosion occurs when a metal comes into contact with an electrolyte, leading to reduction and oxidation reactions between the metal and elements within the electrolyte, ultimately resulting in metal dissolution. This section will provide a theoretical foundation for comprehending the mechanisms of corrosion on stainless steel within fish processing facilities. Refrigerated Seawater (RSW) is the most common electrolyte present in these facilities. The terms seawater and electrolyte will be used interchangeably throughout this section.

2.1. Stainless Steel Alloys and Their Properties

Constructions exposed to marine environment or marine atmosphere require effective corrosion protection to prevent deterioration and subsequent failure over time. The preferred material is often a stainless steel alloy due to its corrosion-resistant properties. There are many different types of stainless steel alloys, and some of the most commonly used are presented in Table 2.1.

Stainless steel alloys get their corrosion-resistant properties through the formation of a thin oxide film on the surface, which effectively shields the underlying metal from direct contact with seawater [8]. This oxide film is generated when steel, containing a minimum chromium (Cr) content of 12% wt, comes into contact with oxygen [9]. In contrast, the rust observed on plain carbon steel is also an oxide, but it is porous and allows the electrolyte to reach the metal substrate [10].

The selection of a steel alloy for industrial equipment heavily relies on the specific environment to which it will be exposed. Different alloys exhibit varying abilities to form and maintain an oxide layer on their surfaces. Hence, the choice of alloy is crucial in ensuring optimal corrosion resistance and long-term performance in a given operating environment.

Stainless steels are categorized based on their metallurgical structure, which includes ferritic, austenitic, martensitic, and duplex stainless steels. Duplex stainless steels are alloys that have a combination of ferritic and austenitic crystal structures. The mechanical properties of these stainless steel groups differ, with duplex alloys generally

Table 2.1.: Composition [% wt] of different stainless steel alloys.

UNS/AISI	C	Cr	N	Ni	Mo	Mn	P	S	PREn
S30400/304	0.08	18-20	-	8-10.5	-	0-2	0-0.045	0-0.03	18-20
S30403/304L	0.03	18-20	-	8-10.5	-	0-2	0-0.045	0-0.03	18-20
S31600/316	0.08	16-18	0.1	10-14	2-3	0-2	0-0.045	0-0.03	24.2-29.5
S31603/316L	0.03	16-18	0.1	10-14	2-3	0-2	0-0.045	0-0.03	24.2-29.5
S32750/2507	0.03	25	0.3	7	3.5	0-1.2	0-0.035	0-0.02	41.4

exhibiting slightly higher yield and ultimate tensile strength compared to austenitic stainless steels. [11]

2.1.1. Alloy Composition

As seen in Table 2.1, minor variations in the composition of alloying elements can result in distinct stainless steel alloys with different properties. One of the most important aspects is the amount of Cr present in the alloy. Cr is the only alloying element that can form a passive film on its own, although the other alloying elements will help in the formation and maintenance of the passive film, and make this more robust [12]. The presence of specific alloying elements can enhance the ease of machining, improve weldability by reducing the likelihood of defects, and increase the thermal stability to withstand high-temperature applications [13]. These are also important factors to consider when selecting an alloy for a specific application.

Nickel (Ni), as an alloying element, helps stabilize the passive film by facilitating rapid film formation. The addition of nickel to stainless steel promotes the formation of an austenitic structure, characterized by a Face Centered Cubic (FCC) crystal structure. Ni readily dissolves in this FCC structure, enhancing the stability and properties of the austenitic stainless steel. In contrast, in the Body Centered Cubic (BCC) structure of ferrite, Ni is insoluble. Therefore, when a ferritic alloy is desired, the addition of Ni is avoided, as it does not contribute to the desired characteristics of the ferritic structure [14].

Molybdenum (Mo) is utilized as an alloying element to enhance resistance against pitting and crevice corrosion. It also promotes the formation of a BCC structure, requiring a sufficient amount of Ni to maintain the desired properties of the FCC structure of austenitic stainless steel.

Alongside Mo and Ni, nitrogen (N) and manganese (Mn) can facilitate the formation of austenite [15]. Nitrogen, in particular, provides improved protection against pitting corrosion. The utilization of high-nitrogen steels is becoming increasingly prevalent, and efforts are being made to enhance the role of nitrogen in stabilizing the austenitic structure and passive film. By doing so, it becomes possible to reduce the reliance on nickel content in stainless steel alloys, while still maintaining the desired properties and corrosion resistance [9].

Other trace metals like phosphorous (P) and sulfur (S) have maximum allowed concentrations. These elements are added in order to improve machinability, although excessive amounts can cause have detrimental effects on the corrosion resistance of the alloy [16]–[18].

To assess the resistance of an alloy to pitting corrosion, a scoring system known as the Pitting Resistance Equivalence number (PREn) is used. This is a rating system that considers the relative amounts of specific alloying elements known for their pitting resistance, resulting in a numerical score. The formula to calculate it is shown in Equation 2.1.

$$PREn = \%Cr + (3.3 * \%Mo) + (16 * \%N) \tag{2.1}$$

To withstand marine environment and seawater applications in ambient temperatures, a material typically should have a PREn value > 40 [19]. This system has been subject to challenges and alternative approaches that weigh the importance and combination of alloying elements differently [20]. Although alternative methods exist, the presented PREn calculation remains widely used and offers practical and effective means of comparing and evaluating the pitting resistance of different alloys.

The most commonly used stainless steel types for constructions today are austenitic or duplex steels, due to the austenitic structures' advantage in weldability and toughness [21]. The types of austenitic steels most widely used are UNS S30400 (AISI 304) and UNS S31600 (AISI 316) stainless steel [22]. The AISI 304L and AISI 316L are almost identical to the AISI 304 and AISI 316 alloys, although with a lower carbon content which aids in weldability and reduces the chance of carbide precipitation in welds. However, the bulk material corrosion resistance properties are almost identical[23]. Thus, the low-carbon variants are often used in welded structures as the ones seen in processing facilities.

Table 2.2.: Composition [% wt] of AISI 304L.

C	Cr	N	Ni	Mo	Mn	P	S
0.03	18-20	-	8-10.5	-	0-2	0-0.045	0-0.03

As seen in Table 2.2, AISI 304L is an alloy consisting of high levels of Cr, and minimal levels of Ni. Despite being cost-effective and having favourable manufacturing, machining, and welding properties, it exhibits limited corrosion resistance, particularly in acidic environments and in the presence of chlorides such as in seawater or marine environments [24].

Table 2.3.: Composition [% wt] of AISI 316L.

C	Cr	N	Ni	Mo	Mn	P	S
0.03	16-18	0.1	10-14	2-3	0-2	0-0.045	0-0.03

The alloying elements of AISI 316L provide enhanced corrosion resistance in acidic and chloride-containing environments, surpassing the corrosion resistance of AISI 304L. This is mainly due to the presence of Mo, as seen in Table 2.3. Elevated Ni levels and the presence of N help stabilize the austenitic structure and improve the PREn value to around 27, depending on the specific alloy. This value is still lower than the recommended score of 40 for seawater applications. AISI 316L stainless steel is generally not recommended for use in seawater applications without any form of corrosion protection, as there can be risks of pitting and other kinds of failures. Nonetheless, it is important to note that the actual performance of the alloys will depend on the specific environmental factors and exposure conditions, as discussed in section 2.3 [25].

Table 2.4.: Composition [% wt] of 25Cr SDSS.

C	Cr	N	Ni	Mo	Mn	P	S
0.03	25	0.3	7	3.5	0-1.2	0-0.035	0-0.02

Duplex stainless steels are characterized by their unique combination of ferritic and austenitic crystal structures, making both the composition and structure crucial factors in their performance.

Table 2.4 shows that AISI 2507, also known as 25Cr Super Duplex Stainless Steel (SDSS), contains a higher content of Cr and N compared to other stainless steel alloys. It surpasses the minimum requirement of a PREn of 40, making it highly suitable for a wide range of applications in seawater environments, up to around 20°C according to NORSOK standards [26], although studies have shown survivability in even warmer waters [27]. Nevertheless, the high cost of SDSS necessitates careful consideration of which areas require its usage versus alternative alloys, to avoid unnecessary expenses in construction and maintenance.

2.1.2. Formation and Breakdown of the Passive Film

As previously mentioned, the formation of a passive film is a critical mechanism in preventing corrosion of stainless steel. These thin oxide layers, typically ranging from 1 to 3 nm in thickness, develop as a result of the alloy's oxidation upon exposure to the surrounding environment [10]. These films are described as passive due to their unreactive nature, and their prevention of further corrosion of the metal, as they prevent the electrolyte from directly contacting the underlying metal. When the passive film is formed, it initially appears as rapid corrosion, but it quickly reaches a steady state where the corrosion rate is significantly decreased, and the metal enters into a passive state [28]. The alloy's ability to create this film in corrosive environments is important, as it is able to self-heal if the metal should sustain damage to the surface [10].

The conditions in which the passive film can form are illustrated in Figure 2.1 where the potential is the given potential of the metal in the electrolyte, and the corrosion current is the rate of the anodic reaction, which is explained further in section 2.2.
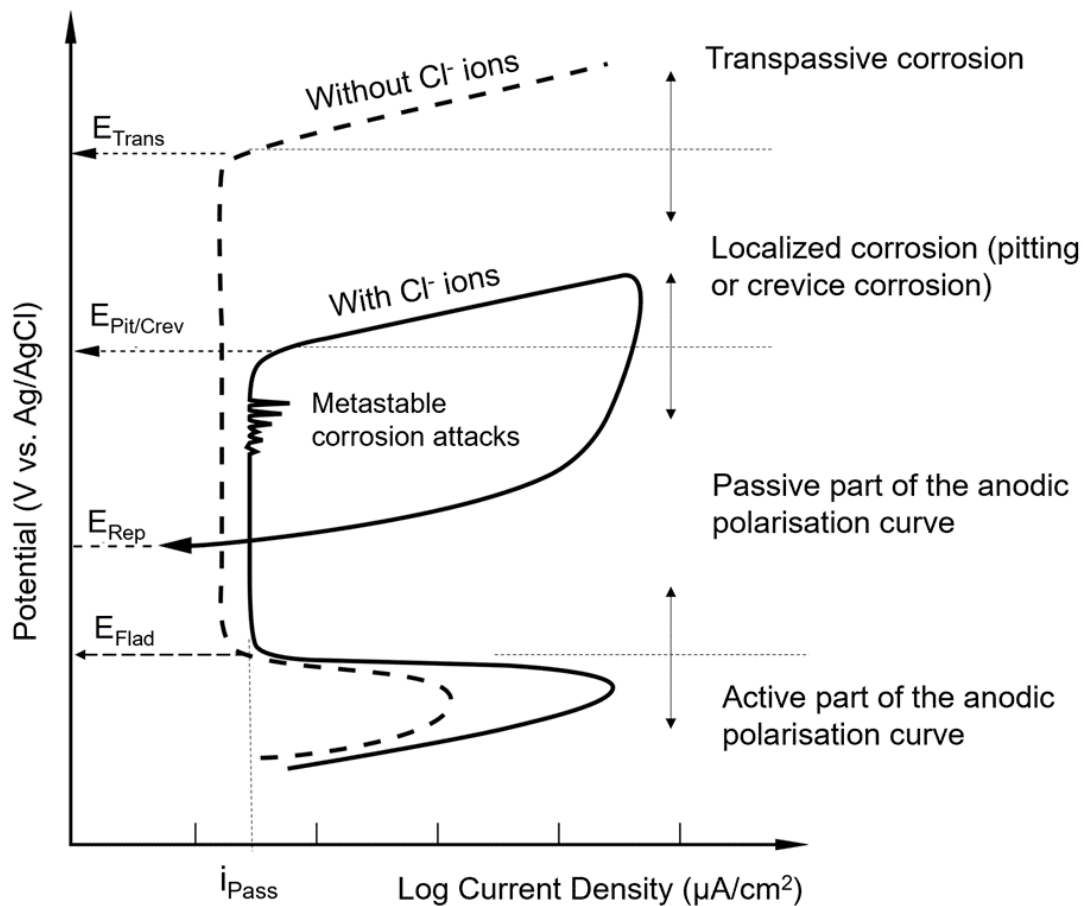
Figure 2.1.: Evans diagram showing corrosion rate compared to potential for chloride-containing and non-chloride-containing environments.

For environments without Cl, the passive film will be stable from the passivation potential E_{Flad} [29], up to a potential E_{Trans}, where the metal enters a transpassive state. Above E_{Trans}, dissolution of the passive film will occur, causing an increase in the

corrosion current [30].

In a chloride-containing environment like seawater, the passive film will still be formed at E_{Flad}, but will experience a different behaviour with increased potential. Above the pitting/crevice potential $E_{Pit/Crev}$, stable pit formation and crevice corrosion can occur. These mechanisms are also described further in section 2.2. At potentials slightly lower than this, metastable corrosion attacks can be seen, where pitting and crevice corrosion is initiated but not sustained [31]. The exact shape of the hysteresis curve seen in Figure 2.1 will be dependent on factors like the specific alloy, chloride content, and temperature, as explained in section 2.3. If the temperature is kept stable, alloys with a higher PREn will typically experience a smaller hysteresis curve, up to the point where E_{Rep} and $E_{Pit/Crev}$ intersect, pitting corrosion is mitigated, and the mechanisms of transpassive corrosion take over [32], [33].

The composition and structure of the passive film formed on austenitic steels vary depending on the pH of the electrolyte. The passive film will normally consist of an outer hydroxide layer and an inner oxide layer, mainly consisting of iron, chromium, and molybdenum, where molybdenum will occur in different oxidation states in the oxide and hydroxide layer [10]. The metal right under the oxide layer will appear to have a higher concentration of nickel since it will not contribute to the formation of the passive film, and stay dissolved in the austenitic structure. This mechanism is illustrated in Figure 2.2.
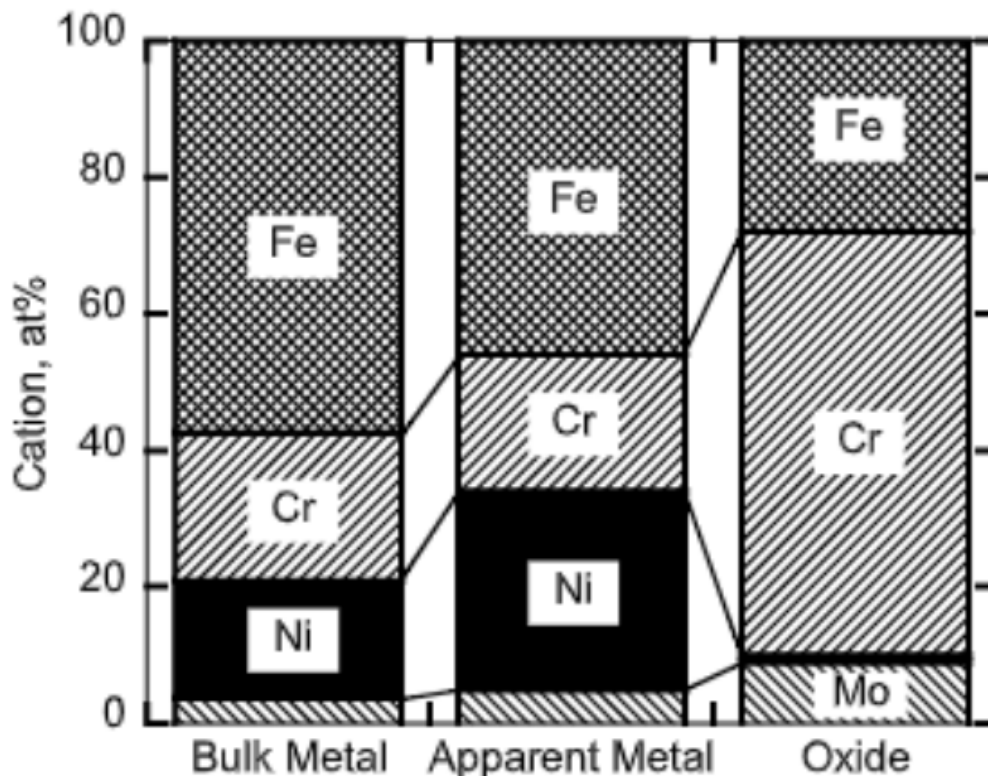
Figure 2.2.: Alloy composition in bulk metal and passive film [10].

2.2. Corrosion and Failure Mechanisms

Corrosion can occur through various mechanisms. To understand what potential problems can occur, and to try to explain corrosion occurrence seen in different facilities, it is important to understand the different corrosion mechanisms that can be at play. Corrosion requires reduction and oxidation reactions within the same electrolyte to establish a closed electrical circuit, enabling the transfer of electrons in the metal and ions externally through the electrolyte. In fish processing facilities, a lot of different electrolytes can be found. However, to explain the corrosion mechanisms, the main focus will be on seawater.

Figure 2.3 illustrates how corrosion in general occur in an oxygen-rich environment, where the oxidation of a bivalent metal is the anodic reaction letting metal ions into solution, while oxygen reduction occurs at the surface of the metal, producing hydroxide, which in turn react with the metal ions forming metal hydroxide, completing the electrical circuit by mitigating the buildup of charges.
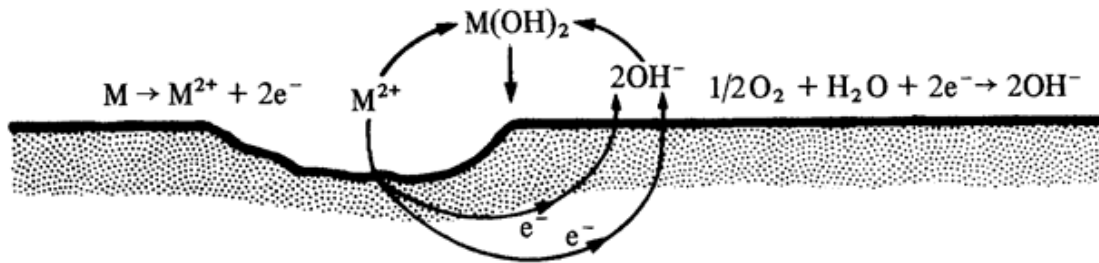
Figure 2.3.: Mechanism of corrosion in aqueous solution [34].

Corrosion current is a term used to determine the rate of these reactions by measuring the electron flow between the anodic and cathodic site, and hence how much metal has been oxidized.

The anodic reaction will depend on the valency of the metal but will normally be shown in the form of bivalent metal as seen in Figure 2.3, and presented in Equation 2.2.

$$M \longrightarrow M^{2+} + 2e^- \tag{2.2}$$

The cathodic reaction presented in Figure 2.3, is called the Oxygen Reduction Reaction (ORR) normally presented as in Equation 2.3 and Equation 2.4 for acidic and alkaline solutions, respectively.

$$O_2 + 2H^+ + 4e^- \longrightarrow 2H_2O \tag{2.3}$$

$$O_2 + 2H_2O + 2e^- \longrightarrow 4OH^- \tag{2.4}$$
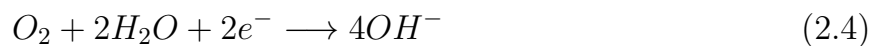
If there is a lack of oxygen, another reaction can occur, which is the Hydrogen Evolution

Reaction (HER). This reaction is shown in Equation 2.5.

$$2H_2O + 2e^- \longrightarrow H_2 + 2OH^- \tag{2.5}$$
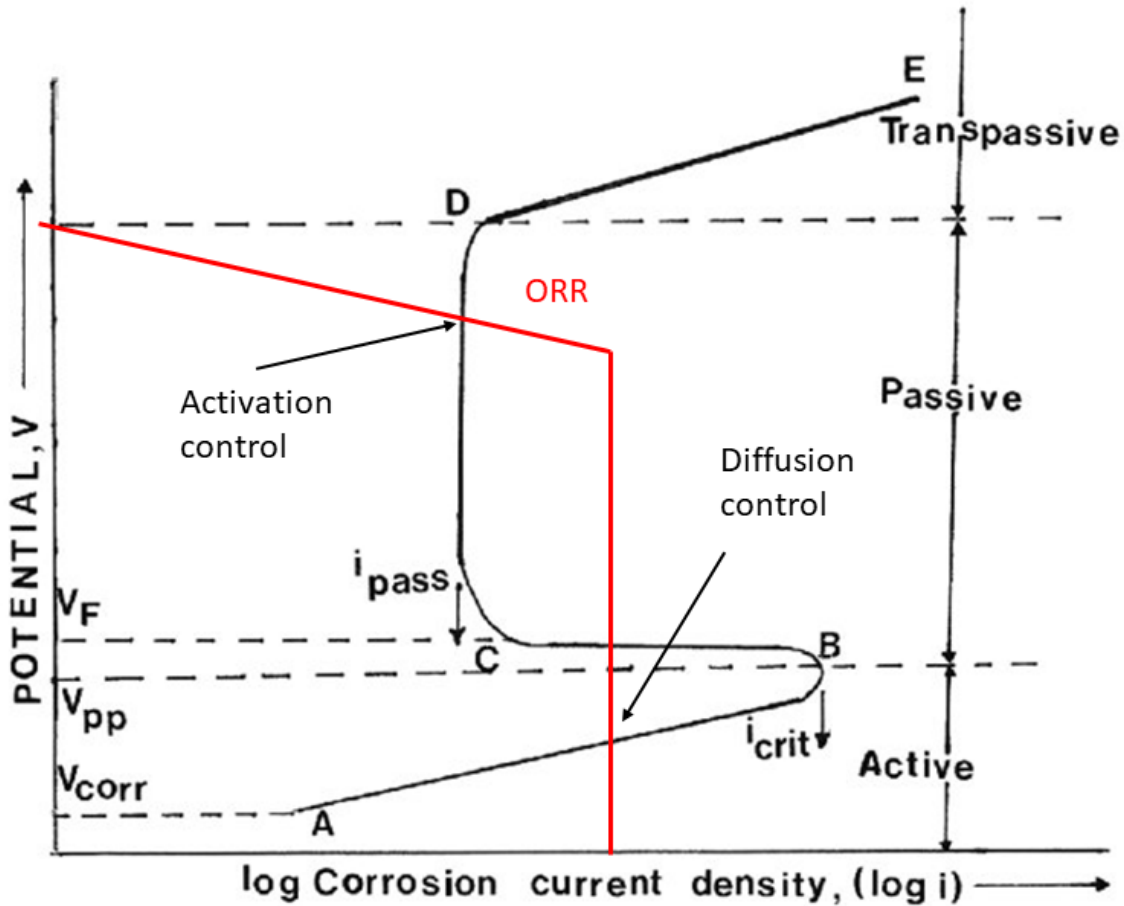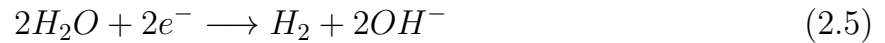
Figure 2.4.: Diffusion and activation controlled ORR [1].

These reactions have a specific thermodynamic driving force (voltage), and which reactions are allowed to occur, together with the pH of the electrolyte, will determine the Open Circuit Potential (OCP) of the metal in the electrolyte [34]. If the bulk solution has an abundance of oxygen, and the transport of oxygen to the metal surface is higher than what the cathodic reaction consumes, the polarization of the metal is said to be activation controlled and promote a higher OCP, as seen in Figure 2.4. If the diffusion of oxygen is lower than what is consumed, the polarization of the metal will depend on the diffusion of oxygen to the surface, and enter a diffusion-controlled state. This will lower the OCP, and as seen in Figure 2.4, this potential will determine if the metal will be in a passive state, or corrode actively[34].

2.2.1. Uniform Corrosion

Uniform or general corrosion is the most commonly seen corrosion mechanism, at objects where no single failure point or damage point is seen, but a general deterioration of the surface due to oxidation of the bulk metal, as seen in Figure 2.3. On a macroscopic scale, the metal dissolution will occur evenly on the surface, and the corrosion product will deposit as porous corrosion product onto the whole exposed surface. This is a corrosion mechanism often seen on carbon steel and other metals not undergoing an active/passive transition [34].

2.2.2. Pitting Corrosion

Pitting corrosion occurs when there is a breakdown of the passive layer, and the metal is unable to reform the oxide layer due to environmental factors, resulting in an exposed bulk metal that is vulnerable to corrosion. This type of corrosion affects metals that exhibit an active/passive transition, which makes it a critical corrosion mechanism for stainless steels.

Pitting is often divided into four stages: Local breakdown, early pit growth, stable pit growth, and repassivation. The mechanism behind the initiation of pits is still unknown, although many suggestions have been proposed [17] [35] [36]. To initiate a pit, a certain potential known as the pitting potential E_{Pit} is required. Above this potential, the metal will enter a state where pitting can be sustained, as shown in Figure 2.1. The value of the critical potential depends on many factors, including the alloy composition, pH of the electrolyte, chloride content, and temperature [37].

After the local breakdown, early pit growth forms a small pit from the local breakdown in the passive film and allows metal dissolution. This stage is not clearly defined, but is typically regarded to last until the pit is visible to the naked eye. To sustain the pit formation, chlorides or other ions with high electronegativity must be present [34].

When a pit is formed, the anodic reaction occurs inside the pit, and the cathodic reaction outside at a site with properties making it a sufficient cathode. This can typically be inclusions or grain variations within the steel. When oxygen is depleted inside the pit due to anodic reactions, hydrogen evolution will occur, making the local pit environment very acidic. This will initialize chloride migration into the pit, which in turn makes the environment even more suitable for pit growth. At the same time, metal ions will travel to the mouth of the pit, where they react with hydroxide from the cathodic reaction and form deposits. These deposits may cover the pit opening, limiting the diffusion of ions and containing the acidic environment in the pit, allowing further metal dissolution and pit formation. This mechanism is shown in Figure 2.5. This is the stable pit formation phase, which will end if environmental factors allow for better oxygen access in the pit and a change of potential. Repassivation of the metal can occur if the potential is changed to or beneath the repassivation potential E_{rep}, and above the E_{flad} as shown in Figure 2.1 [38].

Pitting is dangerous due to its spontaneous nature and is hard to monitor and discover.

The localized corrosion can penetrate constructions at a much faster rate than general corrosion [39], and can in facilities cause spontaneous leaks in piping systems.
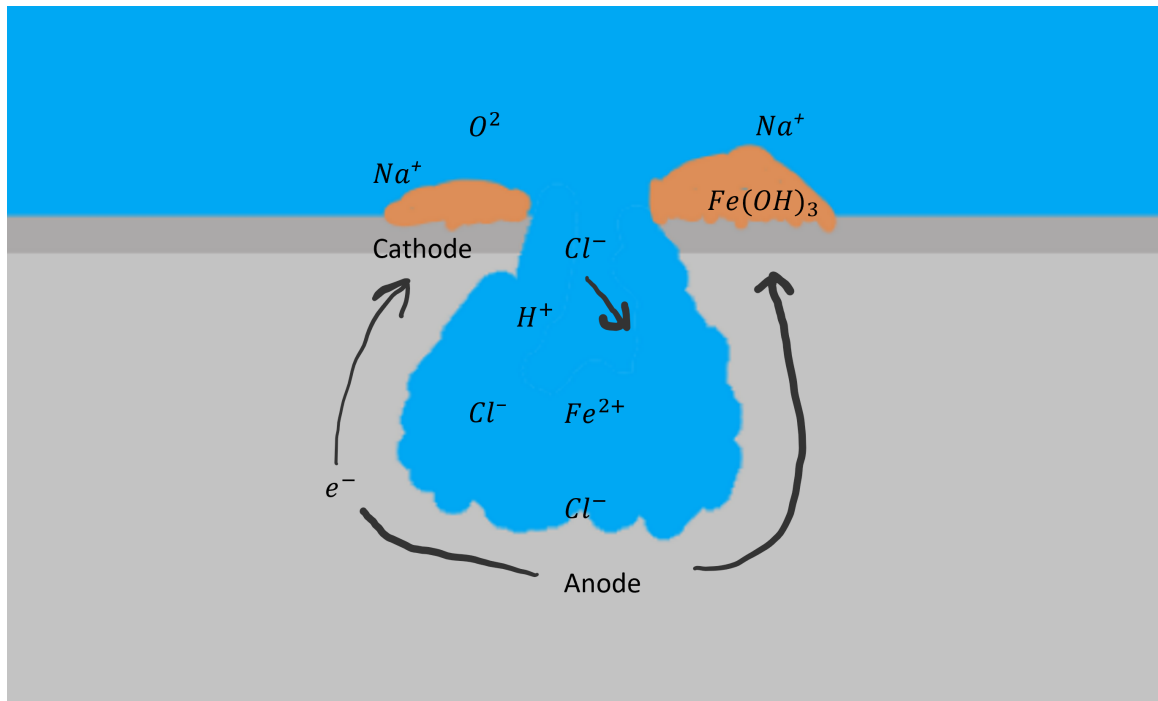
Figure 2.5.: Mechanism of pitting corrosion [1].

2.2.3. Crevice Corrosion

Crevice corrosion follows a similar mechanism as pitting corrosion, but it occurs in small gaps or crevices within the construction. As with pitting, to initiate crevice corrosion, a certain potential E_{crev} must be reached. Whereas in pitting, an initial region with oxygen depletion has to be formed, in crevice corrosion, the gap acts like the initial pit and allows oxygen depletion to occur. This will in turn create similar conditions as in the pit, although at a larger scale. This mechanism is shown in Figure 2.6 for a crevice between two stainless steel plates. However, non-metallic components like rubber gaskets and any other object that can form small gaps between itself and a metal substrate can cause crevice corrosion initiation [34]. An important note is that crevices will have a capillary effect, which can cause small gaps exposed to a humid, chloride-containing environment to accumulate water and similarly initiate corrosion even though there is little exchange of ions with an external electrolyte.
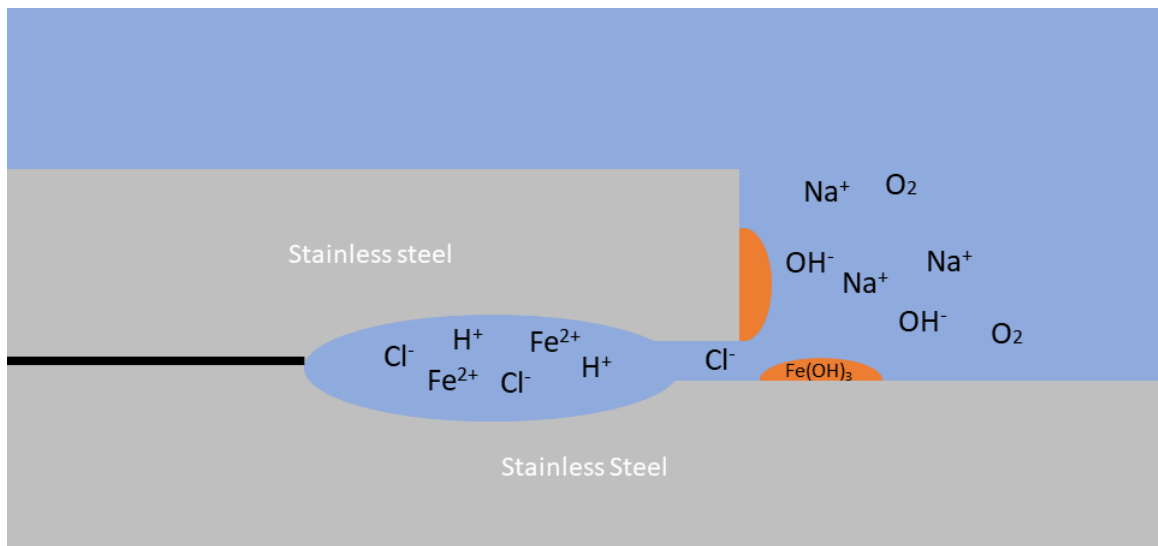
Figure 2.6.: Mechanism of crevice corrosion [1].

2.2.4. Microbiologically Induced Corrosion

Microbiologically Induced Corrosion (MIC) is a phenomenon that occurs when the formation of a biofilm on a metal surface leads to corrosion. Biofilms are created by bacteria that encapsulate themselves in a slimy substance called extracellular polymeric substance (EPS), which provides a stable environment and protection against the outside environment. [40]. Biofilms are created by various bacteria, including aerobic or anaerobic bacteria, such as sulfide-reducing bacteria or iron-oxidizing bacteria. Although the mechanisms are not fully understood, it is observed that the ORR can be catalyzed by biofilm, resulting in ennoblement of the steel [10], [41], [42].

Other factors like the change in pH under the biofilm and the fact that the biofilm acts like a physical barrier to the bulk solution can also be enabling factors in the increase of the OCP. As described in subsection 2.2.2, in order to begin pitting, the metal has to exceed E_{pit}. Hence the formation of biofilm can cause the initiation of pitting corrosion even though the conditions in the bulk solution would not facilitate this. The evolution of the stages from initiation to fully developed MIC can be seen in Figure 2.7, where the buildup of different bacteria and the encapsulation in EPS is shown together with Scanning Electron Microscopy (SEM) images of the corresponding stage. This illustration does not show which reactions occur under the biofilm since this can vary depending on what bacteria are present in the film [40].
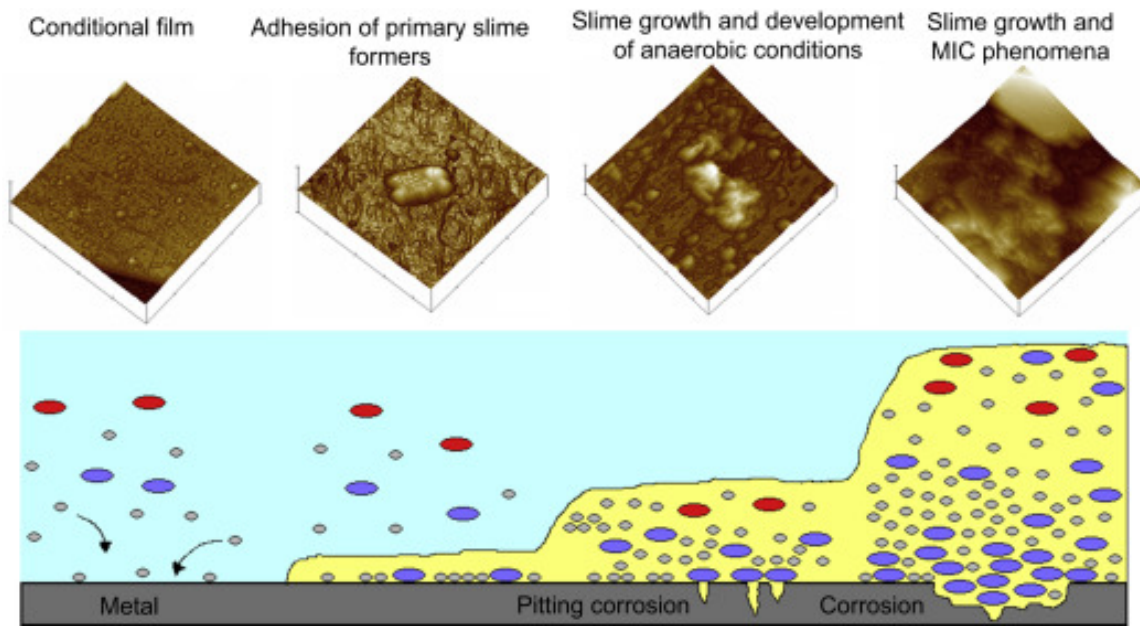
Figure 2.7.: Evolution of biofilm, and initiation of MIC [40].
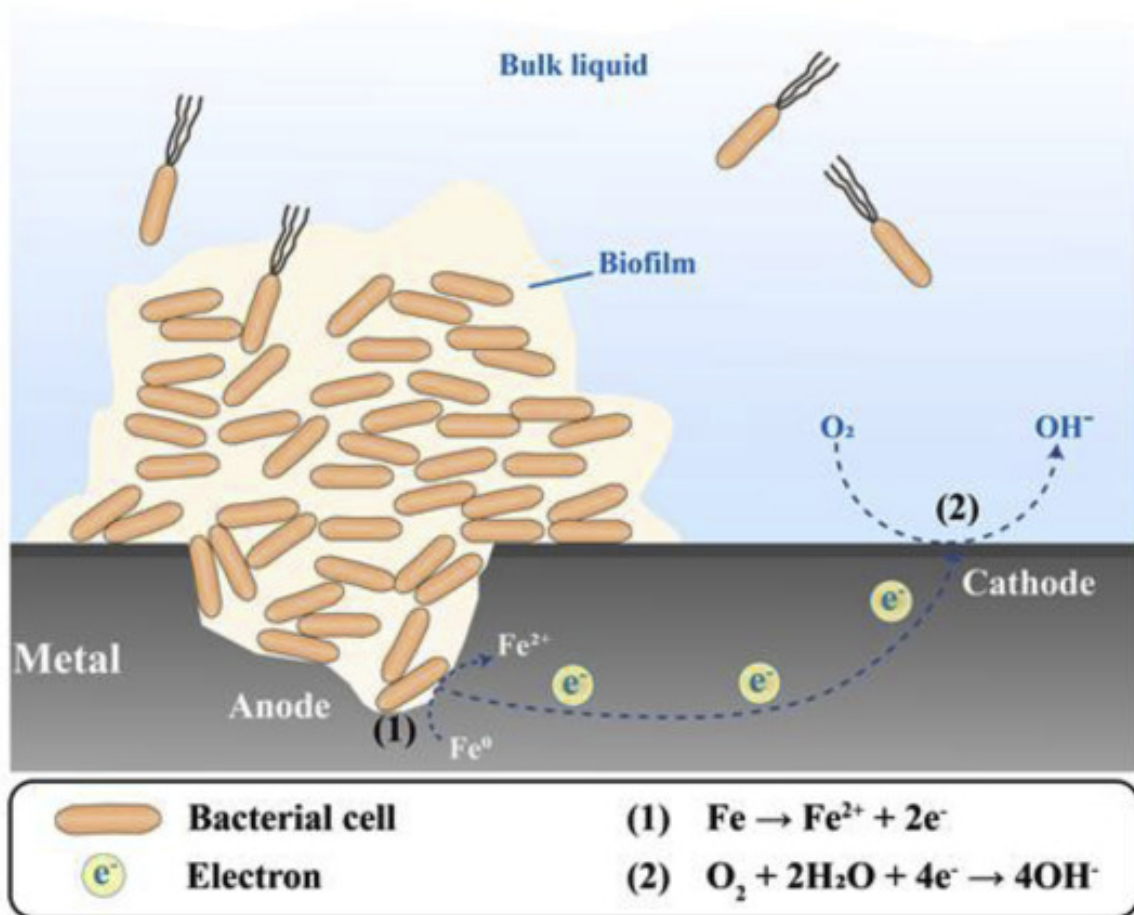
Figure 2.8.: Mechanism of pitting corrosion under biofilm [43].

2.3. Factors Affecting Corrosion of AISI 316L

As previously mentioned, AISI 316L is the alloy mostly used in fish processing facilities, especially for components in contact with fish and/or seawater. The corrosion susceptibility of AISI 316L is highly dependent on environmental factors, some of which are discussed in the following section.

2.3.1. Electrolyte

The electrolyte or environment AISI 316L is exposed to, plays a significant role in whether corrosion will occur or not. The pH of the electrolyte is one important factor in determining what type of reduction reactions will be dominating, and if AISI 316L is able to passivate or will be forced into active corrosion. For seawater this pH is normally around 8 [44]. The oxygen saturation of the electrolyte is also crucial since no ORR can occur if there is no oxygen present. The presence of ions with high reduction potentials like Cl will also affect if the metal will corrode or not, and can accelerate reactions like pitting massively, as seen in Figure 2.1, by lowering the potential at which the passive film can be susceptible to corrosion attacks.

Seawater is corrosive to AISI 316L under the right circumstances. The salinity of around 3.5% wt NaCl is one of the determining factors, where the chloride content is the driving force behind corrosion mechanisms like pitting and crevice corrosion. Together with the presence of microorganisms that can induce MIC, these are the main factors that facilitate the corrosion of AISI 316L in seawater [45].

For electrolytes like cleaning agents, especially the presence of chlorine and the pH of the solution are significant in determining if they are corrosive for AISI 316L or not, though the exposure time of the different electrolytes is also vital to determine if these initialize corrosion. Facilitating repassivation by rinsing in fresh water will also improve survivability [28].

The reason why marine environment and the splash zone are often regarded as very corrosive for AISI 316L is due to the onset of small droplets of water with high chloride content, which can allow for the initiation of pitting corrosion. Since these droplets are not in contact with a general bulk volume of water, and due to wet-dry cycles, a concentration of Cl is also possible. This will in turn increase the chance of initiation of pitting corrosion [45].

Compere and Le Bozec [46] show that the influence of bacteria and other microorganisms in natural seawater can greatly affect the probability of pitting and crevice attacks, hence identifying specific numbers for values like E_{pit} and Critical Pitting Temperature (CPT) is difficult.

2.3.2. Temperature

General metal dissolution does not normally occur on AISI 316 in seawater since it will normally be passivated. However, if the temperature is high enough, pitting or crevice corrosion may occur, which in turn can cause active corrosion. The temperature at which stable pitting may occur is referred to as the metals Critical Pitting Temperature (CPT). A similar temperature relation is found as the Critical Crevice corrosion Temperature (CCT), and this is lower than the CPT. Due to the semi-random nature of pitting corrosion, it is challenging to predict the CPT and CCT for a specific situation.
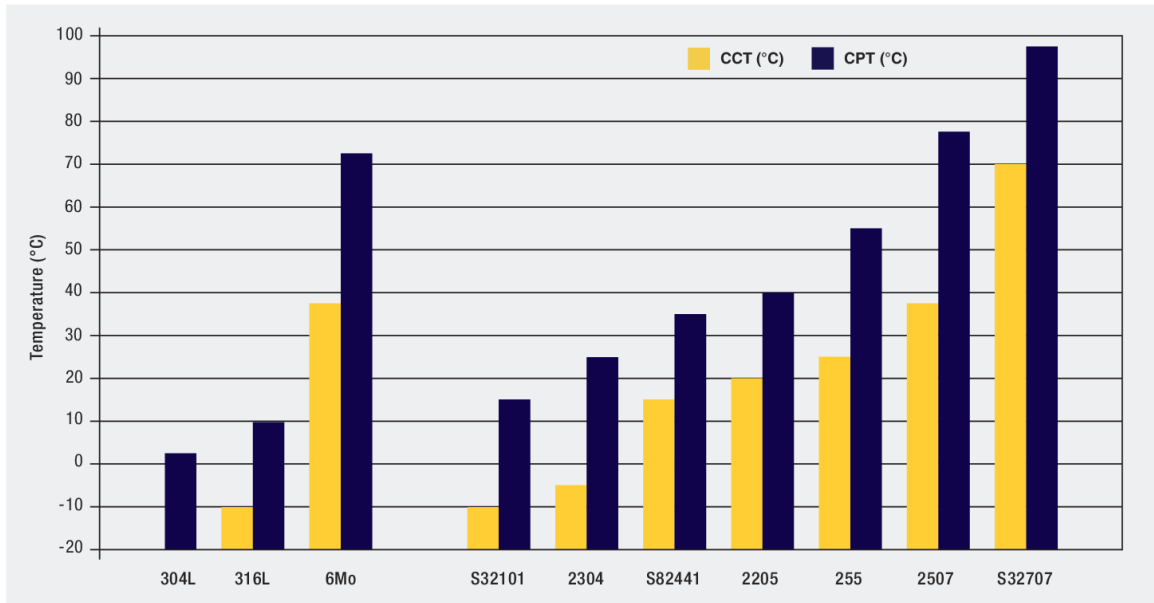
Figure 2.9.: Critical Pitting and Crevice corrosion temperature of selected stainless steel alloys (evaluated in 6% ferric chloride by ASTM G 48) [11].

There are a couple of different methods to perform CPT and CCT tests, which yield different results. The ASTM G48 test shown in Figure 2.9 gives a value of 10 °C for the CPT, and -10 °C for the CCT of AISI 316. However test done in seawater collected in Trondheim, performed by AvestaPolarit [47] in accordance with the ASTM G150 test, show a CPT of around 30 °C for AISI 316. These tests will not take into account effects due to biofilm formation due to the short time from immersion to result, and these tests show the difficulty in obtaining representative real-world values of CPT and CCT. The CPT values from AvestaPolarit are also backed up by tests performed by Alleima (former Sandvik Material Technology), which results are shown in Figure 2.10. The chlorine content in seawater is normally higher than 1.2% wt Cl, which is shown in the tests from Alleima. However, the figure illustrates that the decrease in CPT is most significant at lower Cl concentrations, with only a small predicted decrease from 1.2% wt to 3.5% wt.

Figure 2.1 does not show the effect of temperature, though if the temperature is below the CCT or CPT, the respective corrosion mechanism will not initiate. However, CPT and CCT are dependent on the potential of the samples, making general predictions difficult [38]. Temperature will also influence the rate of other corrosion mechanisms,

as many chemical reactions will happen faster at elevated temperatures.
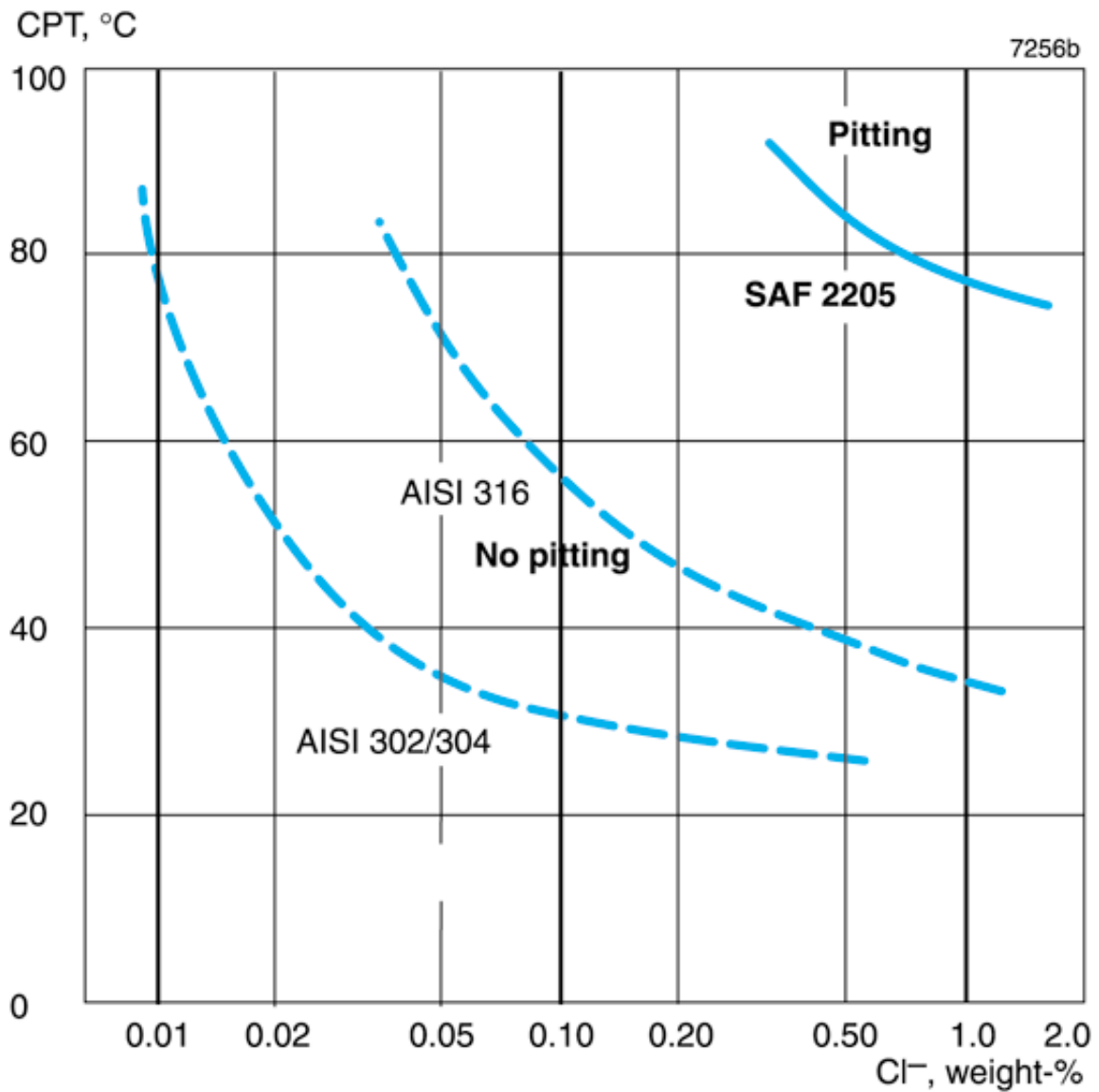
Figure 2.10.: CPT of selected stainless steel alloys in different Cl concentration [48].

2.3.3. Flow and Access to Oxygen

In stationary systems, diffusion of oxygen to the metal surface may be a limiting factor for the ORR. If pitting is initiated on the surface, this lack of oxygen will make repassivation difficult. By introducing flow in the system, the diffusion of oxygen to the surface can increase and promote repassivation of the surface, preventing further corrosion [34]. This effect will only be beneficiary for low and moderate flow velocities as other mechanisms like erosion corrosion can take over as the primary corrosion mechanism at flow velocities over 12 m/s [49].

Flow can also help reduce the formation of biofilm due to the mechanical shear forces between the film and the water. This effect will only increase with the flow velocity. Nonetheless, for lower velocities, like ones seen in the processing facilities, this effect will be negligible, and biofilm can still form [40].

2.3.4. Welding and Heat Treatment

There are many different methods to weld stainless steel, but the most common method used in the facilities is Gas Metal Arc Welding and Gas Tungsten Arc Welding. These methods, although different, both rely on joining the metal by creating an electrical arc which melts the base material and adding a filler material to join the parts together. When welding stainless steel, the alloy in practice becomes liquid, and the grain structure will be redefined by the cooling rate and eventual impurities and inclusions which might have contaminated the weld. The weld will also be hot for a prolonged time, and if it is exposed to the atmosphere, different oxides than those normally found in the passive film may form.

A shielding gas, typically Argon, is used to displace the oxygen in the vicinity of the weld to prevent oxidation of the weld. When welding thin structures like piping, back coverage with shielding gas is also important in order to avoid oxidation of the backside of the weld. This may involve purging the piping section with the shielding gas. However, post-treatment of the weld, such as pickling, grinding, or electropolishing, may be necessary to restore material properties in the Heat Affected Zone (HAZ) [50]. Pickling involves using hydrofluoric acid and nitric acid to remove unwanted oxides and free iron from the weld zone, allowing the naturally forming chromium oxide to protect the steel surface [51]. Grinding mechanically removes oxide precipitation and exposes the metal substrate to be able to form a proper passive layer. Electropolishing includes oxidizing the surface in a controlled manner, removing any other oxide buildup on the surface and allowing for a proper passive film to grow [52].

If welding is not performed properly, weld zones can act as local anodic regions due to the lower potential, and galvanic corrosion of the weld may occur [39]. In addition, pores and other structures in the weld zone can act as crevices, leading to many different forms of active corrosion, with resulting rapid weld deterioration and subsequent failure of the component. Factors like the wrong type of filler material and shielding gas, together with difficulties in identifying improper back shielding when a piping section is mounted, can contribute to making the welds susceptible to corrosion [53].

An example of improper weld procedures is seen in Figure 2.11, where visible discolouration is seen. This corresponds well with the example weld in Figure 2.12.e) or f). A weld with sufficient shielding would have little to no discolouration, as seen in Figure 2.12.a. This resembles the vertical weld seen in the bottom half of Figure 2.11.
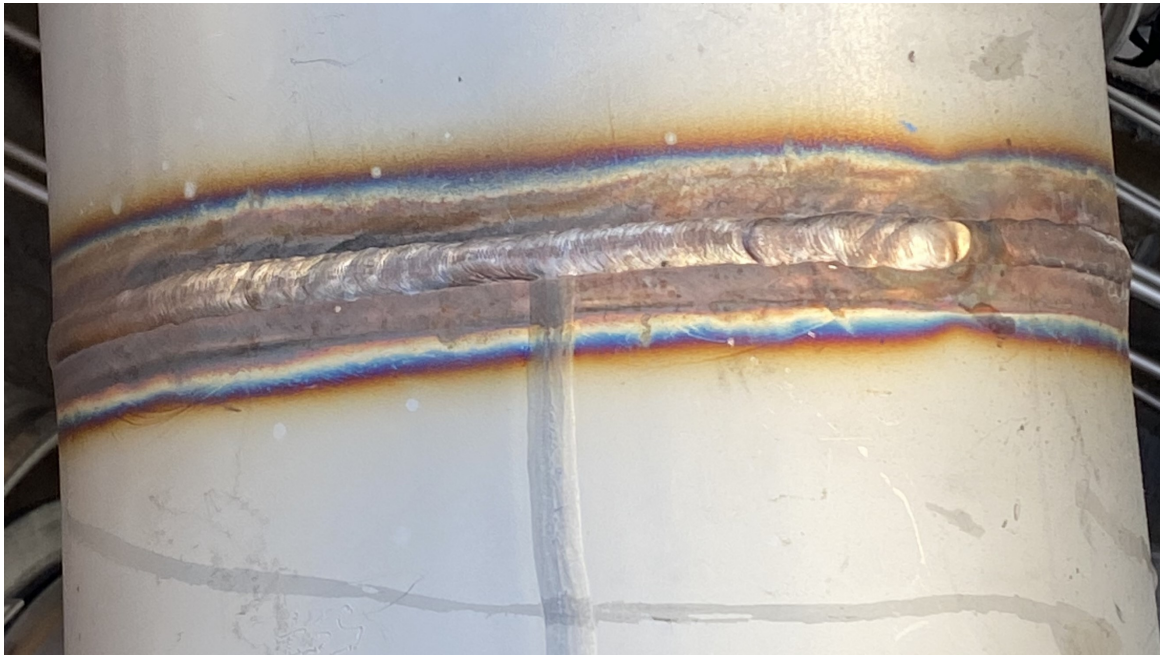
Figure 2.11.: Poor weld of AISI 316L piping at InnovaNor, with significant discolouration. The vertical seam is properly welded and post-treated, with no signs of discolouration.

a) Good gas protection

b) Acceptable gas protection.

c) Acceptable provided the blue areas are intermittent.

d) Acceptable provided the brown coloured zone close to the weld is as shown, narrow and light coloured.

e) Poor back purge. Not acceptable

f) Poor back purge. Not acceptable.
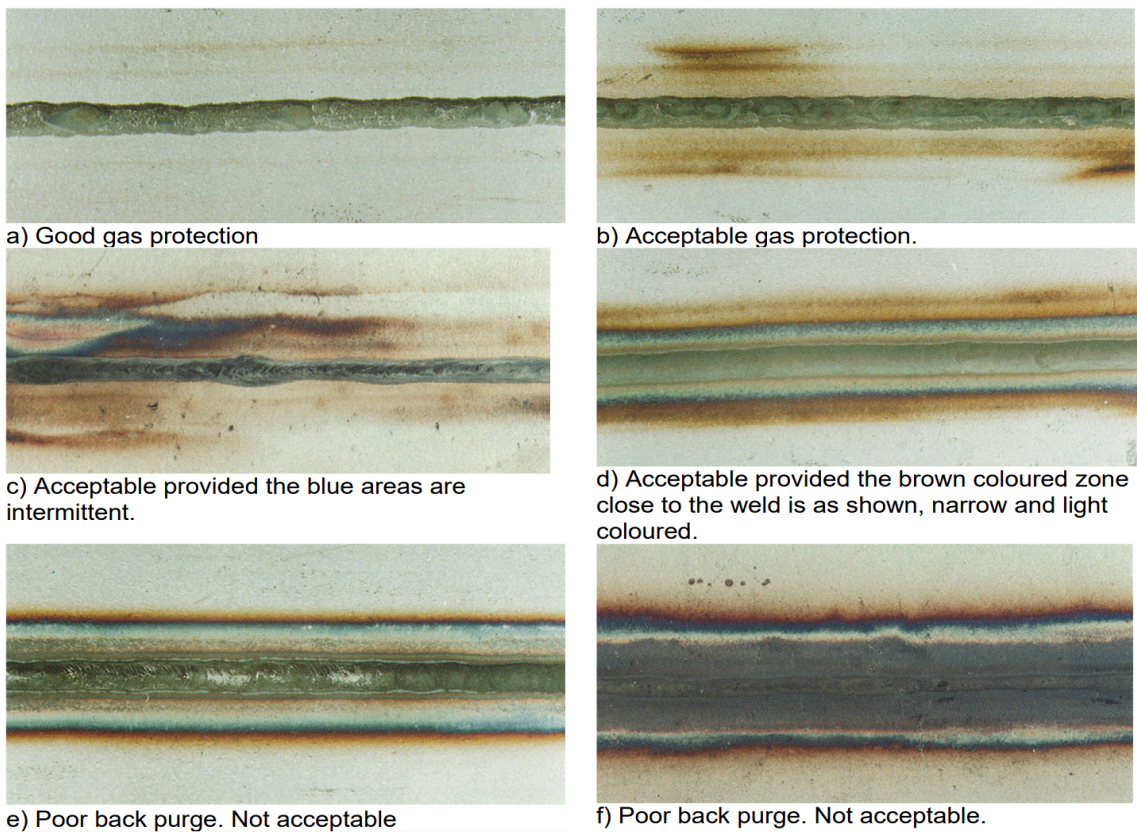
Figure 2.12.: Overview of acceptable and unacceptable weld discolouration according to NORSOK M601 [54].

Figure 2.13, show the relation between temperature and the potential at which pitting can occur on different alloys and weld qualities. At lower temperatures, E_{crev} is drastically lowered on a poor weld compared to a good weld. Though different from AISI 316L, the trend does still apply.
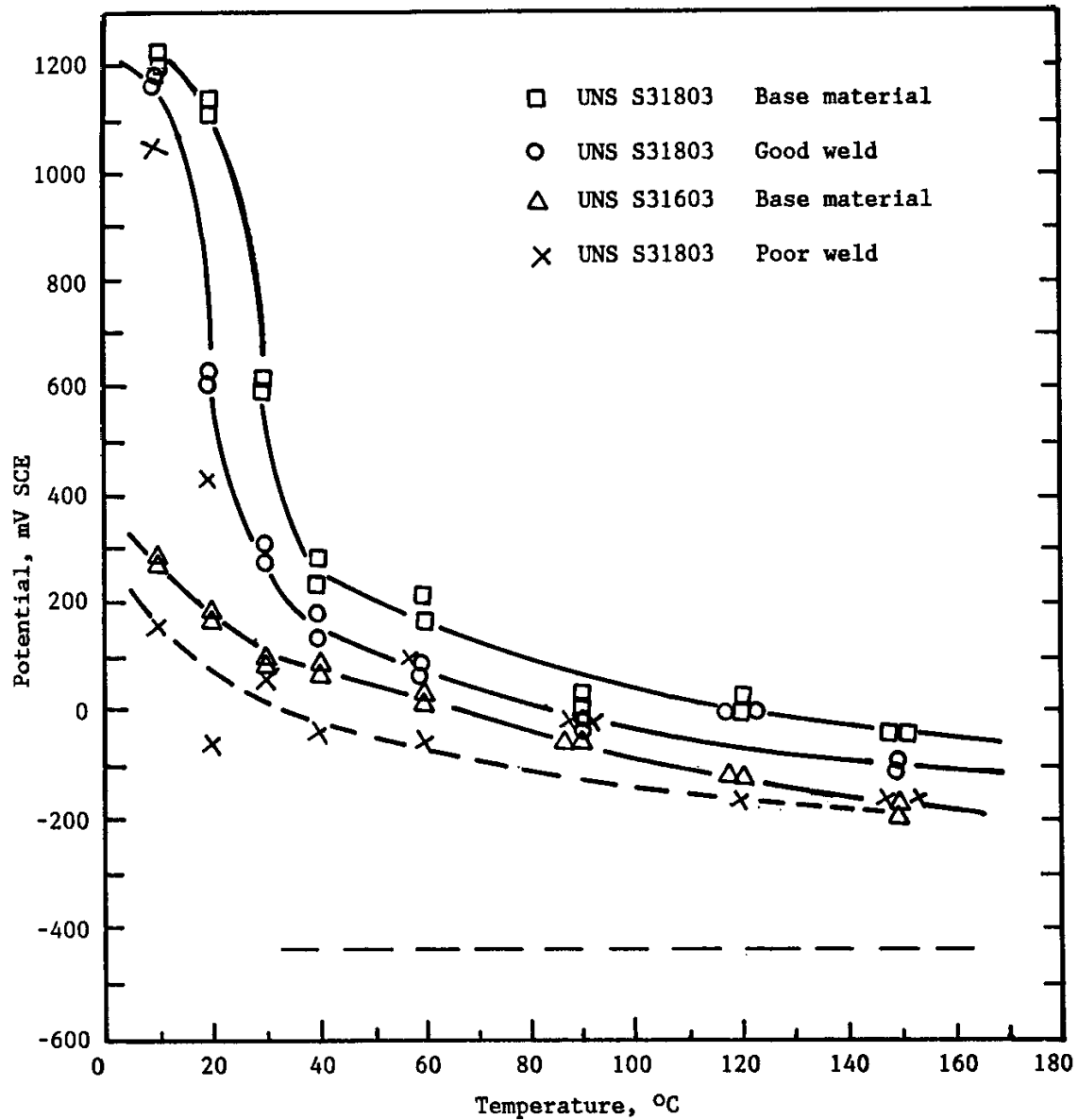
Figure 2.13.: Critical potential vs temperature determined by use of long duration tests in 3% NaCl at 2.5 bar CO2 for base material of UNS S31803 and base material of UNS S31603 (AISI 316L) and good and poor quality welds of UNS S31803. [55]

2.3.5. Biofilm Formation

As seen in subsection 2.2.4, biofilm formation will affect the OCP evolution of AISI 316L, which in turn can cause the onset of pitting or crevice corrosion. The rate at which this biofilm forms, hence changing the OCP, is highly dependent on temperature. This effect can be seen in Figure 2.14, where the fastest biofilm formation occurs at 30°, with decreasing speed at lower temperatures due to a longer incubation time of the film. At 40°C, the biofilm no longer forms, and no ennoblement is seen. These exact temperature relations will be dependent on location in the world [56]. Light level can also affect the onset of biofilm [41].
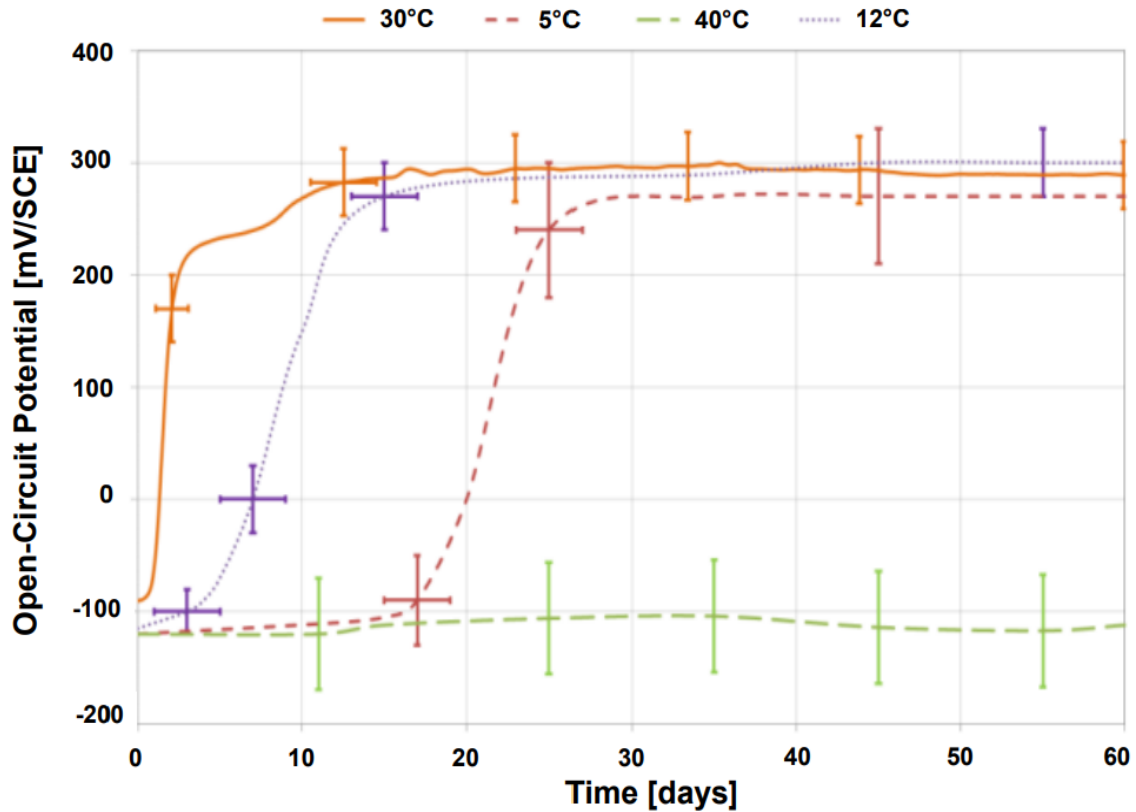
Figure 2.14.: Open Circuit Potential development at different temperatures, due to biofilm formation. No ennoblement indicates that no biofilm is formed [56].

By connecting samples of 25Cr SDSS to a sacrificial anode through a shunt resistor, and measuring the cathodic current, pseudo-polarization curves were made by Larche et al [56]. These curves, seen in Figure 2.15, show the cathodic current demand of the stainless steel drastically increases with the onset of biofilm, indicating the initiation of pitting. It is important to note that this current reduction is specific for 25Cr SDSS as lower alloyed metals can initiate pitting at these temperatures without the onset of biofilm. The trend is nevertheless relatable to current demand with and without the onset of biofilm in regard to pitting corrosion.
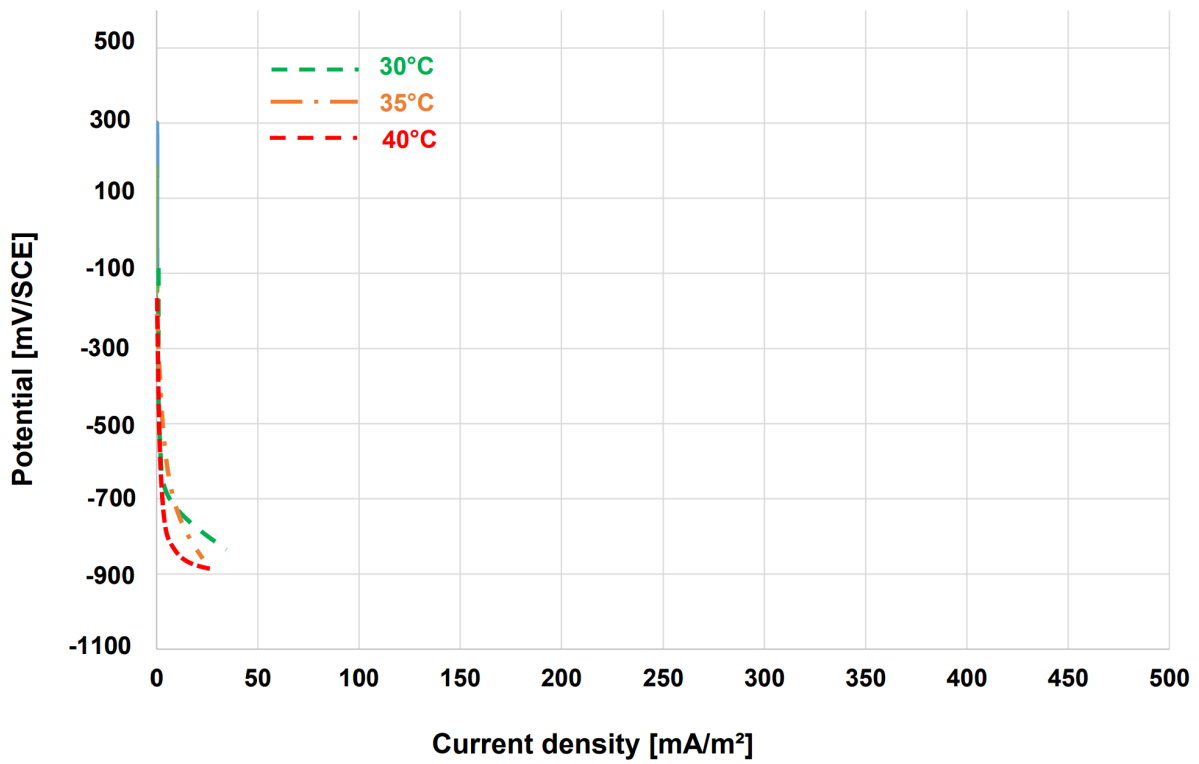
(a) Cathodic current before biofilm formation
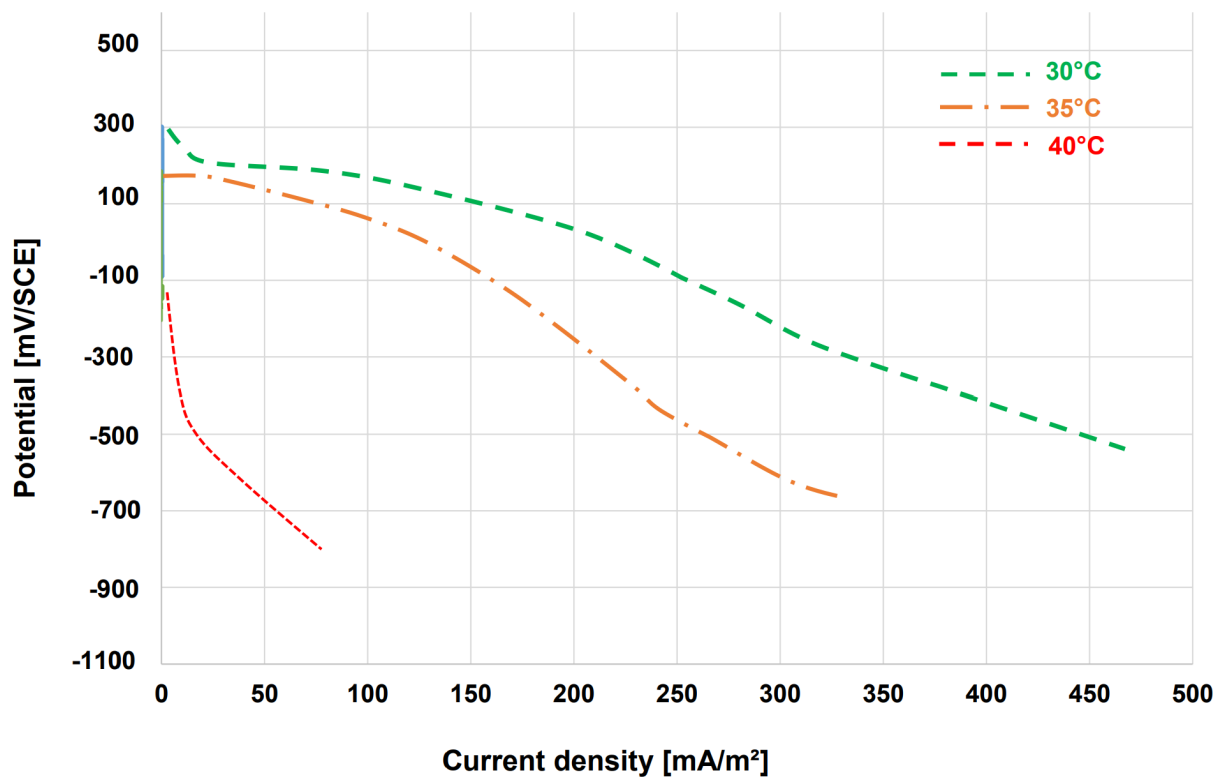
(b) Cathodic current after biofilm formation

Figure 2.15.: Pseudo-polarization cathodic current density curves created by repeated potentiostatic measurements at different potentials. [56].

Chapter 3.

Harsh Environment Multi-channel OCP-test Setup (HEMOS)

An Open Circuit Potential (OCP) measurement involves measuring the potential between a reference electrode and a test sample immersed in the same electrolyte. By analyzing continous OCP measurements of stainless steel, one can determine if pitting and crevice corrosion initiates. An initiation is identified by a rapid decrease in the OCP, and can be followed by a similar increase in potential when the steel re-passivates. For measurements in the facilities, a Comet Systems MS6d data logger [57] was used to monitor the OCP of 15 samples as well as the temperature of the seawater.

To be able to install this setup in a fish processing facility's harsh environment, a couple of design issues had to be resolved. The test setup is split into three main components: the test chamber, the electrical cabinet, and the control PC and Power supply (PSU). This system and its components will be presented in this chapter.

3.1. Test Chamber

The test chamber is a plastic box measuring L60xW35xH40 cm, with a water inlet and outlet.

As seen in Figure 3.1, the water inlet and outlet are placed high on the wall of the box, to ensure that there always will be water to cover the samples, even when the facility is shut down. The inlet side has a pipe on the inside that leads the inlet water to the bottom of the chamber. This is to ensure circulation of the water in the entire chamber. The water flow rate on the inlet side is controlled by a ball valve connected to the water source.

To hold all the samples in place, a mount was designed consisting of two girders along the length of the box, with overlaying beams to hold the samples, reference electrode

Figure 3.1.: Test chamber during the design stage.

and temperature sensor (thermocouple). The girders are mounted to the sidewall with three M6 bolts, and the holes are filled with silicone to prevent leaking. On the top of the girders, small nylon pegs are mounted, which match up with corresponding holes in the beams, to prevent transversal movement of the beams while still making them easy to remove.

The beams have four equally spaced 4mm holes to accommodate the mounting of the samples either by platinum wire or by thread rods, both of which were tested in the facilities. The middle beam holds the reference electrode and the thermocouple.

A slot is cut into the side of the box to facilitate cable routing out of the box, as seen in Figure 3.2. After mounting the first samples on Frøya, it became clear that stronger support for the inlet was beneficial due to the heavy inlet valve assembly. To accommodate this, an extra plate of PVC is mounted to the outside of the box to stiffen the wall, seen in Figure 3.3. This plate is fastened with four M6 bolts and the holes sealed with silicone.

The setup at Senja proves that this is a viable solution, and the connection can now handle a heavier inlet valve assembly.
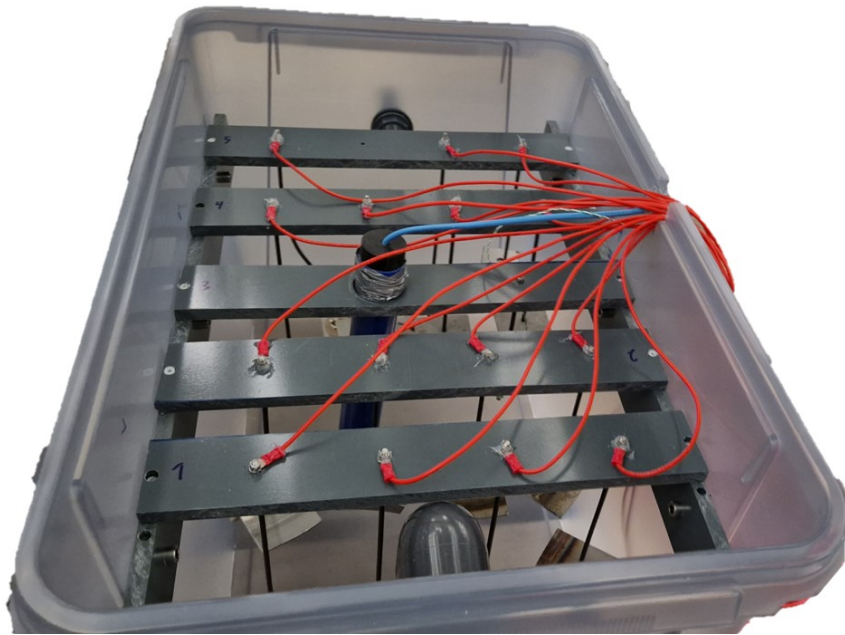
Figure 3.2.: Test chamber with mounted samples at InnovaNor.

Figure 3.3.: Support for the inlet valve assembly, constructed and implemented for the setup at InnovaNor.

3.2. Electronics Cabinet

The electronics cabinet is designed to withstand humid conditions as well as direct splashes of water, while providing a safe and stable environment for the datalogger and allowing it to monitor the samples. This cabinet is built with an IP44 rated box, which is splash proof. All holes in the box walls are sealed with silicone to provide a watertight seal. The most noticeable feature on the electronics cabinet is the input for all the samples, seen in Figure 3.4. These banana connectors are mounted to the side wall of the box, with an additional laser-cut plywood support behind to relieve some strain from the wall of the box. This piece of plywood also serves the purpose as a drill guide when boring the holes in the box. All banana plugs eventually got a seal like the one in the upper left corner, to seal the interface between the male and female plug. The rectangular thermocouple connector is also sealed with silicone to make the connection waterproof. Cables like the one shown in Figure 3.5a are used to connect the samples to the Electronics cabinet. These are prepared with one male banana plug connector for the cabinet, and one ring-formed cable lug to connect to the sample.
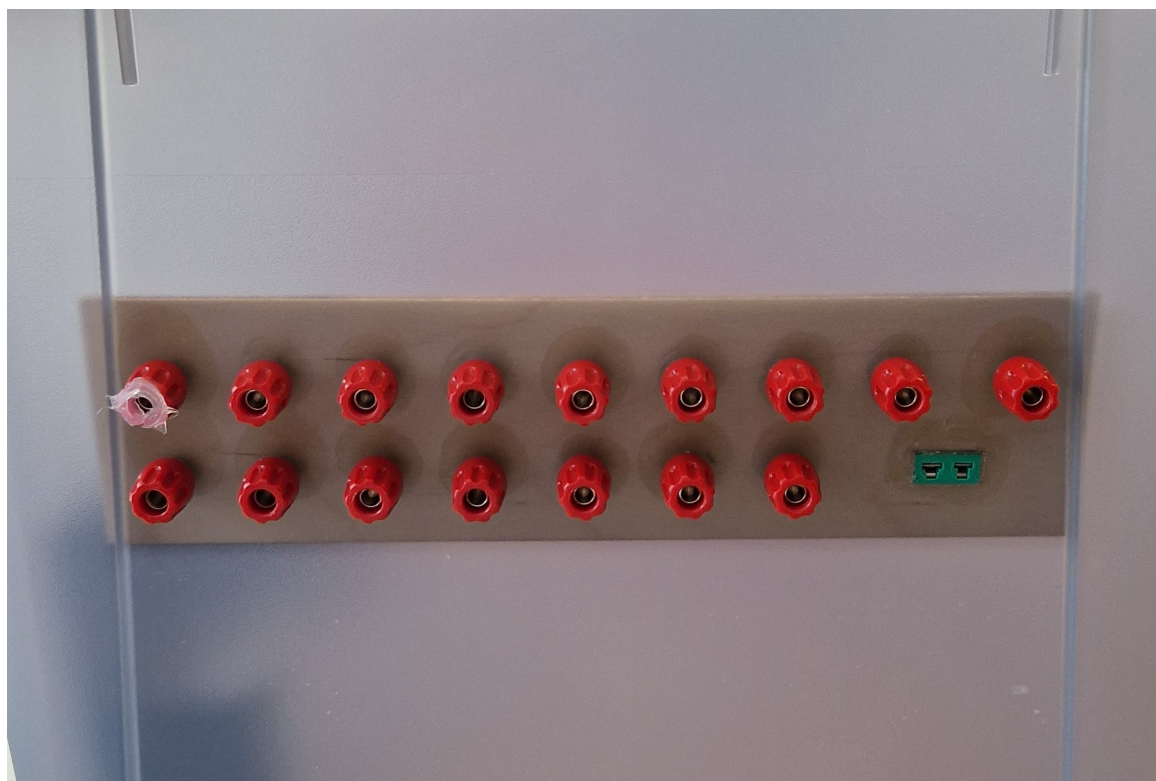
Figure 3.4.: Signal cable interface for the electronics cabinet, Allowing for 15 samples, 1 reference electrode, and a thermocouple to be connected.

One common ground/reference cable, Figure 3.5b, connected all the COM-ports on the datalogger to the common reference electrode in the test chamber

In order to make the thermocouples used in the test setup waterproof, their exposed sensor tips were coated with polyurethane, as seen in Figure 3.6.

(a) Signal cable.

(b) Common ground cable.
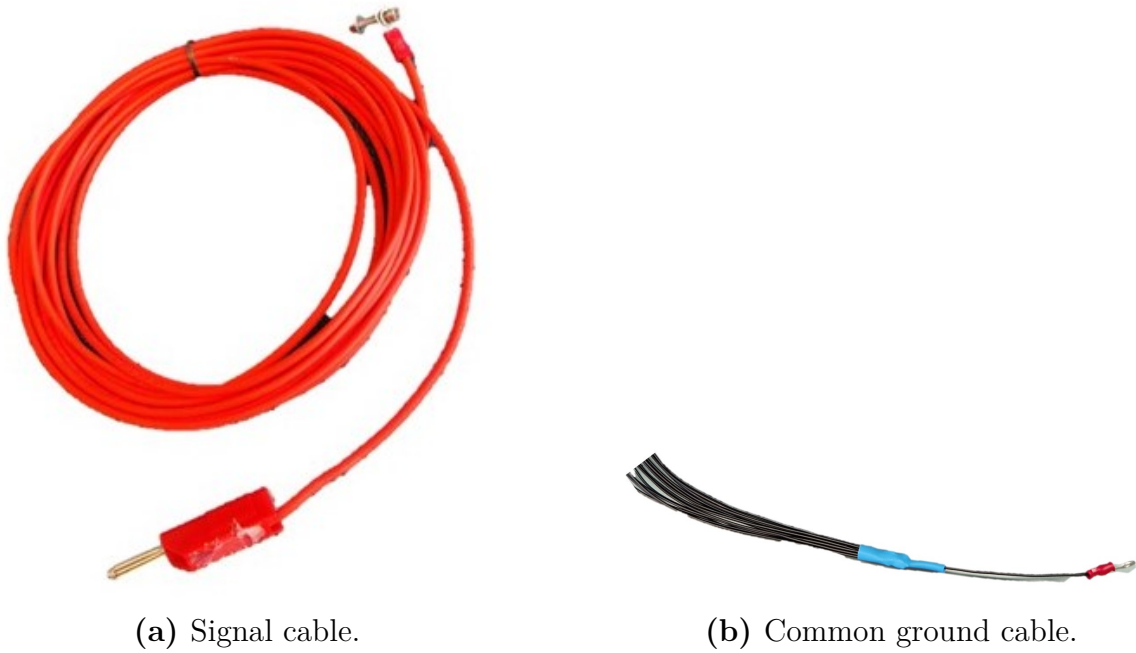
Figure 3.5.: Custom cables made for the test setup. The signal cables are terminated with banana plugs and ring-formed cable lugs. The Common ground is soldered with 15 cables to 1, to connect all samples to the same reference.
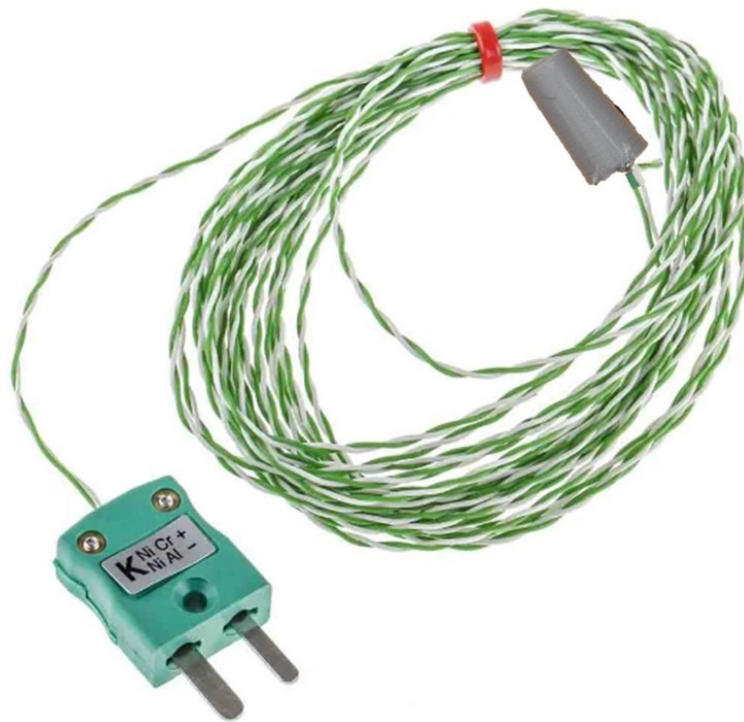
Figure 3.6.: K-type thermocouple used in test chambers. The sensor is coated with polyurethane to make it waterproof. Adapted from RS components[58].

The data logger is mounted on the wall of the cabinet in a 3d printed holder,Figure 3.7a, and two cable glands are mounted to facilitate the power and ethernet cables routing to the data logger, Figure 3.7b. The complete electronics cabinet assembly can be seen in Figure 3.7c.

In an effort to minimize the humidity inside, small bags of silica gel were placed in the electronics cabinet during installation.
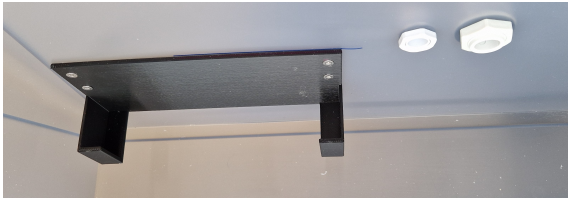
(a) 3D-printed logger holder.
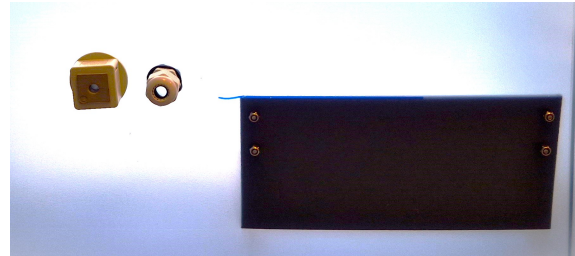
(b) Cable glands.
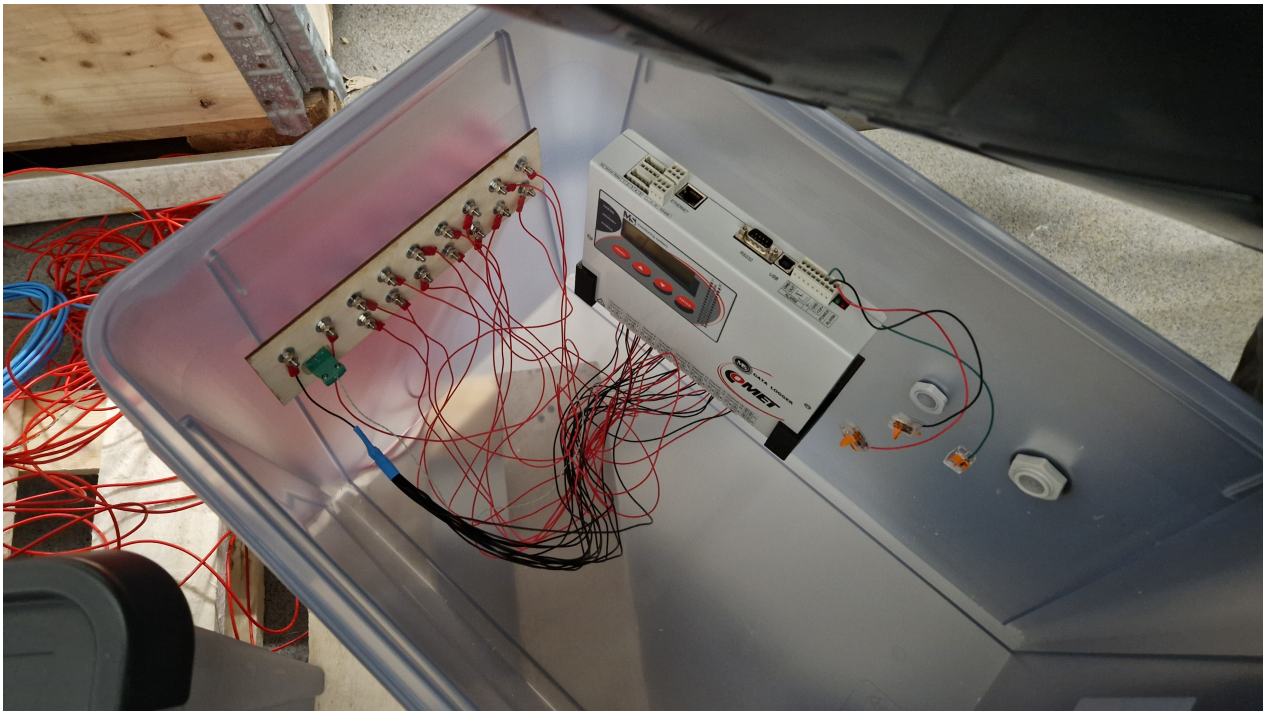
(c) Mounted datalogger.

Figure 3.7.: Data logger mounting and interface for Ethernet and power.

3.3. PC and Power Supply (PSU)

The PC and PSU are mounted in dry locations separate from the rest of the setup, with power and Ethernet cables brought to the data logger. This is to protect the electronics of the PC from moisture, as well as making sure the electronics do not overheat, as they could if placed in the enclosed box together with the data logger.
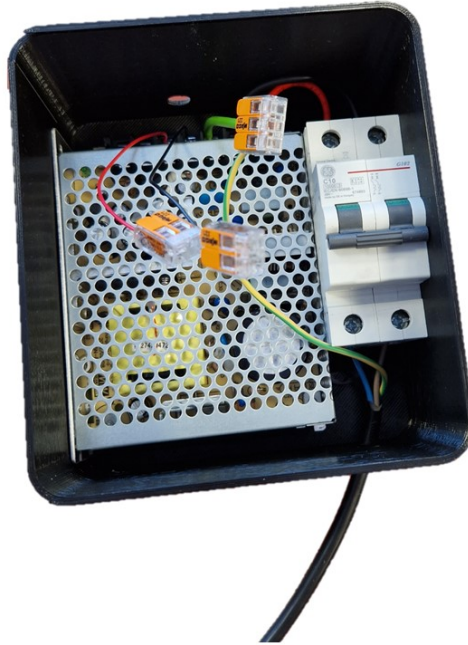
Figure 3.8.: Powersupply for the data logger, with integrated circuit breaker in order to protect the system should a short circuit occur.

The PC is a Windows computer running the data loggers' custom software which auto-downloads the data from the logger every 8 hours. (This is configurable to an interval of liking). The computer is also set up to automatically boot, and log in as a local user immediately after it receives power, to eliminate issues with power failures. The data program also launches automatically, and data collected from the logger is synchronized to a remote drive, accessible from anywhere so that data can be monitored and analyzed in real-time without having to be present at the location. The computers are also configured with TeamViewer to be able to resolve any issues remotely, as long as they are connected to the internet.

The PSU casing, Figure 3.8, is designed with a 24V power supply, and its own circuit breaker. This is done to limit the influence of the equipment on the rest of the facility in case something should fail. The circuit breakers in the facility are of a higher current rating, so if a short circuit should occur in the setup, it would hopefully only trigger the local circuit breaker, and not interrupt normal production in the facility.

3.4. Design for Transportation

One important aspect of the HEMOS is that it can be mounted in remote locations, and subsequently needs to be transported there. One criterion for the setup was to be able to transport it within the footprint of one case. This is done by making all internal structures of the Test chamber removable so that the other cases can stack within, as seen in Figure 3.9. The electronics cabinet must have all external features removable for the same reason. When stacked, the inner case holds all the electronics, PC, PSU, samples and equipment needed, so that everything can be shipped as one package. This makes shipping and transportation easier, at the cost of longer assembly time at the test location. Whether the HEMOS should be transported as one unit or pre-assembled, has to be decided on a time-to-time basis depending on the transportation method and efficacy.

Figure 3.9.: The HEMOS system packed for transport to InnovaNor.

Chapter 4.

Experiments

4.1. OCP-setup at the Corrosion Lab at NTNU

OCP test setup at the corrosion lab was initiated in the middle of February 2023. The samples used were a combination of new 316L samples, and samples made from different pipe sections cut from the discarded AISI 316L pipes at Innovanor, together with a SDSS sample as a control expected not to corrode. All the samples were cut with a band saw or hack saw, and carefully filed and sanded in order to not alter the alloy properties by heating it. The sample combination for all three OCP test sets is presented in Table 4.1.

Table 4.1.: Types of samples used in the OCP-test setups.

Sample type	Amount	Note
304L	3	Free Surface samples (only at Senja)
316L	2	Crevice samples
316L	3	Good weld samples
316L	2	Bad weld samples
316L	1	Pitted weld sample
316L	3	Mid Section from piping
SDSS	1	Control sample

The good weld samples were cut from a piping section where both the inside and outside of the weld had sufficient gas coverage, and no weld discolouration was present, as seen in Figure 4.1.

The bad weld samples were cut from a piping section where the outside of the weld appeared to have had sufficient gas coverage, while the inside of the pipe had sputtering, and bad oxidation and discolouration in the HAZ, Figure 4.2.
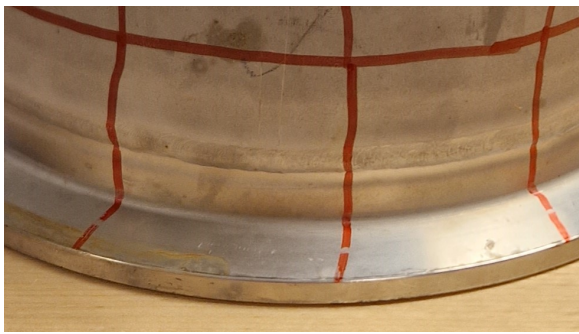
(a) Outside of pipe

(b) Inside of pipe

Figure 4.1.: Pipe flange cut into the good weld samples.
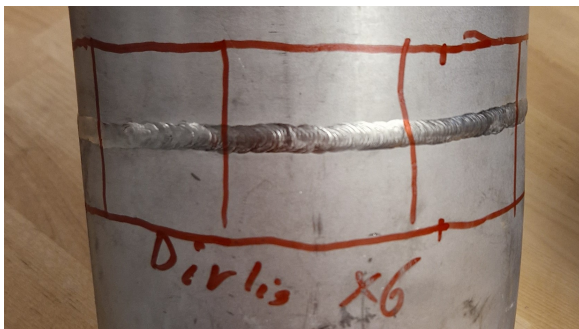
(a) Outside of pipe

(b) Inside of pipe

Figure 4.2.: Pipe weld cut into the bad weld samples. The weld appears good from the outside, but has bad discolouration and oxide precipitates on the inside.

(a) Outside of pipe

(b) Inside of pipe

Figure 4.3.: Pipe section from which the pitted weld samples were cut. the weld zone is badly discoloured, with pitting attacks on the inside.

The pitted weld samples were cut from a piping section where there were severe pitting attacks in the weld zone, seen in Figure 4.3b, and holes through the pipe. The samples were made from sections of this weld without any visible pits or holes.

The midsection samples were cut from the same piping as the good weld, in an effort to reduce the effect of poor weld quality on the bulk metal.

For the setup in the Corrosion Lab, seen in Figure 4.4, the samples were suspended

from platinum wires over the test chamber, and connected to the integrated data logger at the lab, which measures the OCP between the Ag/AgCl reference electrode and the samples. The chamber was filled with seawater brought from Sea Lab in Trondheim, and filled to an extent where all samples are covered. An air hose connected to an aquarium pump was immersed to provide circulation in the chamber. The water was topped up frequently due to evaporation losses. The rest of the water was stored at room temperature in the lab in translucent plastic containers, where the room was lit with artificial lighting during day time.

During the experiment, a crack was discovered in the test chamber, and the setup needed to be moved to another chamber to avoid leaks. This, together with a power outage, might have affected the data recorded.
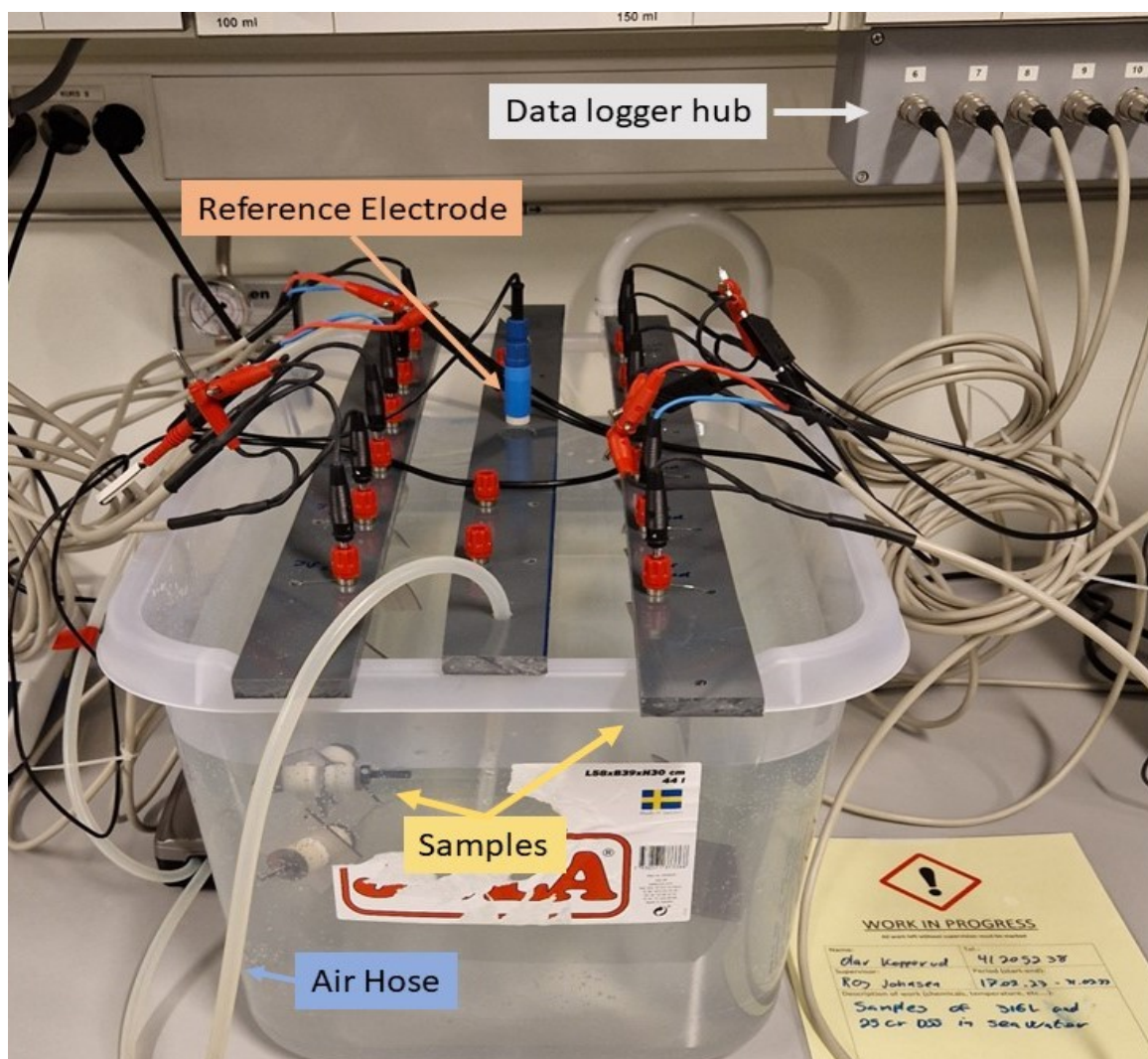
Figure 4.4.: OCP setup at the Corrosion Lab. The samples are immersed, and connected to the data logger through the data logger hub.

4.2. OCP-setup at InnovaMar - Frøya

The HEMOS setup at Frøya, seen in Figure 4.5, was mounted in late February of 2023, with all equipment transported to the facility by car. The HEMOS was mounted in the production area, under the RSW cooler, and supplied with water directly from this. The samples were suspended in the water using platinum wire and connected to signal cables prepared to connect to the data logger. The setup was prepared in the facility's workshop before being carried out to the production area and connected to water and power. Before departure to Frøya, all samples were cleaned with soap, rinsed with water, and cleaned with ethanol, to remove all dirt and grease. The samples were packed in separate plastic bags and only handled wearing gloves. The water inlet was connected to the RSW, and the flow rate was controlled with a ball valve. This was set to a stable flow of around 2 litres per minute. The cables connected to each sample were connected to their respective port on the electronics cabinet, and the OCP was measured with a multimeter to verify the potential and data logger readings. Cables for Ethernet and power were drawn from the service floor above and connected to the electronics cabinet. Subsequently, the PC and power supply was mounted on the service floor and connected to mains power. The PC was brought online with a 4G USB modem, and an initial synchronization of data was performed using the method described in the appendix subsection A.1.9.

After the first few weeks of running the test, it was apparent that the measured values probably were too high. A few suggestions were made, and after around 10 weeks, it was discovered that the protective cap on the reference electrode was still mounted. This was removed by service personnel in the facility, and the test continued.
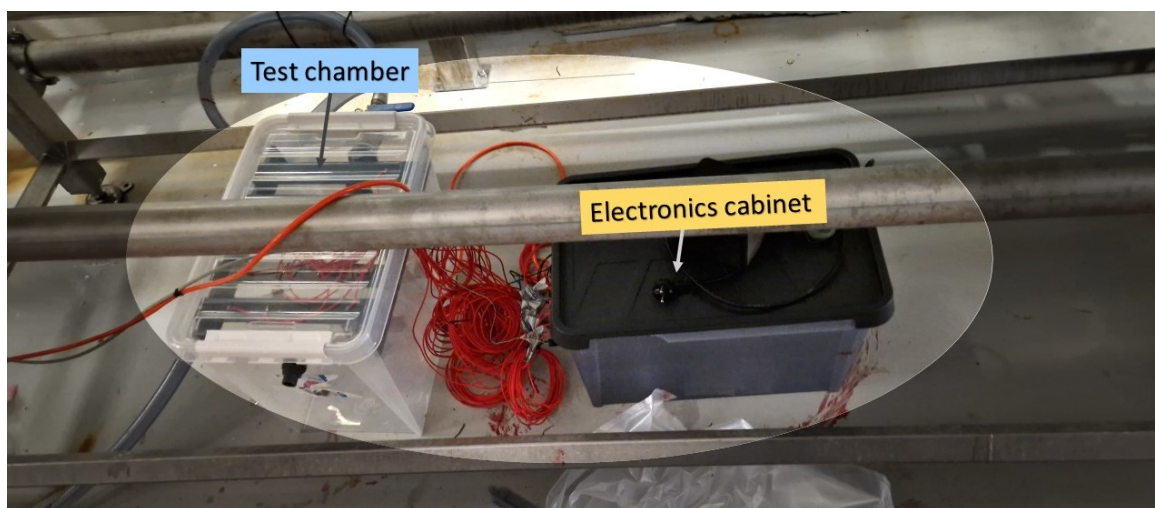
Figure 4.5.: HEMOS setup at InnovaMar - Frøya. The system is mounted in the production area and connected to the RSW cooler.

4.3. OCP-setup at InnovaNor - Senja

The HEMOS at Senja, seen in Figure 4.6, was mounted at the beginning of March 2023 after implementing a few design modifications based on the experiences from Frøya. In addition to making a functioning test setup, this setup had to be easily transportable and have some redundancy in case something was to break during transportation. The HEMOS was shipped with Nor-Lines from Trondheim to Finnsnes, while personnel transport was with a plane to Tromsø and a ferry to Finnsnes. The last part of the trip went by car to the facility, and the mounting of the test setup began. The redundancy turned out to be important, as the electronics cabinet was cracked during shipping and had to be remade. Luckily, an extra case was shipped, and a new cabinet was made within an hour.
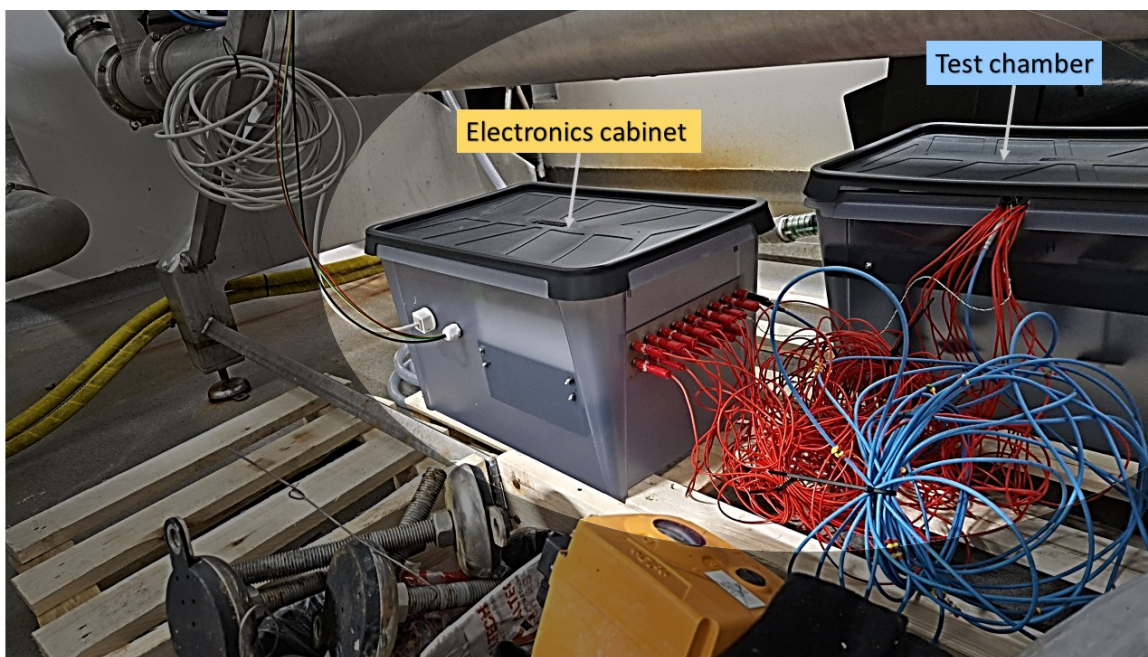
Figure 4.6.: HEMOS setup at InnovaNor - Senja. The system is mounted in the room with the RSW cooler.

As with Frøya, the samples were cleaned with soap and ethanol before departure and packed in plastic bags. These samples were threaded with M3 threads and mounted using A4 grade (AISI 316) threaded rods. These rods were cut from longer pieces of threaded rod and covered in heat shrink tubing to protect them from direct water contact. When mounting, the test specimen was threaded onto the rod, and the exposed tip was covered with heat shrink and silicone, as seen in Figure 4.7. This was done to prevent a potential initiation of crevice corrosion and subsequent erroneous measurements.

A robust field electrode (Stelth Ag-AgCl Model SRE-004-SFB from Borin Manufacturing [59]) was used to provide reliable measurements for the whole period.

After mounting the samples, the HEMOS was placed by the RSW cooler, however, this

<center>(a)   (b)</center>

Figure 4.7.: Specimen mounting on threaded rods. Heat shrink tubing and silicone were used to shield the threaded rod, and the connection between the sample and rod.

was located in a separate room, so it was easier to mount it. Water was connected with roughly the same flow rate as in Frøya, and power and Ethernet cables were drawn to a nearby room, which was dry, to place the PC and PSU. The PC was brought online using a wired connection to the local network. To achieve this, communication with the local IT department was crucial to maintain the data security and integrity of the network. This is important to mitigate the risk of creating an easy point of entry into the network from potentially malicious actors seeking to interrupt the production. As in Frøya, a synchronization test was performed to check if all systems functioned correctly before leaving.

Both the setup at Frøya and Senja experienced connectivity and synchronization issues during the experiment period, but with the help of on-site personell and TeamViewer, all problems were resolved without having to return to the facility. This shows the importance of the redundancies in the system to ensure the data was continuously logged for several months. The setup at Senja also experienced a temperature probe failure and should have had a redundant backup probe at the location. Due to a mistake, this was not in place, and some temperature data was lost. This failure occurred once again at the end of the testing period.

Facility service personnel reported that there was a production halt during the time from 14th to 23rd of April due to maintenance work, resulting in the equipment being shut down and the samples being exposed to stagnant water and higher temperature for a prolonged time.

4.4. Potentiostatic Measurements in Refrigerated Seawater

Potentiostatic tests were performed to determine the connection between the potential and CCT/CPT of stainless steel in refrigerated seawater. Containers containing freshly gathered seawater from Sea Lab in Trondheim were cooled in a cooling bath controlled by a simple temperature probe which cut power to the cooler at the target temperature. Crevice corrosion samples of AISI 304L and AISI 316L, were prepared using crevice formers in accordance with ASTM G48 Method F [60]. Samples of AISI 316L, cut from the same piping as the OCP test samples, were also tested to determine the weld's quality. Different setups and combinations of polarization and temperature were performed as shown in Table 4.2. These potentials and temperatures were chosen to match the expected potential and temperature combinations due to ennoblement from biofilm formation, and identified in the facilities by the OCP test setups.

Table 4.2.: Parameters for different test setups.

Sample Type	Temperature [°C]	Polarization [mV vs. Ag/AgCl]
304L Crevice	2	300
	2	400
	5	100
	5	300
	10	100
316L Crevice	2	300
	2	400
	5	100
	5	300
	10	100
	10	300
316L Weld	2	300
	5	300
	5	100
	7	0
	10	100
316L Free surface	7	500
	10	400

The samples were connected to the potentiostat as shown in Figure 4.8. By connecting the samples through shunt resistors (R1-R3), and measuring the voltage drop over them, an increase in the anodic current of the sample is identified.

The shunt resistors used were 1 Ohm resistors, making the potential drop measured in Volts identical to the current in Ampere. An increase in this current indicates the initiation of crevice or pitting corrosion, which is verified by observing the formation of corrosion product and discolouration of the water. When initiation was observed,
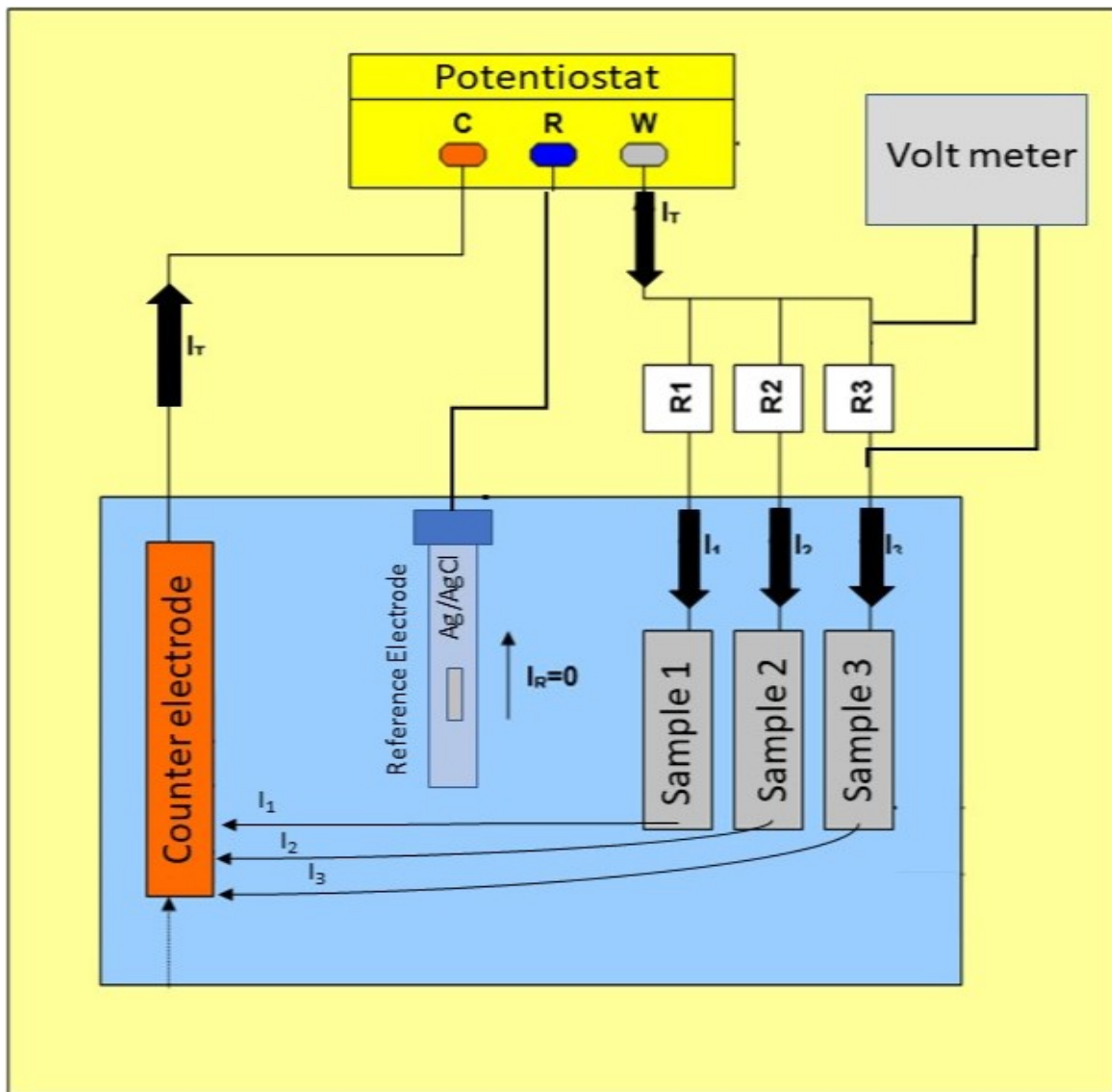
Figure 4.8.: Schematics of the Potentiostatic Test Setup.

the sample was left for a day to monitor the evolution before removing it and changing the water in the test beaker. The replenished water was left to cool down before the remaining samples were once again polarized. If the samples did not initiate within a week, the current setup was terminated. After some initial tests were performed, the subsequent test parameters and sample combinations were determined by the result of the preceding tests, in order to identify how the change in both temperature and polarization caused initiation of the samples.

4.5. SEM and EDS of Weld Samples

In order to document the corrosion properties and damage of the pitted weld samples, Scanning Electron Microscopy (SEM) images were taken to visualize this damage. SEM allows for high magnification imaging, allowing for detailed images of the corrosion attacks [61]. Questions were raised about the composition of the weld bead on the same weld samples, and if the weld filler material was actually an AISI 316L alloy or not. Energy Dispersive Spectroscopy (EDS) can determine the chemical composition of an alloy, and this was utilized in order to identify the composition of both the weld filler and the base metal.

These tests were performed on samples that were subject to severe corrosion damage during the potentiostatic tests. One of which is the sample seen in Figure 4.9.

Figure 4.9.: One of the samples scanned by SEM and analyzed by EDS. This is the sample exposed to the potentiostatic test at 400mV 2°C.

Chapter 5.

Results and Analysis

5.1. OCP-tests at the Corrosion lab, InnovaMar, and InnovaNor

The OCP measurements from Frøya, Senja, and the Corrosion lab are presented in this section. Due to noise in the data, the raw data is filtered through a Savitzky–Golay filter [62] in order to emphasize the overall trend and reduce the noise. This filter is utilized in figs. 5.1, 5.4 and 5.6, where the filtered data is the main graph, and the unfiltered data is the opaque plot.

5.1.1. Corrosion Lab at NTNU

The data from the setup at the corrosion lab at NTNU are seen in Figure 5.1.

The crevice samples seen in figs. 5.2a and 5.2b, clearly have initiated crevice corrosion, which is relatable to Figure 5.1d. The biofilm similar to the one seen in Figure 5.2e, was present on all samples. After cleaning the samples from this biofilm, it was clear that the 25Cr SDSS sample, Figure 5.2d, was more or less unaffected by the exposure. Both the AISI 316L midsection, and Good weld sample had some minor signs of pit initiation, seen as small brown spots in figs. 5.2c and 5.2f. The other samples from this setup can be seen in Figure B.1
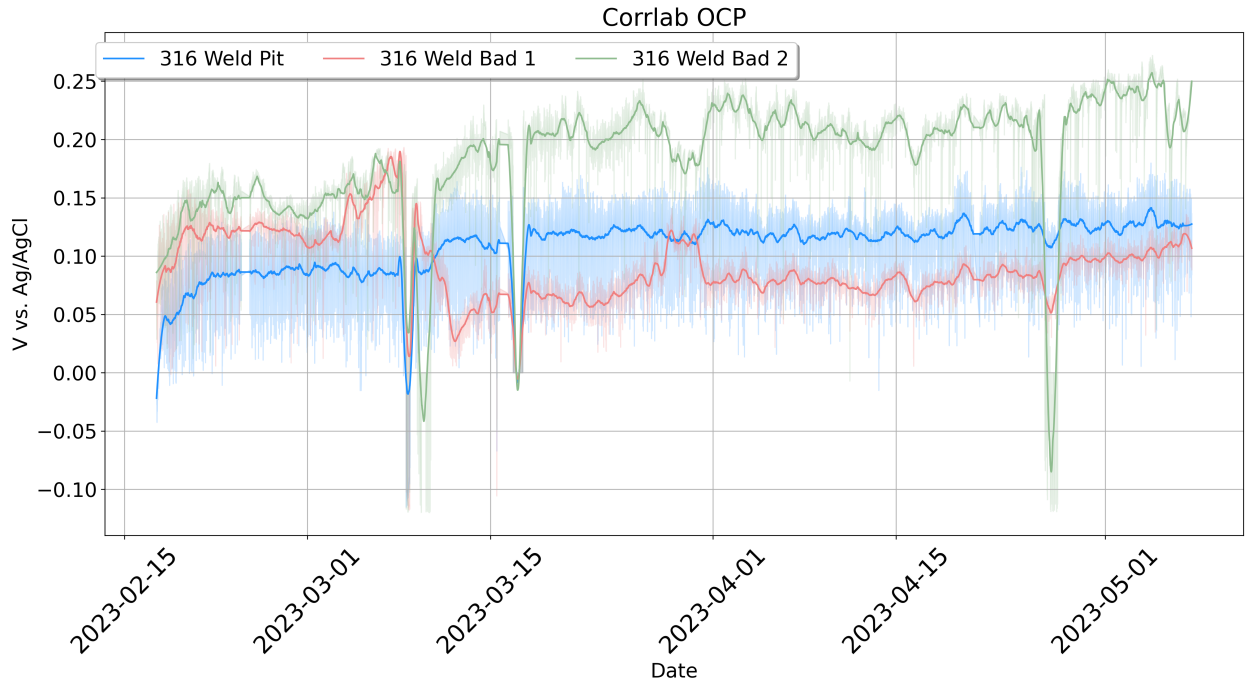
(a) OCP evolution of pitted and bad weld specimens.
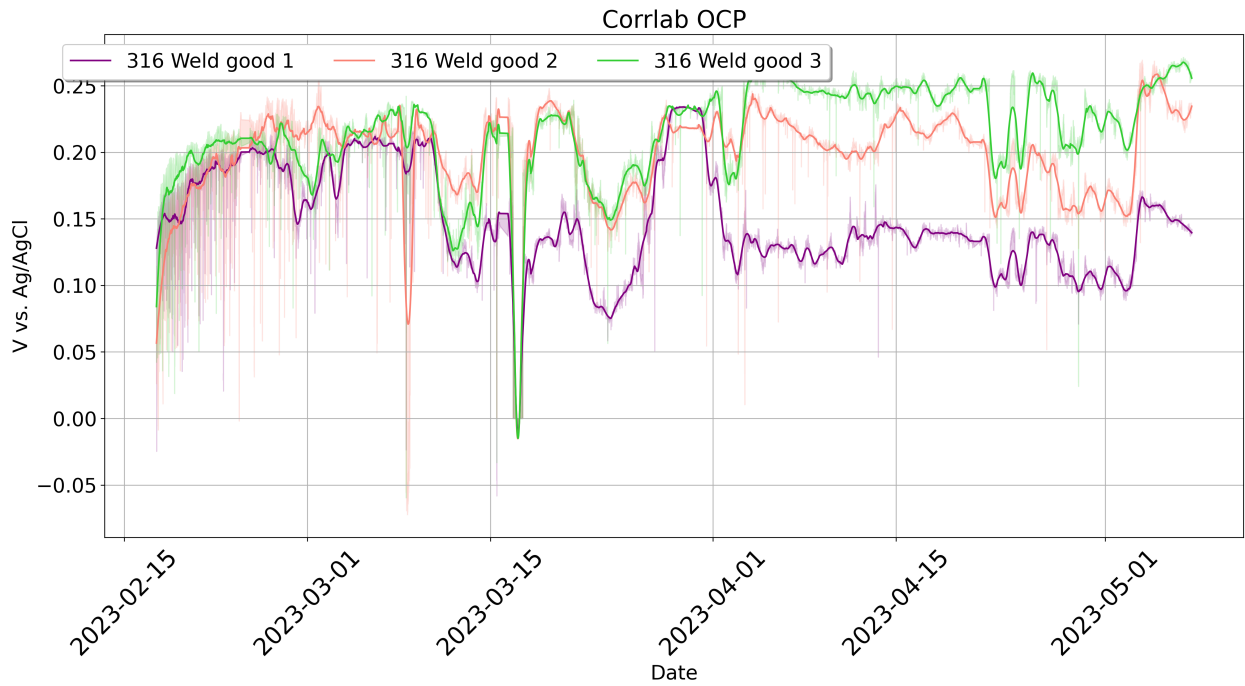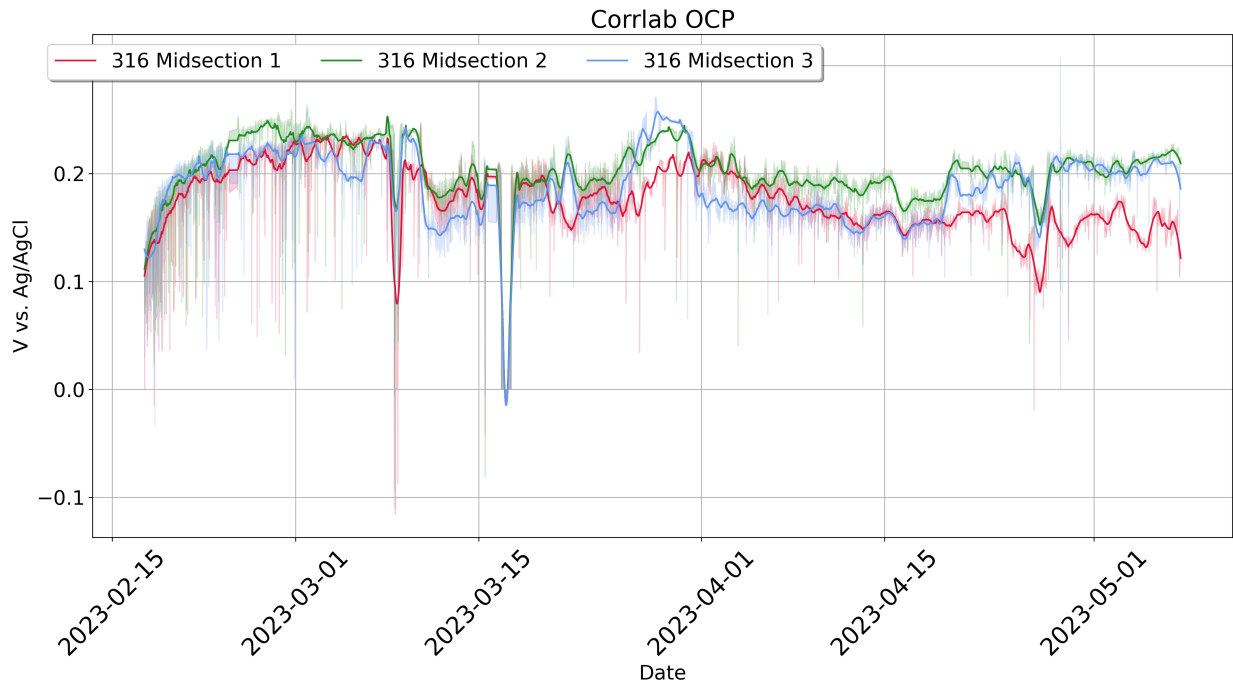
(b) OCP evolution of good weld specimens.

(c) OCP evolution of AISI 316L piping mid-section specimens.
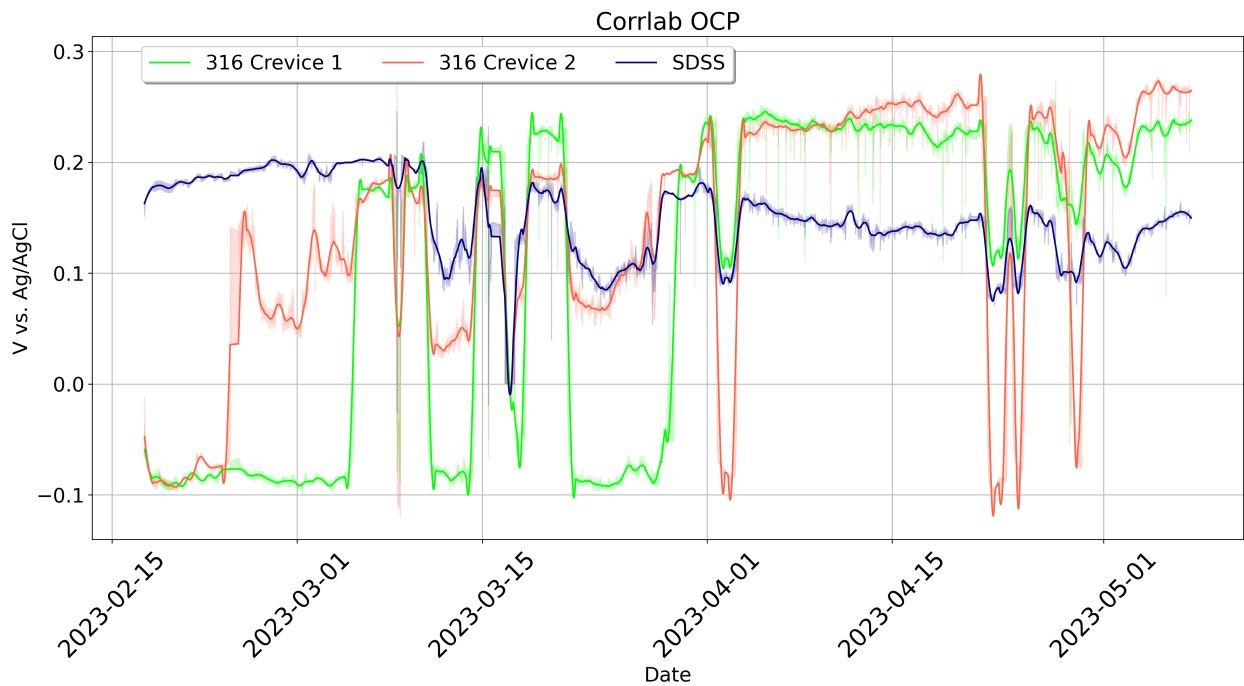
(d) OCP evolution of AISI 316L crevice and 25Cr SDSS specimens.

Figure 5.1.: OCP data from the test performed at the Corrosion lab - NTNU.
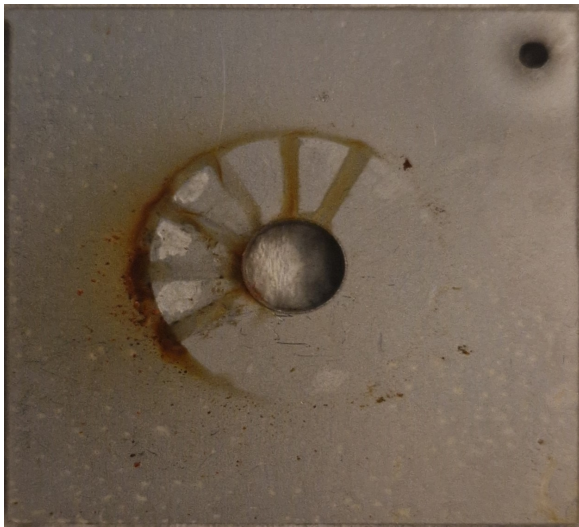
(a) 316 Crevice 1.

(b) 316 Crevice 2.
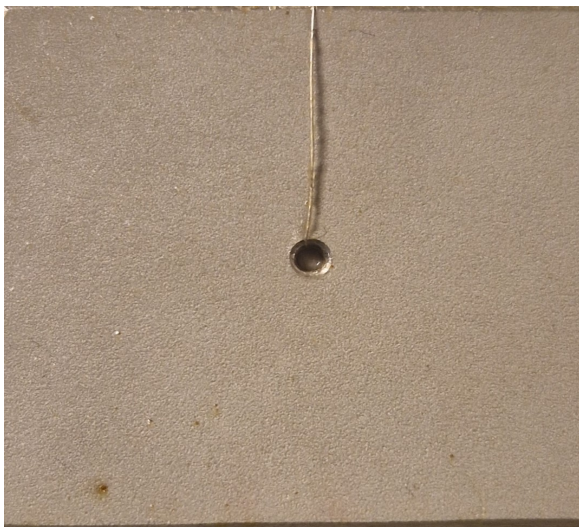
(c) AISI 316L Midsection.

(d) 25Cr SDSS.
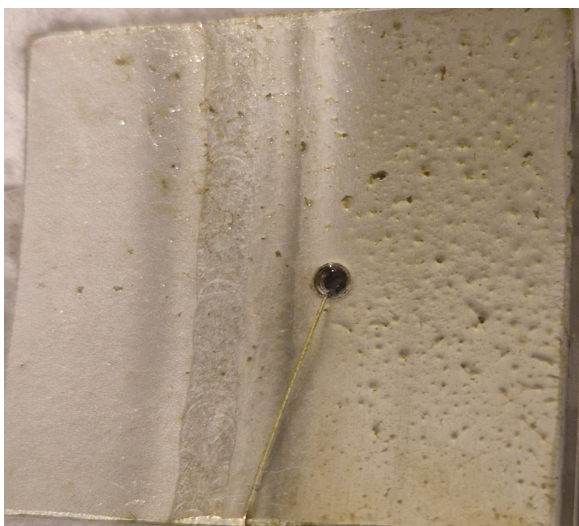
(e) Biofilm formation on good weld.

(f) Good Weld.

Figure 5.2.: Samples after exposure to the OCP setup at the Corrosion Lab.

5.1.2. InnovaMar - Frøya

The results from the facility on Frøya are as seen in Figure 5.4.

Due to a lack of AISI 304L Samples at the time the test setup was mounted, these were not included. One of the weld samples fell off during the experiment's mounting, and was subsequently removed from the data set.

Figure 5.4a and Figure 5.4c show that the samples that are improperly welded, together with the pipe midsection samples, experience larger deviations in the measured potential. These samples show signs of initiation of pitting and rapid repassivation, by the many significant drops in potential, which quickly returns back to the original state.

Figure 5.4b and Figure 5.4d show that the properly welded samples and the crevice samples provide more stable results and have less deviation in the measurements. These measurements also become less noisy when the temperature rises.

Figure 5.4b show that no significant initiation of corrosion appears to occur on the properly welded samples. In Figure 5.4d, it appears that both crevice samples initiated, and re-passivated after one and three weeks. After roughly two months, one crevice sample re-initiated.

The removal of the protective cap on the reference electrode is highlighted by a vertical red line in the graphs. The 25Cr SDSS sample and one of the crevice samples appeared to drop in potential immediately after this. This distinct change was not seen in the other samples, although the midsection samples experienced larger deviation in the OCP after this. After the initial drop in OCP, the 25Cr SDSS and the crevice sample increaed in OCP again and stabilized at around 400 mV vs. Ag/AgCl.

Observations made by personnel at the facility, together with pictures of the setup after three months of exposure, show visible biofilm formation in the test chamber, Figure 5.3. Visible corrosion was seen on the crevice samples, Figure 5.3a, but no other samples showed visible signs of corrosion product, seen in part in Figure 5.3b and Figure 5.3c.

(a) Corrosion on crevice samples.

(b) Free surface AISI 316L samples.

(c) Welded samples without visible corrosion.

Figure 5.3.: Samples at InnovaMar - Frøya, after three months of exposure in the HEMOS.
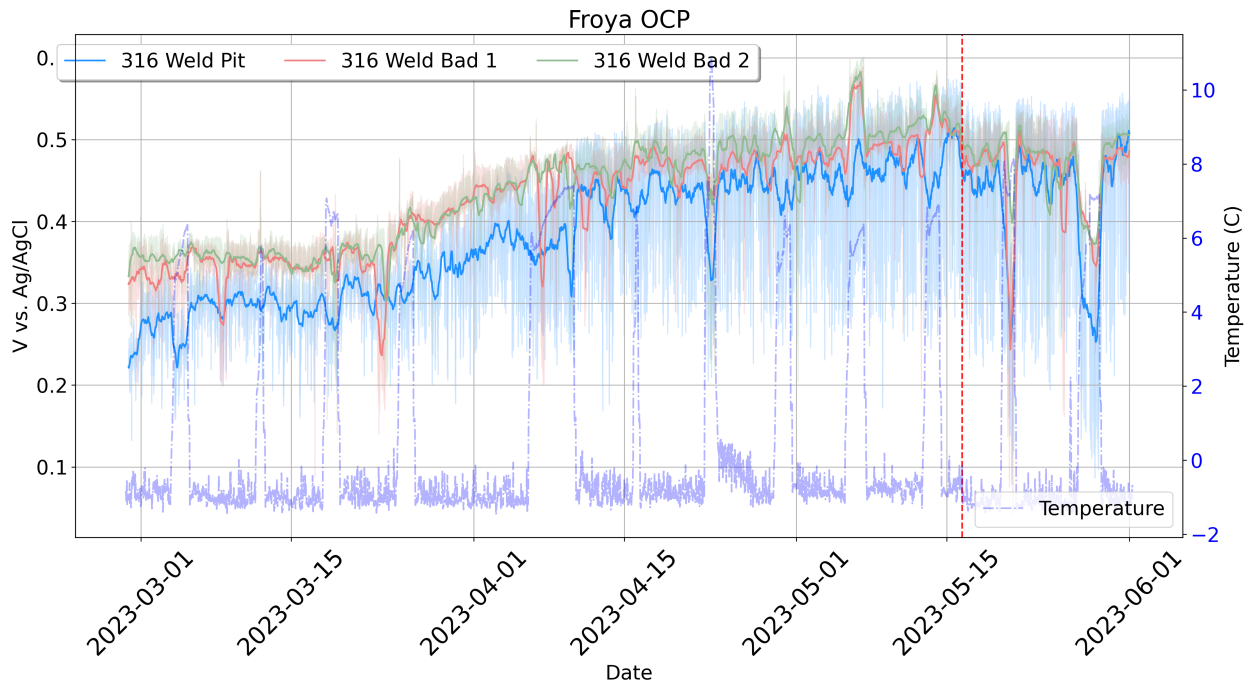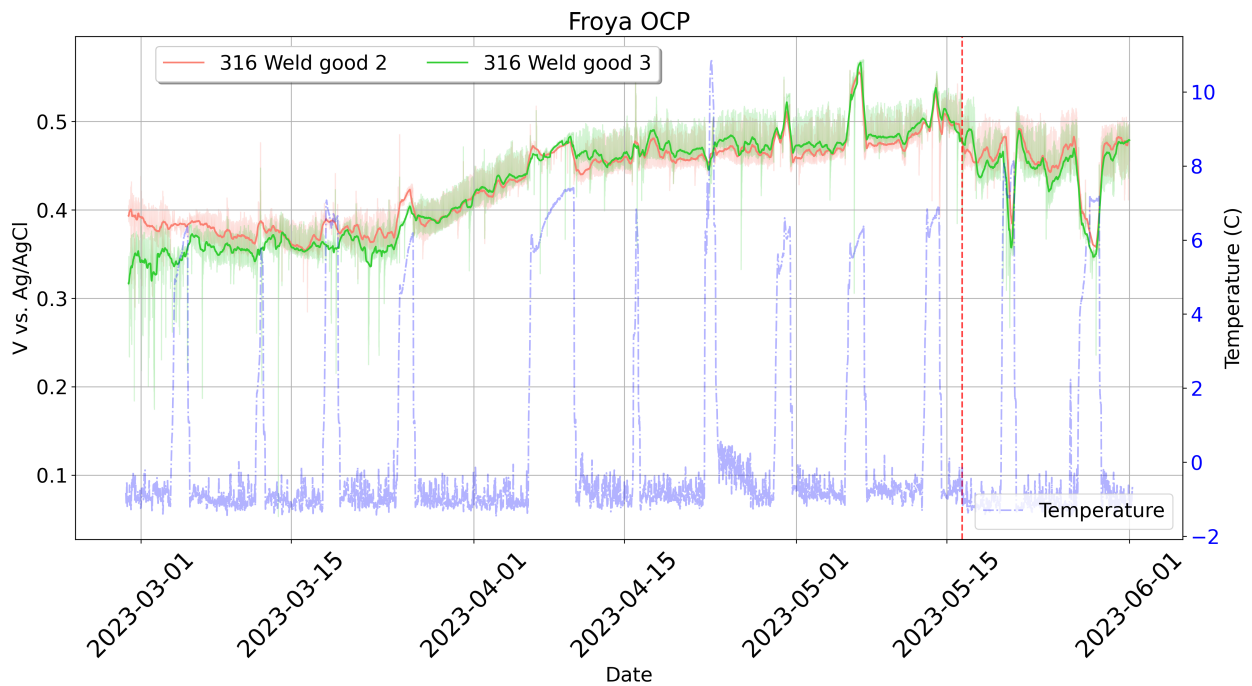
(a) OCP evolution of pitted and bad weld specimens.

**(b)** OCP evolution of good weld specimens.

(c) OCP evolution of AISI 316L piping mid-section specimens.
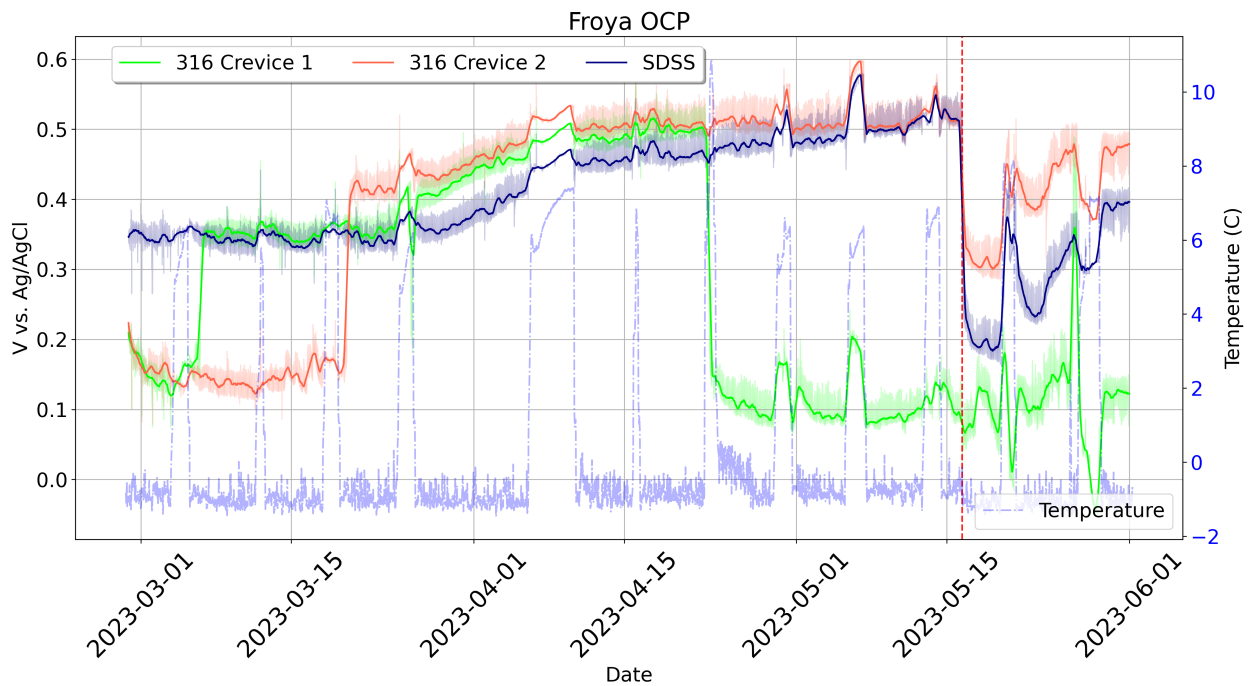
**(d)** OCP evolution of AISI 316L Crevice and 25Cr SDSS specimens.

Figure 5.4.: OCP data from the test performed at InnovaMar - Frøya.

5.1.3. InnovaNor - Senja

The results from Senja are seen in Figure 5.6 with images of the samples in Figure 5.5. The AISI 304L samples seen in Figure 5.6a show that there was an ennoblement period of around 4 weeks before the samples stabilized at around 350 mV vs Ag/AgCl. One of the samples seemed to initiate at the beginning of May. This is the same sample having visible corrosion between the threaded rod and specimens, in Figure 5.5b. At the end of the testing period, the other AISI 304L samples also show signs of initiation.

The improperly welded samples, seen in Figure 5.6b, experienced more fluctuations in the measured values compared to the other samples. Especially the pitted weld sample experienced large variations, before settling at a potential of around -50 mV vs. Ag/AgCl. A lot of corrosion product is seen in the weld zone of this sample, shown in Figure 5.5b.

The good weld samples seen in Figure 5.6c show a steady ennoblement of the samples for the first month. After this, a stable OCP of around 350 mV vs. Ag/AgCl was measured on all samples, before one sample started deviating slightly, decreasing the OCP during the next month. The samples seen in Figure 5.5c show clear signs of biofilm formation, but no significant corrosion product is seen.

Like in Frøya, the 316 midsection samples at Senja, seen in Figure 5.6d, have quite noisy data, but a more steady ennoblement is seen, although with some variation and potential minor initiations. From the end of April, these samples appear to have stabilized a bit more, at around 320 mv Vs Ag/AgCl.

Figure 5.6e show that both the crevice samples appear to have initiated, one initiated twice, both for prolonged times, while the other sample initiated very briefly around the 23rd of April, and quickly repassivated. In the image of these, Figure 5.5a, no visible corrosion is seen. However, only a small section of the crevice formers is seen in this image. The 25Cr SDSS sample experienced a steady ennoblement like the other samples, and stabilized at 360 mV vs. Ag/AgCl.

The maintenance period between the 14th and 23rd of April show very fluctuating data on all samples except for the 25Cr SDSS and AISI 316L crevice samples. The same is seen for the Easter holiday from the 7th to the 10th of April.

The temperature measurement for the first week is a bit off due to a wrong setting in the data logger. This was updated remotely and provided accurate temperature readings afterwards. Temperature data was lost between the 5th of April and 12th of May due to a faulty temperature probe. The replacement probe failed on the 28th of May, and was not replaced before the end of the testing period.

(a) Crevice samples and 25Cr SDSS.
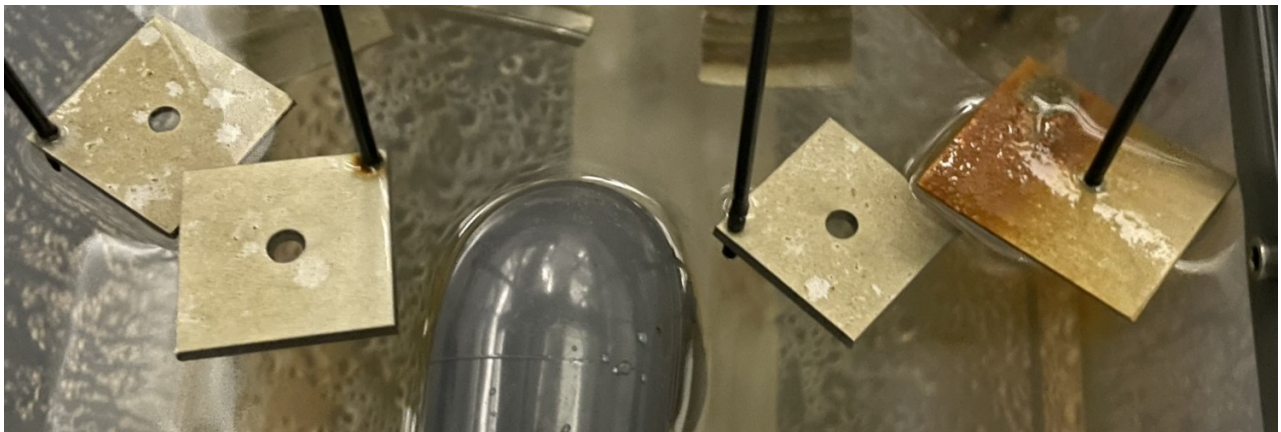
(b) AISI 304L samples and pitted weld.
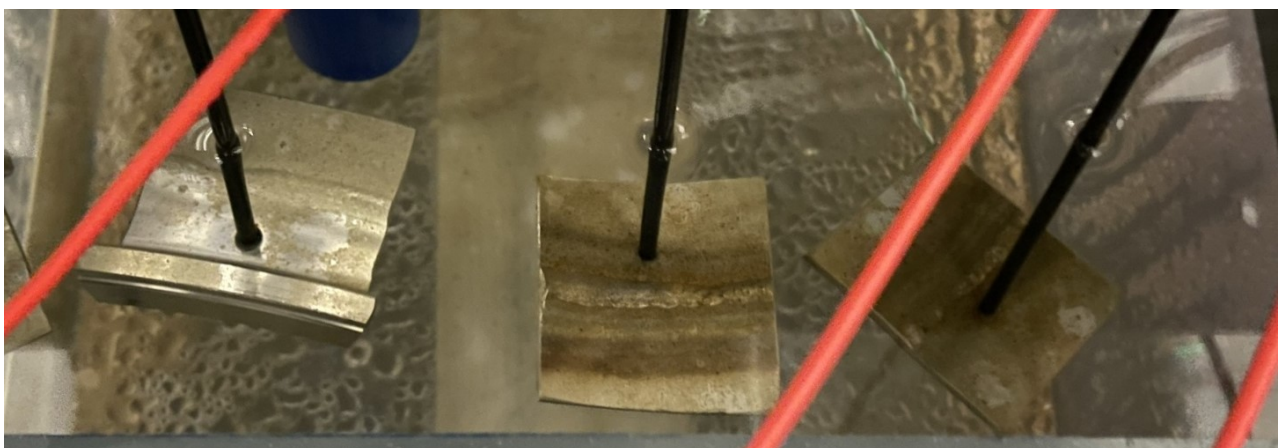
(c) Good and bad weld samples.

Figure 5.5.: Samples at InnovaNor - Senja after three months exposure in the HEMOS.
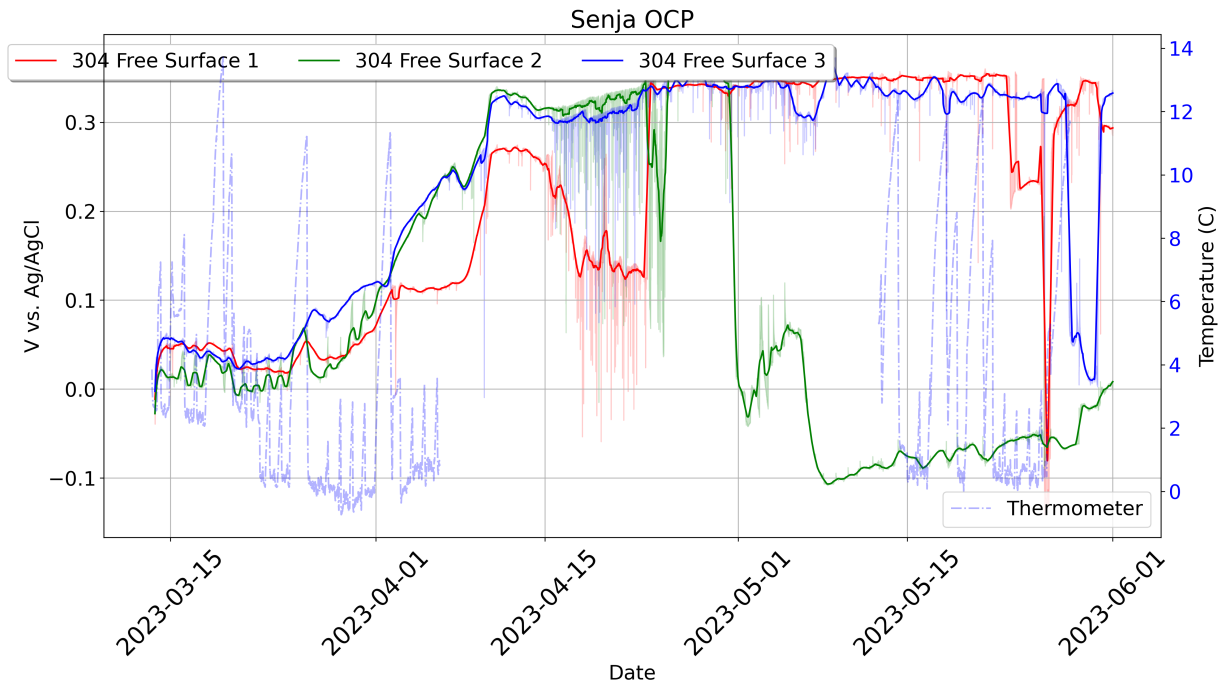
(a) OCP evolution of AISI 304L specimens.
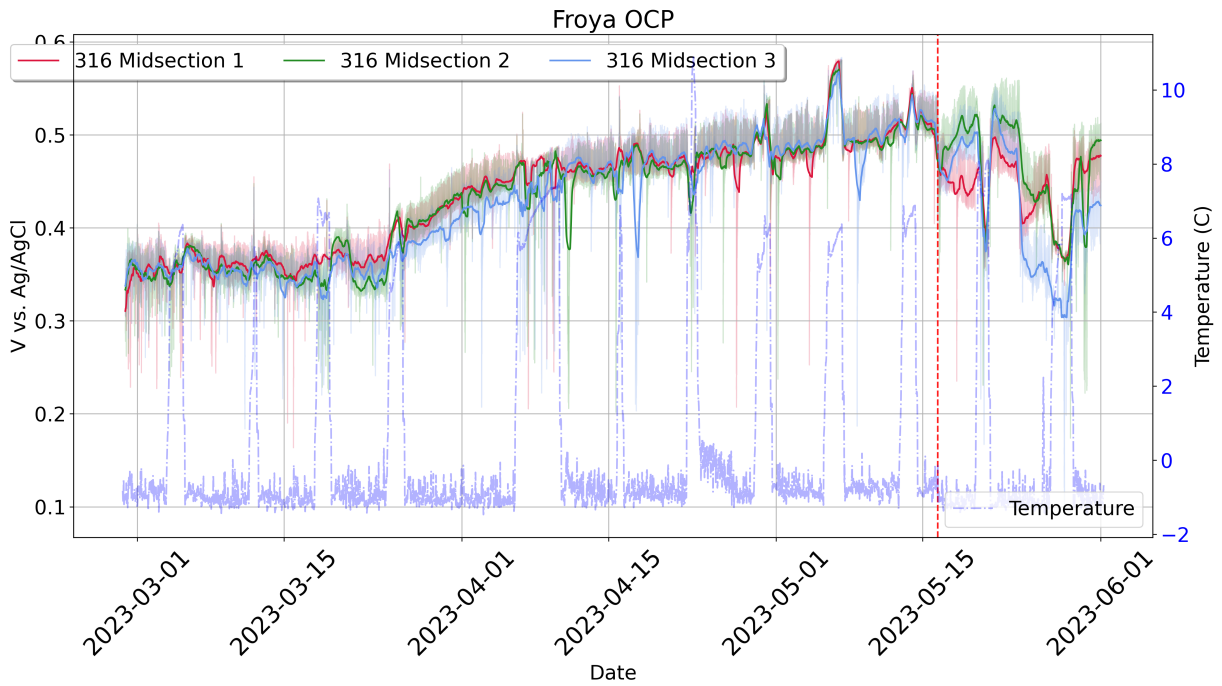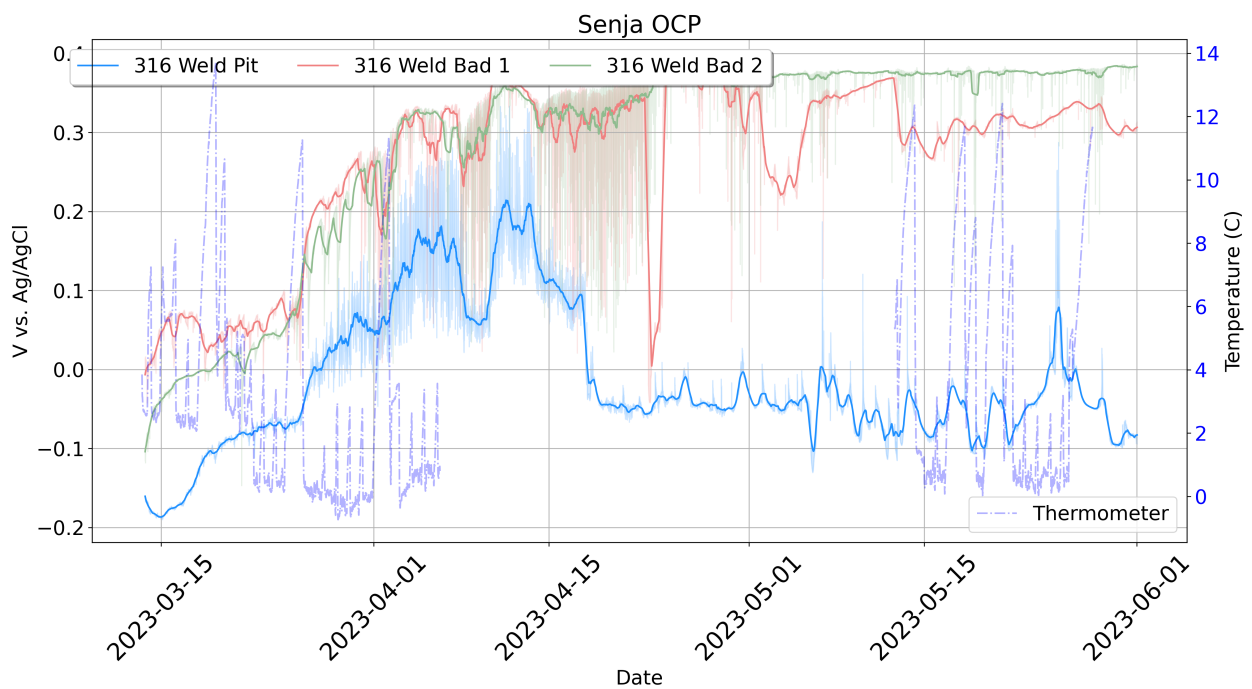

(b) OCP evolution of pitted and bad weld specimens.
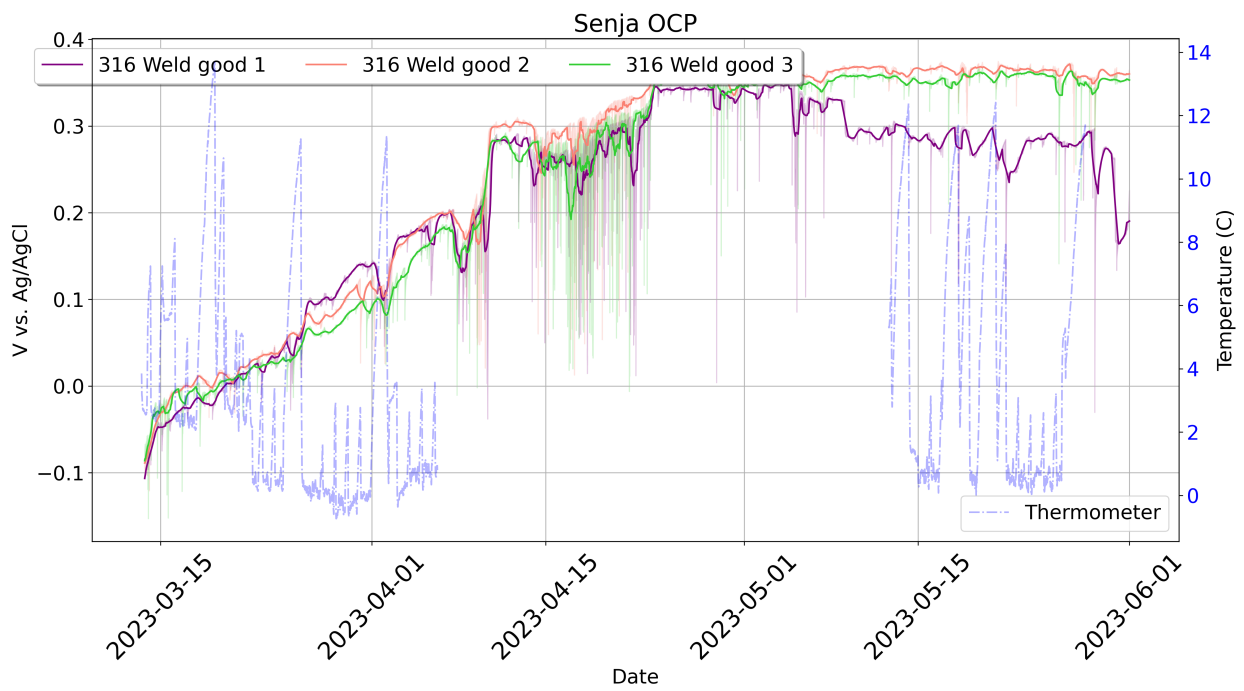
(c) OCP evolution of good weld specimens.
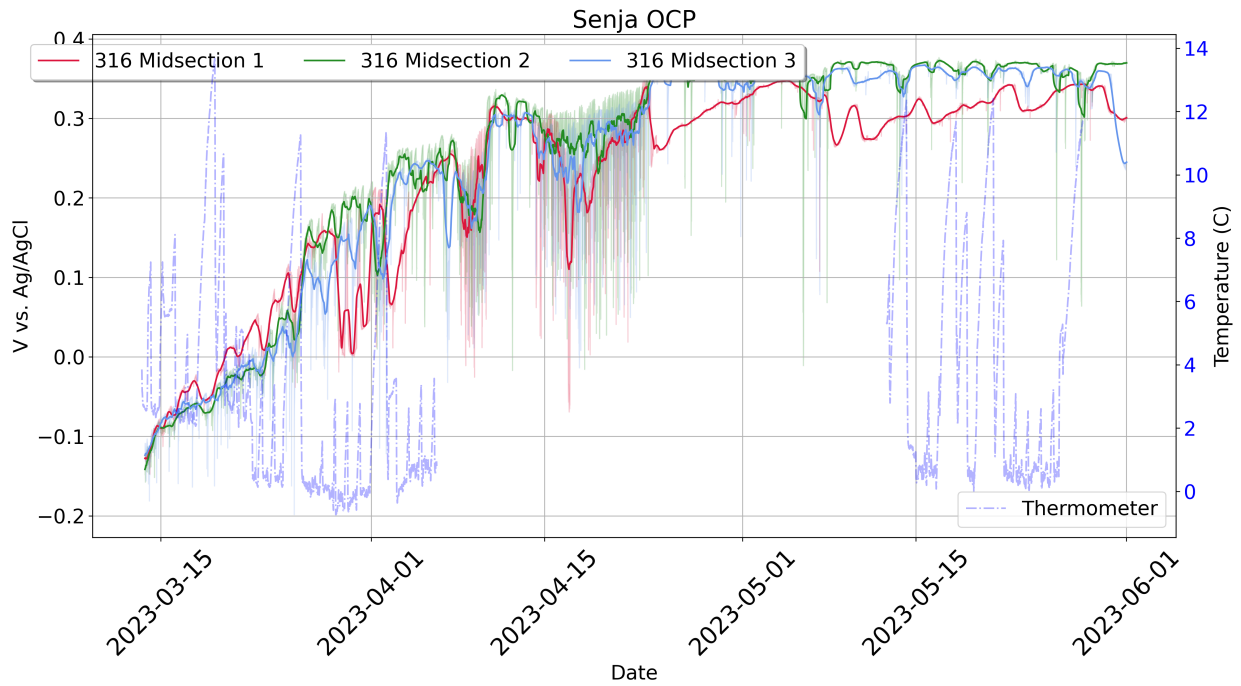
(d) OCP evolution of AISI 316L piping mid-section specimens.
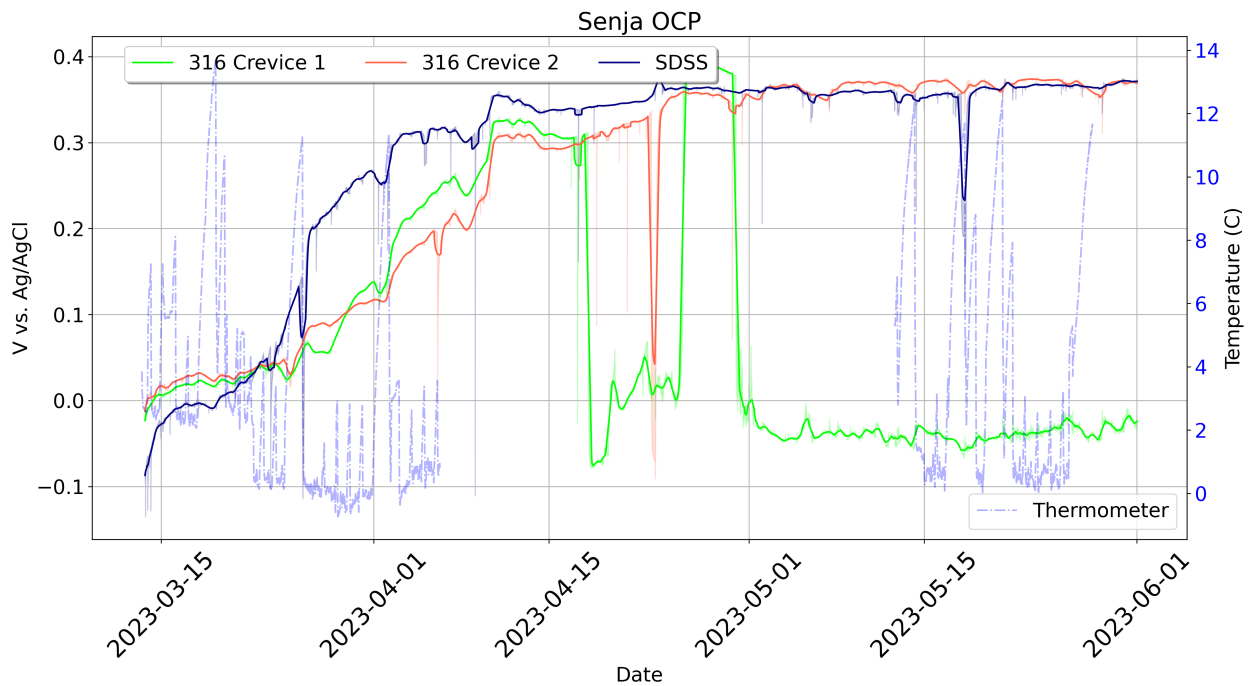
(e) OCP evolution of AISI 316L crevice and 25Cr SDSS specimens.

Figure 5.6.: OCP data from the test performed at InnovaNor - Senja.

5.2. Potentiostatic Measurements in Refrigerated Seawater

The results from the different potentiostatic tests are presented in the following section. As seen in Figure 5.7, the initiation of the different samples was determined and monitored by the voltage drop over the shunt resistor.
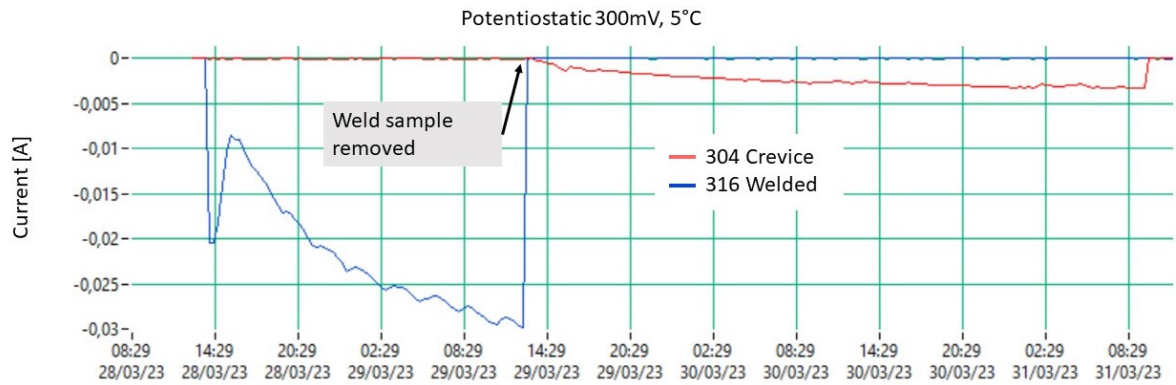
(a) 300 mV vs. Ag/AgCl at 5°C.
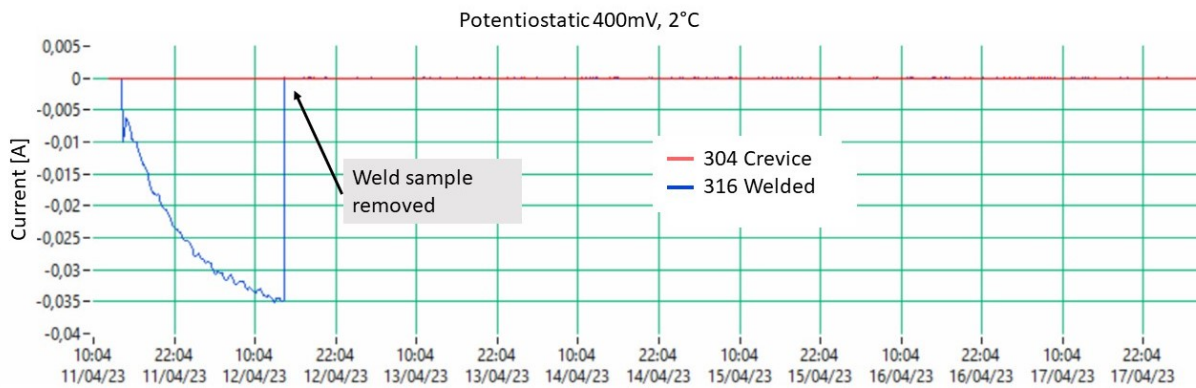
(b) 400 mV vs. Ag/AgCl at 2°C.

Figure 5.7.: Current measurement on welded AISI 316L and AISI 304L crevice samples in the potentiostatic test setup.

Most of the welded samples that initiated, initiated almost immediately, as seen in Figure 5.7. After taking the sample out after 24 hours, it appeared only to be minor surface pitting, seen in the green circle of Figure 5.8a. The area under the blue line in Figure 5.7, which is the total corrosion current, indicated more corrosion than what was initially discovered. After further investigation, the weld zone appeared to have a few grey spots, seen in the red circle in Figure 5.8a. These spots turned out to be very brittle and porous, and the metal in these spots was removable with fingernails. When this metal was removed, subsurface pitting corrosion attacks were revealed, seen in the red circles in Figure 5.8b. Similar behaviour was observed on all the welded samples that initiated.
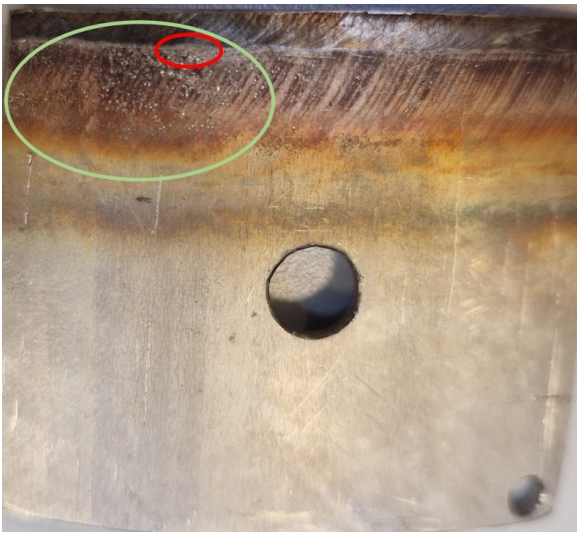
(a) Welded sample after pit initiation.
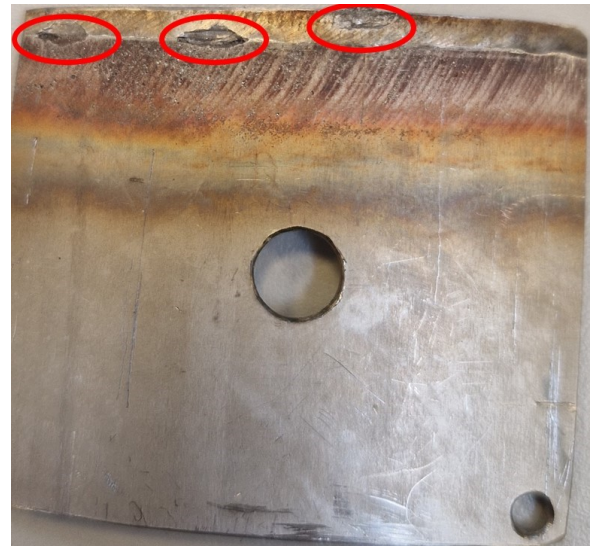
(b) Welded sample after the revelation of sub-surface pitting.

Figure 5.8.: Previously pitted weld sample after exposure to the potentiostatic test at 2°C, 300mV vs. Ag/AgCl. Severe pitting attacks are seen in the weld after exposure.

Figure 5.9 shows the outcome of the potentiostatic tests for all the samples tested. The red areas are overlayed in regions where the combined temperature and potential is expected to cause pitting or crevice corrosion damage on the respective samples, given the results from the potentiostatic tests. The yellow areas are areas of uncertainty, while the green areas are where the samples are likely to avoid corrosion damage.
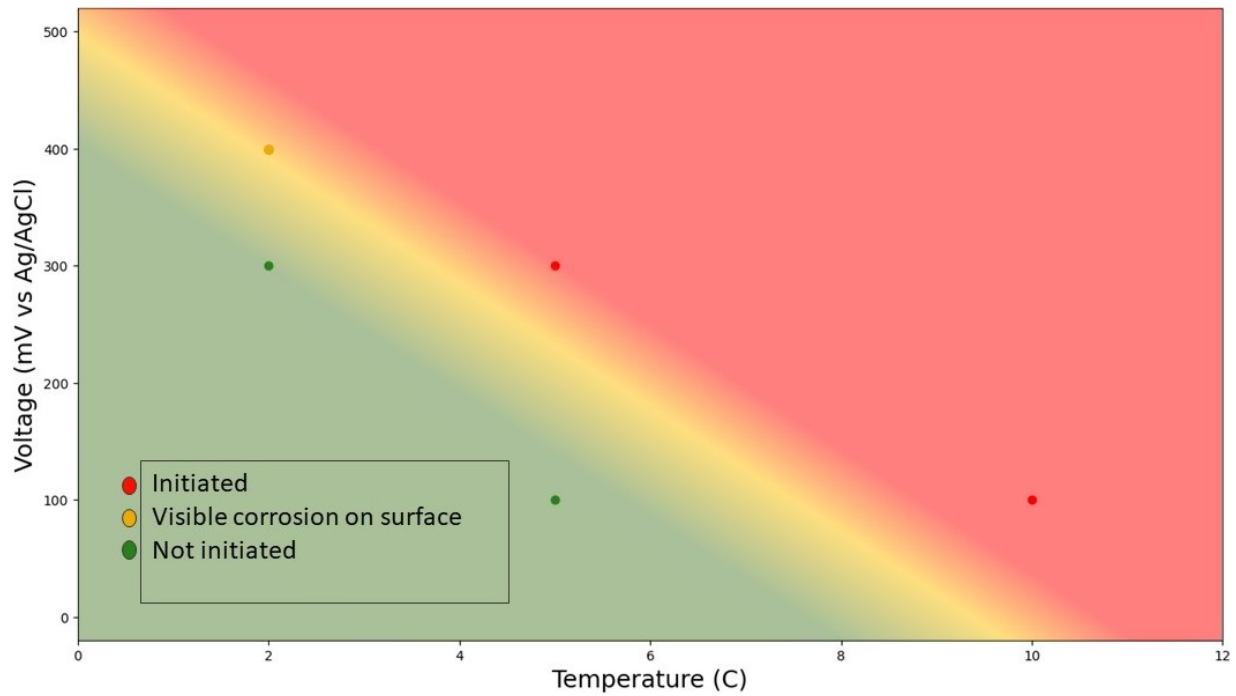
(a) Temperature-Potential dependency on crevice corrosion initiation of AISI 304L.
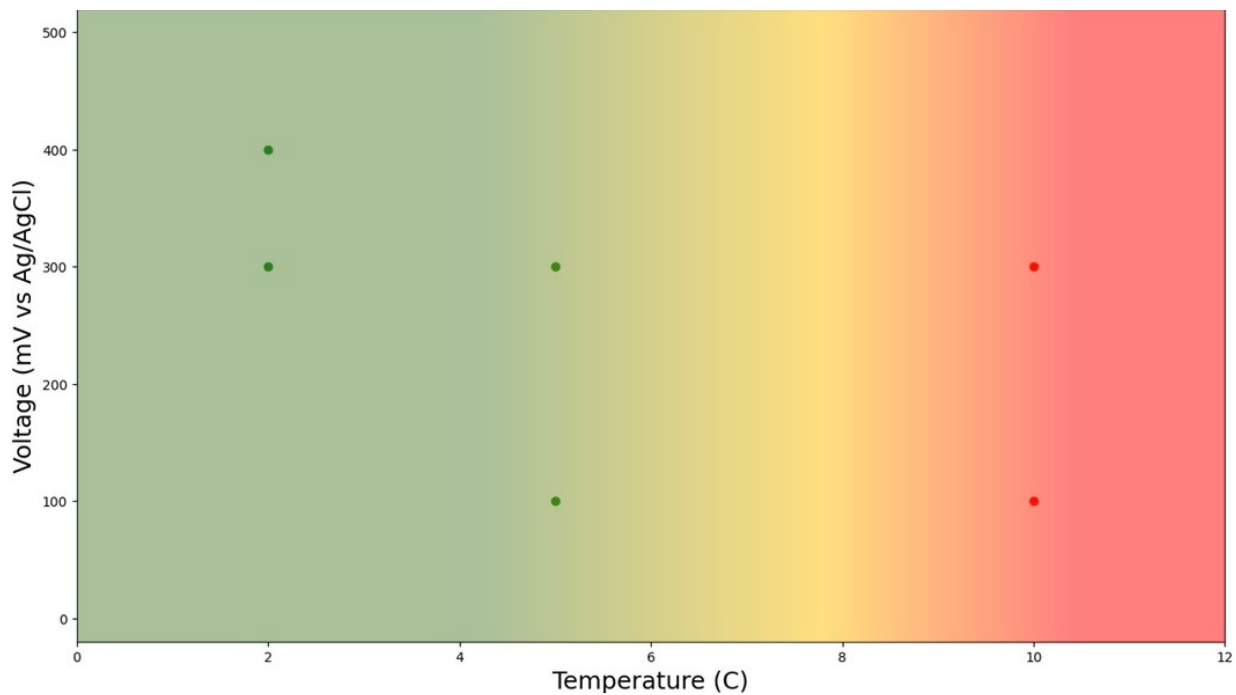
(b) Temperature-Potential dependency on crevice corrosion initiation of AISI 316L.
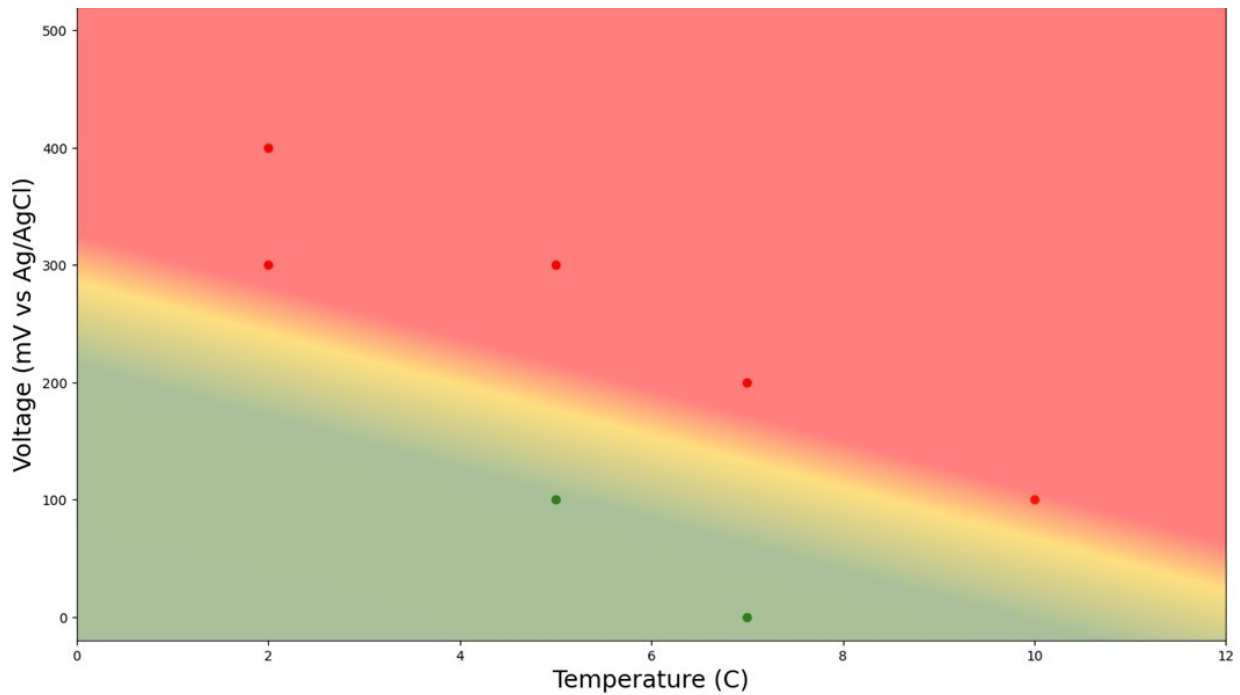
(c) Temperature-Potential dependency on initiation of pitting corrosion on previously pitted AISI 316L weld samples.
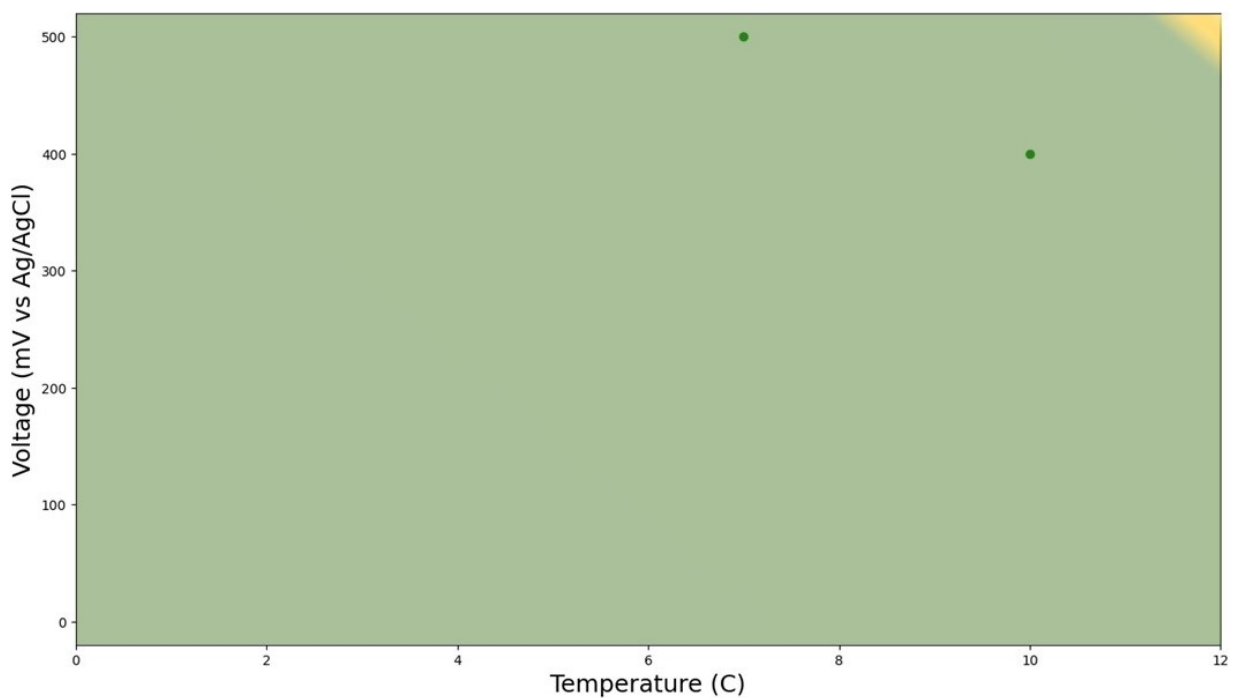
(d) Temperature-Potential dependency on pitting corrosion initiation of free surface AISI 316L.

Figure 5.9.: Temperature-Potential dependency on the initiation of pitting and crevice corrosion on selected samples, found from potentiostatic testing.

The crevice samples showed a significant decrease in crevice corrosion resistance at elevated temperatures. For the AISI 316L crevice samples, seen in Figure 5.10, this occurred between 5°C and 10°C, at both potentials tested. Similar trends were seen for the AISI 304L samples, Figure B.2, although these initiations both varied with temperature and potential. These samples also showed signs of uniform oxidation on the surface.
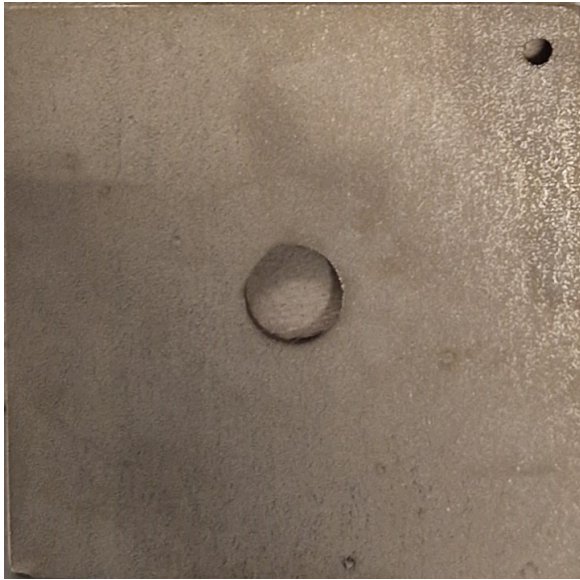
(a) 5°C, 100 mV.
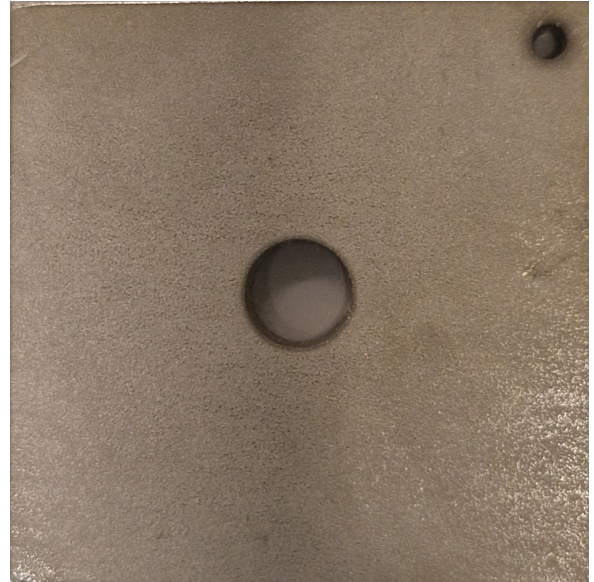
(b) 5°C, 400 mV.
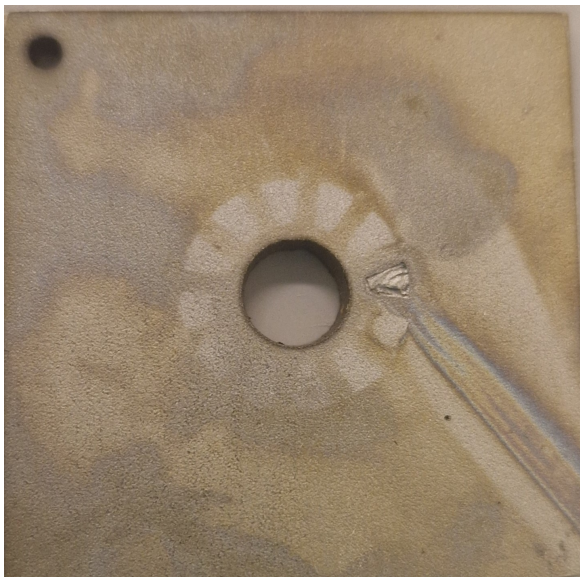
(c) 10°C, 100 mV.
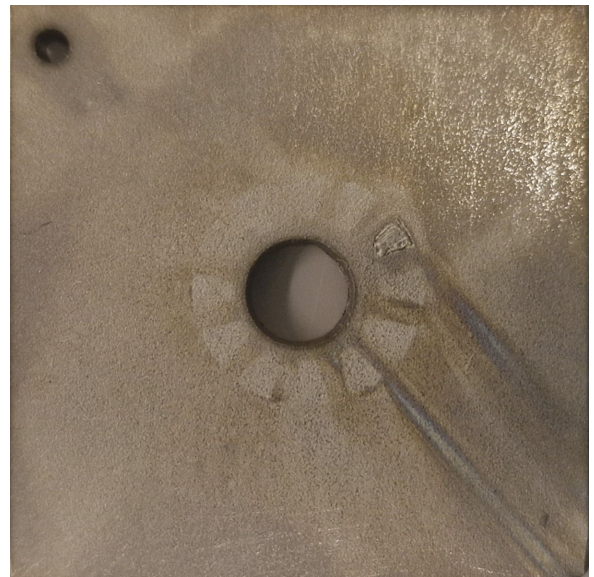
(d) 10°C, 400 mV.

Figure 5.10.: AISI 316L crevice samples after exposure to potentiostatic test. The two samples at 10°C show clear signs of crevice corrosion.

5.3. SEM and EDS

The images from the SEM, seen in Figure 5.11, show the severe corrosion damage on the pitted weld samples from the potentiostatic tests at 400mV at 2°C, and 300mV at 5°C. The weld filler is in the upper half of the images. The corrosion attack has mostly affected the weld filler material, although with some corrosion on the base metal as well. Figure 5.11d show signs of pit initiation on the base metal in the HAZ, close to the filler material itself. The porosity of the weld filler material after the corrosion attack in the potentiostatic test is visible in Figure 5.12

(a)

(b)

(c)

(d)
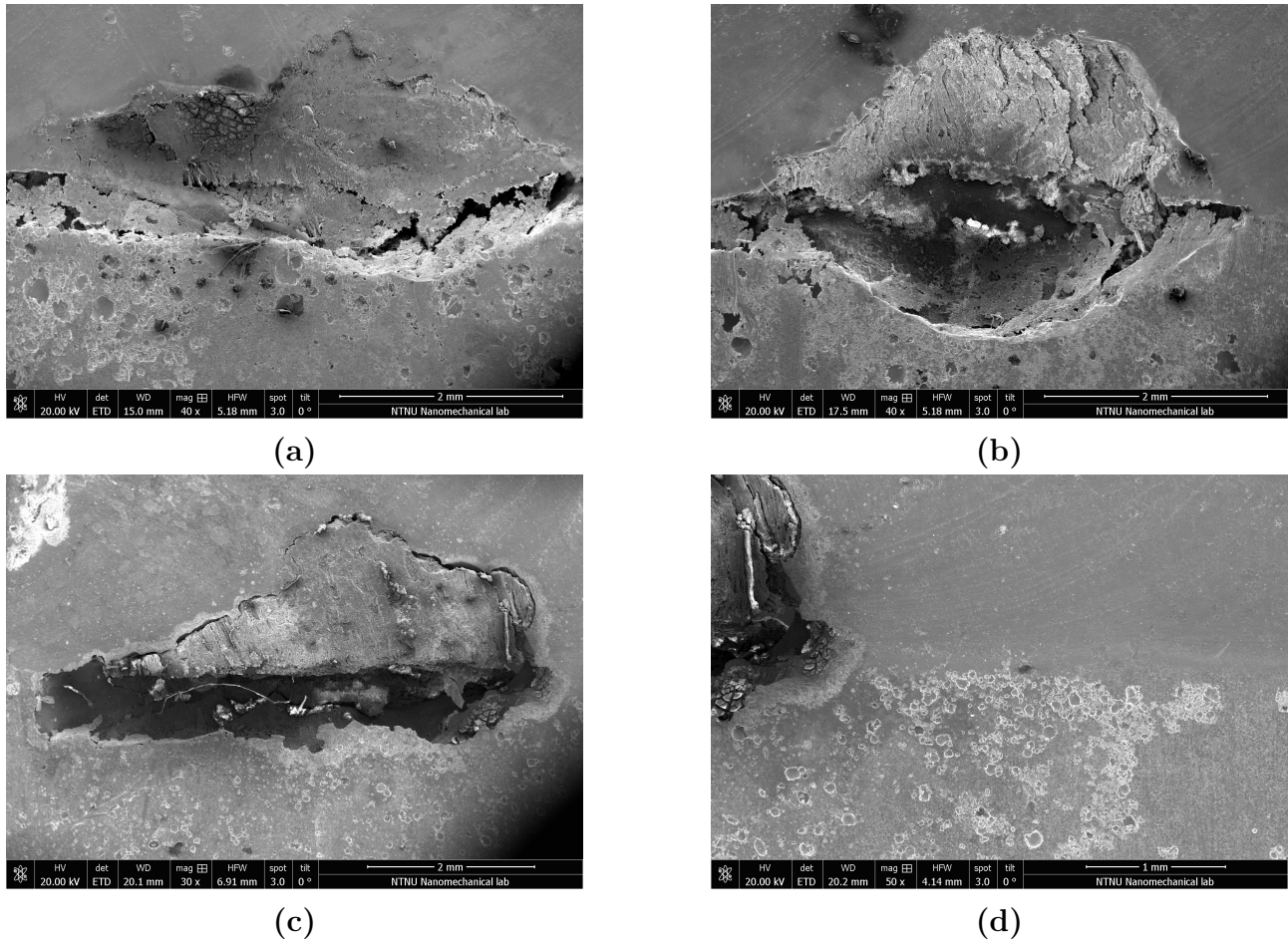
Figure 5.11.: SEM images of the pitted weld samples. The majority of the corrosion damage affects the weld filler material, but pitting attacks are mostly seen on the base material.

The chemical composition of the weld and the base material is presented in Table 5.1. These values have a degree of uncertainty ranging from 5% to 30%, making them suitable to verify the presence of certain elements, although it is difficult to pinpoint exact alloy compositions. Sulfur is only found present in the weld, while molybdenum was only seen in the base metal. The position at which these measurements are taken is seen in Figure 5.13. The measurements were taken within a millimetre of the transition between the base and filler material.

HV	det	WD	mag ⊞	HFW	spot	tilt	⟵ 500 µm ⟶
20.00 kV	ETD	16.3 mm	100 x	2.07 mm	3.0	0 °	NTNU Nanomechanical lab
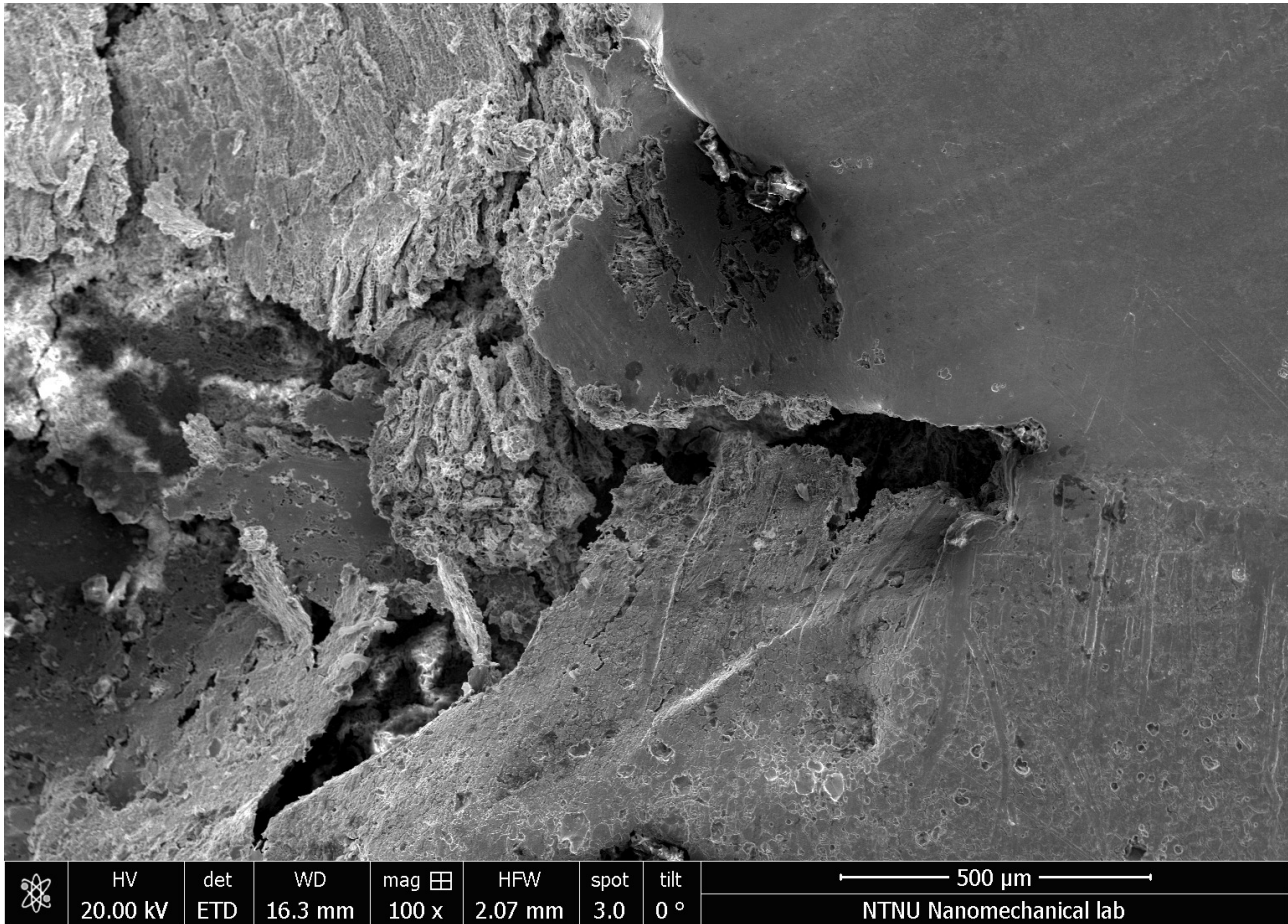
Figure 5.12.: Porosity of weld material after potentiostatic test

Table 5.1.: Composition of weld filler and bulk metal matrix by EDS on three different places on the sample

Elements	Weld [%wt]			Base metal [%wt]		
	Pos 1	Pos 2	Pos 3	Pos 1	Pos 2	Pos 3
Fe	33,1	53,0	37,4	50,5	34,7	48,5
Cr	33,4	29,9	25,1	30,8	32,2	24,5
Mo	-	-	-	-	2,1	0,47
Mn	-	-	1,6	-	-	-
Ni	15,5	10,2	19,7	11,2	6,6	16,2
O	11,1	1,8	8,4	3,0	10,0	5,3
Si	1,2	0,7	1,0	0,9	1,1	1,1
C	3,7	3,0	5,0	3,5	13,4	4,1
S	2,2	1,3	2,0	-	-	-
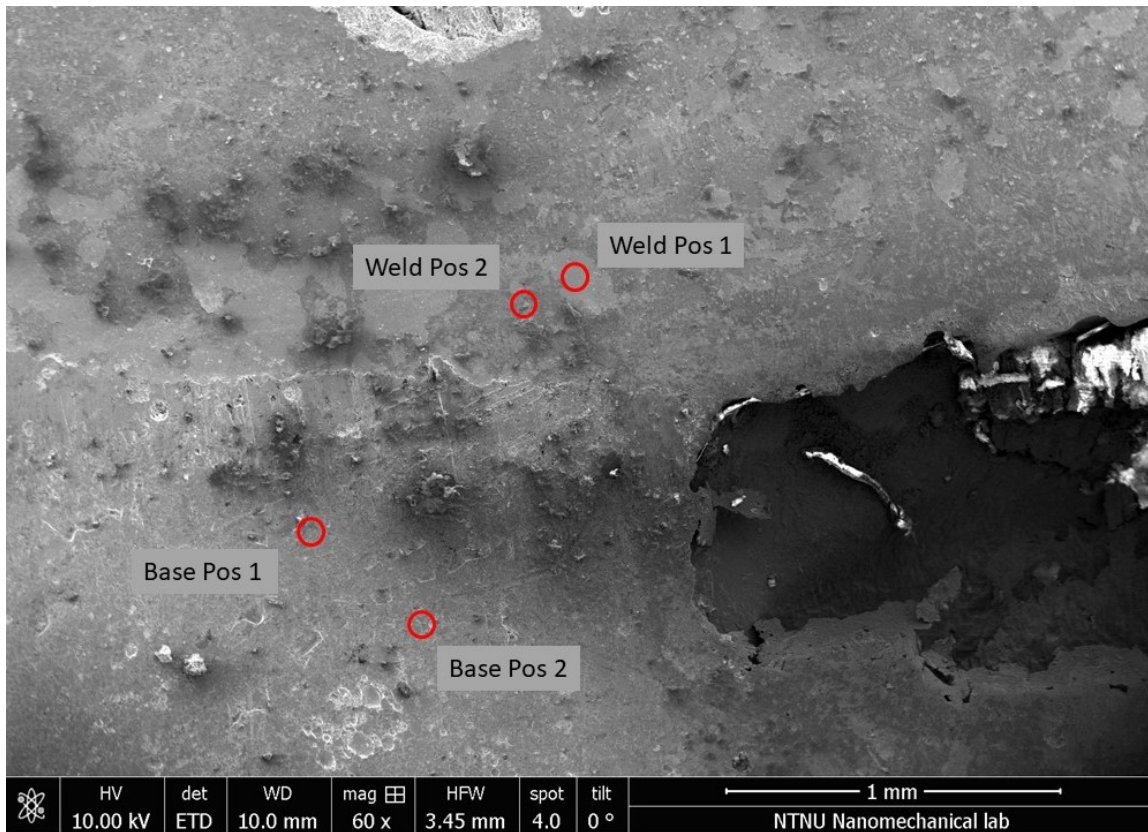
(a)
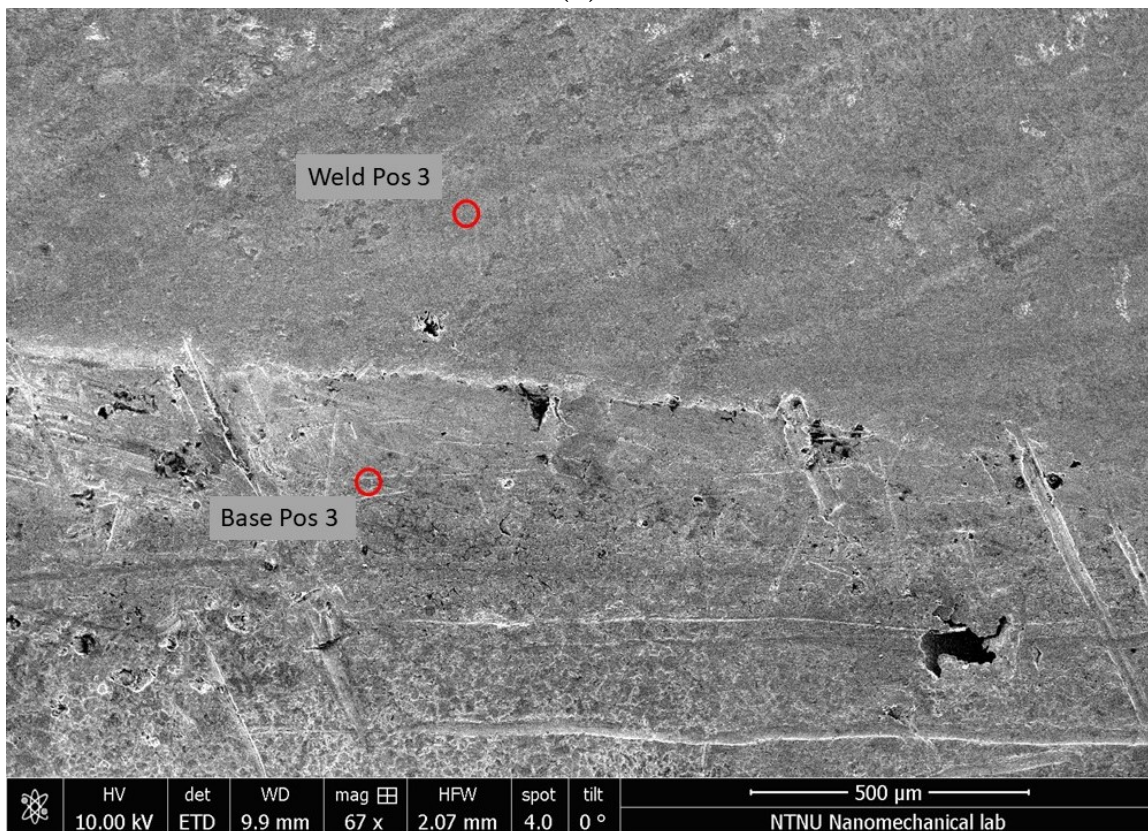
(b)

Figure 5.13.: Position of the different EDS measurements.

Chapter 6.

Discussion

6.1. HEMOS Design and Construction

The design and construction of the HEMOS was done within a limited time period at the beginning of the project, to be able to both construct the system, install it in the facilities and retrieve data over several months. Several limiting factors were encountered, and a lot of trial and error with different configurations was needed.

6.1.1. Mechanical Design

The first test setup was designed with two different types of boxes, a larger one as the test chamber, Figure 3.1, and a smaller one as the electronics cabinet. The electronics box was not water- nor splash-proof, and was replaced by an IP44 rated, polypropylene box with a 5 mm wall thickness to strengthen the construction.

Early in the design stage, it was uncertain whether the computer responsible for logging the data needed to be mounted within the electronics cabinet. The new boxes were ordered in a size capable of housing the computer, as well as being a test chamber. Utilizing the same kind of box for the test chamber and electronics cabinet made the setup easier to transport, as the boxes were stackable.

The dimensions of the hardware in the test chamber were mostly determined by what was at hand during the design phase, and the solutions for mounting inlet valves and outlet hoses were adapted on-site to fit the infrastructure present. The infrastructure in the facilities is designed to deliver several litres of water each second, making the reduction of flow down to around two litres per minute with a single ball valve hard to regulate. A valve system with higher precision would be beneficial to have better control of the flow. This can be performed by either a series of ball valves, or by using a globe valve.

In the test chamber, ensuring enough spacing between the samples was crucial during the construction of the sample holders. Given the dimensions of the box, a setup with 4 sample carrying beams and one central beam to hold the reference electrode and thermocouple proved to be the most efficient. This allowed for 16 samples to be mounted,

although only 15 were mounted due to the channel limitation of the data logger. The beam closest to the inlet had to be mounted closer to the centre of the box to avoid interfering with the pipe guiding the inlet water to the bottom of the chamber. After the necessary spacing on both the inlet and outlet sides was determined, the beams were equally spaced. If the samples were mounted at the same height in the chamber, some samples had the possibility to interfere. To avoid this, some sample holding rods had to be cut shorter. This could have been mitigated by making the mounting holes in the beams off-center, creating a larger distance between the samples, however this was thought of after construction was complete.

The mechanical design proved to work at both Frøya and Senja, although with some issues. One of the boxes broke during transport to Senja, necessitating the use of the redundant box shipped. During mounting, some minor cracking was observed in the test chamber at Senja, and one part of the edge of the electronic cabinet fractured at Frøya due to rough handling, proving the need for more sturdy boxes for future setups. The thermocouple at Frøya survived for three months, while the thermocouple at Senja broke twice during the testing period. The reason why is unknown, but it shows there is a need for a more reliable temperature sensor. This might be done by protecting the cable itself with a wire sock, or providing better sealing of the sensor tip itself. Adding additional sensors for redundancy might also be beneficial

These failures might also be related to service personnel interacting with the setup, and potentially causing damages to the probes. In addition to a protective sock, implementing a camera in the test chamber would reduce the need for interaction in order to take pictures of the setup. This addition would require a lot of prototyping and testing in order to make it reliable, but it would be an interesting addition to the setup.

The reinforcement plate for the inlet at Senja would probably only need fastening to the box at the top corners, limiting the need for plate fixation below the waterline of the test chamber. This would reduce the number of holes needed to be sealed with silicone.

All the fasteners used in the test chamber and electronics cabinet are A4 grade (AISI 316), the survivability of which was to be tested with the setup itself. This was the most corrosion-resistant fastener type that was available without long lead times when constructing the setup. This was an allowable compromise, as the setup was designed to be installed in the facilities for three months. In addition, potential leaks from the setup through corroded fasteners are non-critical, and the forces held by the fasteners are very small. Observations made after three months of exposure show that no visible corrosion damage has occurred on these fasteners, proving that this design choice was allowable in these circumstances.

6.1.2. Electronics Design

The limiting factor of the electrical design was the MS6d data logger. The proprietary system and data format requires the licensed accompanying software to convert the data into a format that is usable in further data processing. This software is only available for

Windows, limiting possible data processing solutions. The initial plan was to connect a Raspberry Pi 4 [63] to the data logger through a Serial connection, and upload data to a Cloud service. Although a serial connection could be established, extracting data from the datalogger proved to be impossible without the proper communications protocol. This made the Raspberry Pi solution unavailable, as the proprietary software would not work on the Linux operating system of the Raspberry Pi.

An Intel NUC mini-computer running Windows [64] was considered and is a viable option for a Windows-based computer for this setup. However, due to accessibility and cost, this was replaced by a desktop computer provided by the IT department at NTNU. This computer was bulkier, heavier, and more powerful than what was required, but it was utilized, being it was the only available option available without a substantial lead time.

The cooling requirement for this computer and the enclosed space of the electrical cabinet was incompatible, risking both the computer overheating, and throwing off the temperature measurements of the data logger. Both InnovaNor and InnovaMar had the option to mount the computer and PSU in a separate, dry area. This was a preferred option to avoid unnecessary exposure of sensitive electronics to the harsh environment in the production area. If this had been determined earlier in the process, sourcing a smaller and more waterproof electronics cabinet would have been possible. This could have fitted within the larger test chamber and eliminated the need for assembling the electronics cabinet on site.

Placing the computer in a separate location also made it more accessible for the personnel at the factory. At Frøya, this resulted in the power cable to the PC being accidentally disconnected once. This was discovered when the synchronization of data stopped, and service personnel was able to reconnect it to power. The automatic boot and initiation of the logging software proved important, as not having it implemented would require more detailed instructions for the personnel at the facilities should the setup fail. Some connectivity and synchronization issues were also discovered after installation, as there was limited time to test the setup in its operating conditions for a prolonged time before deployment. USB power disconnection after 4 hours, and wifi guest network disconnecting after a week was some of the problems experienced after deployment. In these cases, local personnel was invaluable in fixing the issues, as well as having a working Team Viewer setup to be able to remotely reconfigure the PC settings.

An Ethernet (CAT5E) cable was used for communication between the PC and data logger, as USB cables have a maximum length of 5 meters [65] due to signal deterioration. The PSU was also mounted in the dry location. This avoided having to route 230V cables to the test setup, and having a potential 230V ground fault if the waterproofing of the Electrical cabinet failed. 230V AC, and the switching of the power supply, could also potentially induce currents in the signal cables nearby, resulting in erroneous measurements [66]. This is avoided when routing 24V DC directly to the data logger. Due to the long distance this DC power needed to be routed, power loss was a concern. To mitigate this, a separate PSU was preferred, due to uncertainties in the reliability and power of the included power adapter of the data logger. The circuit breaker should, in

addition to the low amperage trigger value, have a Ground Fault Circuit Interrupter (GFCI) to monitor potential ground currents. This mostly to protect the personnel potentially handling the power supply when powered, and to mitigate the influence of ground faults on the facility's own electrical system.

To get the most accurate data readings possible, shielded cables should have been utilized the entire way from the sample to the datalogger, to reduce the risk of interference. This type of cable was not available at the moment of construction, and long lead times resulted in standard 16 AWG copper wire being used instead. In addition, the shielding of shielded cables would have to be grounded to Protective Earth (PE) in order to function correctly. This would further complicate the design of the Electronics cabinet and prolong the time to deployment.

Due to uncertainties regarding the possible placement of the electronics cabinet in relation to the test chamber, the signal cables were made 5 meters long. This proved to be excessive in both setups. The flexibility in length was good to have during mounting. However, the excessive cable length was coiled up and might enhance the interference from nearby AC sources. If unshielded cables are to be utilized in similar setups, cable length should either be determined before installation or adjusted in place to mitigate the amount of unnecessary cable between the test chamber and the electronics cabinet.

The silica gel within the electronics cabinet was implemented with the aim of mitigating the effects of humidity on the data logger's electronic components. Although the efficacy of the silica gel in this regard remains unknown, it is noteworthy that the datalogger, which is only IP20 rated, successfully endured the entirety of the testing period, with the humid marine atmosphere outside the cabinet.

6.2. OCP Measurements

The different OCP test setups have provided good data and allowed for monitoring the condition of different stainless steel samples in the facility's operating conditions and in the lab. It is important to note that these samples are not cleaned regularly, like the equipment in the facilities. The small number of identical samples used in these tests limits the statistical significance of the tests, but does still provide useful indications of the expected results.

6.2.1. Corrosion Lab

The most noticeable difference between the data from the facilities and the corrosion lab is that the OCP is significantly lower. While the samples in the facilities surpass 350 mv vs. Ag/AgCl, the lab samples barely surpass 250 mV vs Ag/AgCl. This is slightly lower than expected, as other experiments, as seen in Figure 2.14, have reached OCP values of 300 mV vs. Ag/AgCl in seawater up to 30°C. This might be an effect of the samples being exposed to the same water for prolonged times in the test chamber instead of free-flowing seawater, as other tests have used. Variation in the biofilm composition and varying light levels can also be contributing factors. Furthermore, the conditions appear to have been worse for the samples in the lab, with overall more signs of initiations and samples initiating.
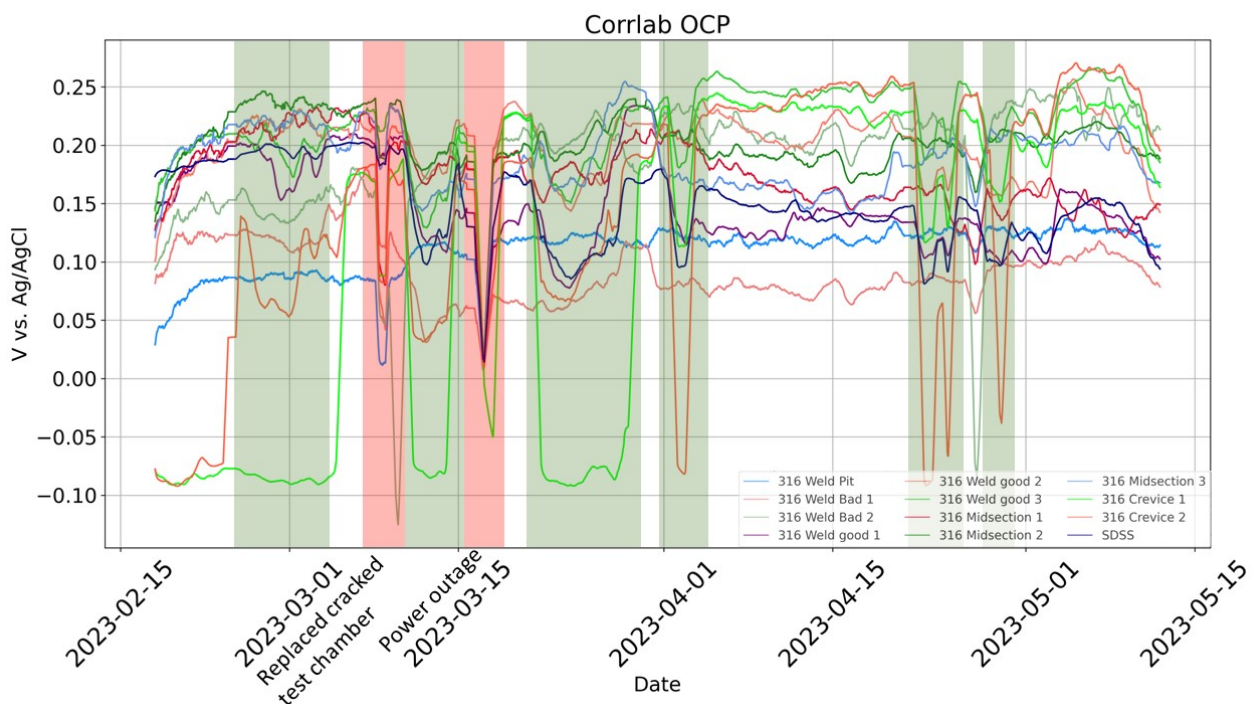
Figure 6.1.: Comparison of all Corrosion lab OCP samples, with areas of error and covariation marked

Figure 6.1 illustrates the measured OCP development of all samples in the Corrosion Lab. The two red sections illustrate periods where the data is erroneous due to external

factors. The first was a temporary break of the experiment due to a leak in the test chamber, necessitating moving the setup into another chamber. The second was a power outage that interrupted data recording for a day.

The sections marked in green show where it is apparent from the recorded data that the AISI 316L Crevice samples have initiated. This initiation and hence decrease in potential seem to affect other specimens in the test chamber as these also drop significantly in potential during the same periods. This might be due to an increased current flowing through the measuring circuit due to an increased rate of the anodic reaction in the crevice. This would cause an ohmic voltage drop in the circuit, hence reducing the measured voltage [67]. However, five of the samples do not experience the same trend. These samples were all connected to the same connection hub, and a possible higher impedance in this hub relative to the other hubs might explain this behaviour. Another possibility is that conditions in the test chamber caused an OCP reduction on many of the samples. This would be quite strange, as some otherwise similar samples experienced different behaviours in these sections. The extent of the influence between the different samples does also vary, so it is difficult to identify one single error source. A possibility to potentially mitigate this issue is to use multiple test chambers, where each test chamber is connected to only one logger hub, as well as mounting crevice samples in separate chambers to mitigate the influence on other types of samples. Limiting the number of samples per electrode could also potentially fix this issue.

The water in the test chamber was changed right before the power outage, so the initial effect of this change was not recorded. However, overall, the change of water did not appear to have a significant effect on the recorded OCP. The water in the test chamber was supposed to be completely changed bi-weekly to have some exchange of water in the system. However, this was not performed as evaporation losses had to be replenished frequently. This would also cause some exchange and agitation of the water, although without the complete substitution of all the water in the chamber. This replenishment could also increase the salinity of the water. However, substantial amounts of saline deposits were found on the edges of the chamber and in the sample holders, indicating that NaCl also left solution, mitigating this effect. No further action was taken regarding this effect, although it is a factor to take into consideration when analyzing the results, as this could lead to changes in the OCP.

Visible algae growth and biofilm formed on the samples after a couple of weeks of exposure, as expected. This biofilm may also affect the OCP development on the samples. The OCP of 25 Cr SDSS, among others, actually reduced overall during the test period, which may have been an effect of the biofilm formation together with the lack of water exchange.

Although an air pump was added to provide oxygenation to the water, it is unclear whether this actually helped in mitigating the effects of stagnant water on the stainless steel. The pump was disconnected for a week at the beginning of April, with no significant difference in the data variations.

Should a similar experiment be conducted, a system for effectively draining and replen-

ishing the test chamber should be created, and a temperature probe included to monitor the temperature in the chamber.

6.2.2. InnovaMar - Frøya

For the first two months of the setup at Frøya, seen in Figure 5.4, the data was overall noisier, and registered less of an ennoblement of the samples compared to the values at Senja, Figure 5.6.

The samples at Frøya stabilized at potentials exceeding 500mV vs Ag/AgCl. These results exceed what is expected and found in other similar setups, which indicated a problem with the reference electrode. After inspection of the electrode by personnel at the facility, the issue was identified, as the protective cap on the electrode was still present. This was removed, and measurements continued, again proving the importance of on-site personnel.

The data gathered before this cap was removed is still usable, as the relative measurements between the samples are still relevant. The OCP of the 25Cr SDSS sample dropping significantly when the cap was removed indicates that the exact values measured may be erroneous. Interestingly, even though the other samples showed some signs of reactions to this change, their OCP quickly stabilized around the same voltage as before this change. This raises the question if there is an issue with the electrode in question or if the data is reliable. This requires comparing the values measured to another reference electrode. This was not performed within the time span of this project due to time limitations. However, this verification will be performed at a later date, as the test will continue for an extended time.

It is apparent that the noise level of the data is reduced when the temperature in the chamber is increasing. This reduction is probably due to the fact that the temperature rises when the RSW cooler and pump in the facility are turned off, and water becomes stagnant in the test chamber. It is possibly the stagnant water that allows for better stability, and hence less noisy data. Another contributing factor can be if there is located AC motors or other equipment using AC power nearby. This kind of equipment can possibly cause noise in the data, which will not be present when the production equipment is turned off. The noise was not reduced significantly when the protective cap was removed, indicating that this did not affect these fluctuations.

An interesting relation in all the samples is the correlation between temperature change and change in OCP. This normally occurs as a slight ennoblement of the samples. As explained in section 2.2, the exact reason for the change in OCP is difficult to explain, although factors like temperature, access to oxygen and biofilm growth all can contribute in this manner. The same was not seen to the same extent in the samples in Senja.

At Frøya, synchronous potential drops as the ones seen at the Corrosion Lab were also seen. The reference electrodes used in both these settings are of identical type, further indicating that there might be an issue with these electrodes. This became especially

visible at the end of the testing period, where all samples decreased at least 100 mV, likely due to the re-initiation of one of the crevice samples.

6.2.3. InnovaNor - Senja

As seen in Figure 5.6, the data from Senja was over all less noisy, and the values were more in line with what was expected from such kinds of measurements. The exception to this is the time from the 7th to 10th, and the 14th to 23rd of April. Due to holiday and maintenance work, the equipment was shut down, and the samples exposed to stagnant water and temperatures up to 12°C for a prolonged time. This appears to have caused favourable conditions for meta-stable pitting for many of the samples, as the values fluctuated rapidly in the area between 300 mV and 0 mV vs. Ag/AgCl.

The sample from the previously pitted weld, seen in Figure 5.6b, had an overall lower OCP and fluctuated much before settling on a stable low OCP. This might indicate that after a period of metastable pitting, stable pitting has initiated, and the weld zone is actively corroding. This sample is cut from the same weld as the sample at Frøya, which did not show signs of initiation, characterising the random nature of these initiations and how small differences in operating conditions or regions of the weld zone can cause the onset of pitting corrosion. One of the untreated welds appear to have initiated on the 23rd of April, before re-passivating after two days. These observations show the importance of proper weld procedures, as corrosion of these welds can cause leaks in the production areas and require maintenance. This is similar to what is seen in Figure 1.3d.

Pit and crevice initiation was also seen in connection with temperature changes, often when the RSW was turned on. This is probably due to the introduction of flow to a stagnant system, enhancing the difference in oxygen concentration inside and outside of the crevices and pits, promoting the pitting and crevice corrosion mechanisms seen in sections 2.2.2 and 2.2.3

The samples at Senja seem to handle the normal operating conditions quite well, except for when the production is shut down for a prolonged time. However, the welded samples which are not properly shielded and post-treated seem to suffer from larger initiations and possibly active pitting. Crevice corrosion can also occur in these conditions, as seen from both crevice samples initiating.

The 25Cr SDSS sample, behaved as expected in all three setups, except for one minor potential drop at Senja. The stable behaviour and no signs of corrosion show that 25Cr SDSS survives well in the conditions of the facilities. While it is probably not viable as a construction material due to its cost, it proves to be a good reference to monitor the conditions of other samples in the test setup.

6.2.4. Factors Affecting Results

As seen in chapter 2, there are several factors affecting the OCP development and corrosion resistance of 316 Stainless steel. Regarding these different setups, the main contributing factors to the differing results are temperature, flow, biofilm formation, pH, and reference electrode differences.

Although the temperature in the corrosion lab is stable, it was not monitored. Therefore, any effects related to changes in temperature were not observable. On the other hand, in the facilities, the temperature was monitored, but due to other factors changing simultaneously with temperature, such as variation between production conditions and maintenance, it is difficult to attribute any observed effects solely to temperature changes with certainty. Flow is in this regard relatable to the temperature changes, since the flow in the chamber stopped when the production stopped. This might have caused stagnant conditions and lack of oxygen diffusion. In the lab, with an air pump continuously pumping and circulating water, oxygen deprivation should not be an issue. However, there was little exchange of the water itself, which would be beneficent to simulate the conditions in the facility more accurately.

The initiation of the crevice samples shows that crevice corrosion can occur in the facility during normal operations. Even though cleaning can affect these results, crevices are inherently difficult to clean, making it probable that crevices within the production equipment can experience similar conditions as these crevice samples.

Exposing the samples to the exact conditions in the production area, with wet and dry cycles, cleaning and rinsing, would be interesting in order to replicate the conditions in the production areas as closely as possible. However, replicating this would require a completely different test chamber setup necessitating long design times to test the concept before deployment.

Underlying factors for biofilm formation also include UV sterilization of the process water, light levels, surface roughness, and pre-treatment, among other factors which have the potential to influence the data. The identification of biofilm in the test chamber corresponds with the ennoblement seen on the samples. As the samples were cleaned with ethanol before installation, this might indicate that the UV sterilization of the water is not 100% effective in killing bacteria and other microorganisms. However, this might not be an issue where the surfaces are regularly cleaned, as the potential biofilm will not be able to form, or will be removed from these surfaces. However, biofilm formation could still occur on parts that are not subject to regular cleaning, or if cleaning is omitted due to maintenance or other factors.

Although it is expected that the pH of the water in the facilities is quite stable, this was not monitored and could be a potential source of error. In the production equipment, the pH might also vary due to the effects of cleaning agents.

Differences in the reference electrodes might also be an issue regarding these measurements. A proper field electrode, such as the one utilized at Senja, yielded good and stable measurements and is preferable when mounting test setups without being able

to monitor them closely and resolve issues regularly. As experienced from the setup at Frøya, being able to trust the measurements is important, and the field electrode seem to provide less noisy data compared to the electrode at Frøya.

The mounting of the samples on Senja uses threaded rods instead of platinum wire. This was a point of concern due to the potential risk of crevice corrosion in the introduced crevices, formed by the thread-sample interface. The sealing of these areas with silicone and heat shrink tubing appears to have worked quite well, with only one of the AISI 304L samples showing signs of corrosion in the vicinity of the threaded rod. The solution with threaded rods proves to be a preferred mounting option, as these provide better support for the samples compared to the thin platinum wire, which is prone to failure, as seen on one of the samples mounted at Frøya.

6.3. Potentiostatic Measurements

The potentiostatic tests shown in Figure 5.9 reveal a noteworthy relationship between temperature and potential with regard to the CPT and CCT of 304L and 316L. While more samples would be needed to verify and obtain more statistically significant results, some interesting relationships can be observed. Specifically, 304L is generally less resistant to crevice corrosion attacks, with the relation being more dependent on both temperature and potential. On the other hand, the crevice samples of 316L show less dependence on potential, with a CCT in seawater ranging between 5 and 10°C. No variation was observed due to potential, although further tests could have identified this within the range of uncertainty.

The welded 316L samples tested performed worse than the 304L Crevice samples, which shows how bad of a condition these samples are in. The weld shows signs of lacking shielding and is not post-treated. This resulted in a very corrosion-prone weld, which experienced sub-surface pitting corrosion and general weld failure. This occurred even in the test of 300 mV vs. Ag/AgCl at 2°C, which are conditions found during normal operation in the facilities.

Figure 5.9, indicate a linear relation of temperature and potential regarding the susceptibility to pitting and crevice corrosion. The relations seen in Figure 2.13 indicate more of an exponential decay in these values. As the potentiostatic tests were performed at a relatively small temperature range of 8°C, the macroscopic relation can still be exponential, while approaching a linear relation at smaller scales.

6.4. SEM and EDS

The imaging with SEM and the results from EDS provide some interesting results regarding the corrosion resistance and quality of the weld. The Cr content appears elevated, likely due to the effects described in subsection 2.1.2, and with the presence of oxygen due to the oxide film formed. The carbon content appears elevated in all the measurements, possibly due to carbide precipitates in the HAZ. One important notice is the presence of Sulfur in the weld filler material, and not in the base metal. This is a strong indication of differences between the base alloy, and the filler metal alloy. The same is relevant for the presence of Molybdenum in the base metal, and not the weld filler.

As explained in subsection 2.1.1, the presence of sulfur can decrease the corrosion resistance of the weld, and can be a contributing factor to the severe damages seen in the weld zone. These attacks are especially interesting, as the pitting attacks are mostly seen on the base metal, as seen in Figure 5.11, but with the major damage mostly affecting the weld filler material. These observations indicate that in addition to poor weld procedures, bad filler material may have been used in these welds.

6.5. Impact on Processing Facilities

The results of the OCP measurements conducted in both the facilities and the laboratory suggest that the OCP is higher in the facility's conditions. Furthermore, the potentiostatic tests indicate that the crevice and pitting potential is higher at lower temperatures. These effects do not cancel each other out, and the higher temperature environment still seems to be more dangerous for the onset of pitting and crevice corrosion.

The UV sterilization and the temperature of the water in the facilities seem to have an effect on the rate of the biofilm formation, as the samples in the facilities experience a prolonged time of ennoblement compared to the lab, where biofilm formation and ennoblement occur rather quickly. However, the presence of biofilm in the facilities proves that the UV-sterilization of the water is indeed not 100% effective, allowing for biofilm-forming bacteria to settle in the test chamber.

Wrong filler material, and improper weld procedures during construction or maintenance create welds susceptible to severe pitting attacks. Difficulties in monitoring and inspecting the backside of welds can be contributing factors, as some welds appear to be good on the outside while still being oxidized inside the pipe, like the ones seen in Figure 4.2.

During normal operation, the facilities and the production equipment are washed daily after the end of production, and with regular thorough cleaning. During this procedure, all seawater-containing equipment is to be drained, hence reducing the corrosive effects of standing seawater in the system. The OCP measurements in the HEMOS were not able to monitor these effects as instead of being drained together with the rest

of the facility, it was left filled with stagnant water until the process was started and flow resumed. However, this does show the effects of stagnant seawater on the process equipment, which have been shown to occur in several facilities due to operational errors. Smaller crevices and prone sections in and around flanges and welds may potentially still hold some seawater even though the system is drained, causing severe crevice corrosion attacks in these regions when the process is turned off, and the temperature in the system is elevated.

Chapter 7.

Conclusion

The OCP results from Frøya and Senja, together with the tests performed in the corrosion lab, provide valuable information regarding the corrosion-resistant properties of AISI 316L and, to some extent, AISI 304L. As an untreated, free surface, AISI 316L has proven to resist corrosion during normal operating procedures, although with signs of instability when the production is halted, causing temperatures up to 12°C and stagnant conditions. The crevice corrosion resistance is not sufficient to withstand initiation, and this effect is influenced by the varying operating conditions in the facilities. If welding is performed according to standards, with proper filler material and gas coverage, the corrosion resistance of AISI 316L is maintained. However, if proper procedures are not followed, the resulting welds are highly prone to corrosion in the operating conditions of the facilities. AISI 304L is shown to have little resistance to crevice corrosion in the operating conditions of the facilities and can be prone to uniform corrosion of the surfaces. The corrosion resistance is documented for conditions where the structures are continuously immersed, while production equipment experience wet-dry cycles and cleaning. This can reduce the effect of biofilm formation and stagnant conditions, which can influence these results.

The testing in the lab suggests critical values for the different materials used. AISI 304L experience a CCT= 2°C, while AISI 316L experience a CCT=10°C. Improperly welded AISI 316L experienced a CPT=2°C, while free surface AISI 316L samples experienced a CPT>12°C.

The HEMOS system proved to work satisfactorily and allowed for remote OCP measurements with live data streaming and processing. Testing one initial prototype setup at Frøya was crucial to gather feedback, and to test how the system worked. This allowed for iterative development of the HEMOS before deployment to Senja. These setups have provided a lot of valuable feedback on the design and construction of the system, which should be implemented if the system is to be utilized for further testing. The system design allows for implementing improvements and modifying the setup to accommodate different types of tests in harsh environments,

Chapter 8.

Further Work

In this thesis, only OCP measurements were performed in order to monitor the samples in the facilities. Other kinds of tests, like linear voltametry or potentiostatic tests, might also be interesting in order to fully understand the corrosion mechanisms of 316L in the facilities.

As this kind of remote setup had to be designed from scratch, the lessons learned from these setups regarding the use of reference electrodes, redundant systems and noise reduction should be implemented and tested further if similar setups are to be made. Separate measurements of water flow and temperature and more temperature probes would also be beneficial for monitoring the operating conditions closely. In addition, measurements of oxygen content and pH could be performed, as well as including a camera in the test setup.

Three samples were the maximum amount of similar samples tested in one location. To obtain more statistically significant data, and minimize the risk of outliers, multiple similar samples should be tested.

Regarding potentiostatic tests, further tests with more samples in the same conditions, and with a clearer history of the weld procedures would be beneficial to establish repeatable tests with statistical significance. Further investigation into the weld composition and filler material used would also be interesting, in order to increase the understanding of the failure of these welds.

As of writing, the OCP tests in the facilities are not concluded and may continue to provide interesting insight into the conditions in these facilities.

References

[1] O. Kopperud, *Corrosion in Fish Processing Facilities: A Study of Causes and Mitigation Strategies*, Unpublished. Available upon request, Dec. 2022.

[2] M. Cassidy, *What is Aquaculture, and Why Do We Need It?* en-US, Mar. 2019. [Online]. Available: `https://www.globalseafood.org/blog/what-is-aquaculture-why-do-we-need-it/` (visited on 12/05/2022).

[3] *Forskrift om desinfeksjon av inntaksvann til og avløpsvann fra akvakulturrelatert virksomhet - Lovdata.* [Online]. Available: `https://lovdata.no/dokument/SF/forskrift/1997-02-20-192` (visited on 05/12/2023).

[4] *Forskrift om godkjenning og bruk av desinfeksjonsmidler i akvakulturanlegg og transportenheter - Lovdata.* [Online]. Available: `https://lovdata.no/dokument/SF/forskrift/2008-06-17-821` (visited on 05/12/2023).

[5] *Forskrift om slakterier og tilvirkingsanlegg for akvakulturdyr - Kapittel 1. Formål, virkeområder og definisjoner - Lovdata.* [Online]. Available: `https://lovdata.no/dokument/SF/forskrift/2006-10-30-1250/KAPITTEL_1#%C2%A73` (visited on 05/12/2023).

[6] Baader, *BAADER Fish Processing Machinery*, English, 2022. [Online]. Available: `https://fish.baader.com/` (visited on 05/26/2023).

[7] Unik, *UV Anlegg for akvakultur*, nb-NO, 2022. [Online]. Available: `https://unikwater.com/uv-anlegg-for-akvakultur/` (visited on 05/21/2023).

[8] P. Marshall, *Austenitic Stainless Steels: Microstructure and mechanical properties*, en. Springer Science & Business Media, Jul. 1984, Google-Books-ID: hhXWZjBclvUC, ISBN: 978-0-85334-277-9.

[9] J. W. Simmons, "Overview: High-nitrogen alloying of stainless steels," en, *Materials Science and Engineering: A*, vol. 207, no. 2, pp. 159–169, Mar. 1996, ISSN: 0921-5093. DOI: `10.1016/0921-5093(95)09991-3`. [Online]. Available: `https://www.sciencedirect.com/science/article/pii/0921509395099913` (visited on 12/04/2022).

[10] C. Olsson and D. Landolt, "Passive films on stainless steels - chemistry, structure and growth," en, *Electrochimica Acta*, Microscopic and Nanoscopic Aspects of Corrosion and Corrosion Protection, vol. 48, no. 9, pp. 1093–1104, Apr. 2003, ISSN: 0013-4686. DOI: `10.1016/S0013-4686(02)00841-1`. [Online]. Available: `https://www.sciencedirect.com/science/article/pii/S0013468602008411` (visited on 05/09/2023).

[11] IMOA, Ed., *Practical guidelines for the fabrication of duplex stainless steels*, en, 2.ed. London: IMOA, 2009, ISBN: 978-1-907470-00-4.

[12] J. H. Potgieter, W. Skinner, and A. M. Heyns, "The nature of the passive film on cathodically modified stainless steels," en, *Journal of Applied Electrochemistry*, vol. 23, no. 1, pp. 11–18, Jan. 1993, ISSN: 1572-8838. DOI: `10.1007/BF00241569`. [Online]. Available: `https://doi.org/10.1007/BF00241569` (visited on 05/22/2023).

[13] A. Vinoth Jebaraj, L. Ajaykumar, C. R. Deepak, and K. V. V. Aditya, "Weldability, machinability and surfacing of commercial duplex stainless steel AISI2205 for marine applications – A recent review," en, *Journal of Advanced Research*, vol. 8, no. 3, pp. 183–199, May 2017, ISSN: 2090-1232. DOI: `10.1016/j.jare.2017.01.002`. [Online]. Available: `https://www.sciencedirect.com/science/article/pii/S2090123217300115` (visited on 12/13/2022).

[14] N. Institute, *Stainless steel: The role of nickel*, en, Oct. 2021. [Online]. Available: `https://nickelinstitute.org/` (visited on 12/04/2022).

[15] N. Suutala, "Effect of manganese and nitrogen on the solidification mode in austenitic stainless steel welds," en, *Metallurgical Transactions A*, vol. 13, no. 12, pp. 2121–2130, Dec. 1982, ISSN: 2379-0180. DOI: `10.1007/BF02648382`. [Online]. Available: `https://doi.org/10.1007/BF02648382` (visited on 05/22/2023).

[16] E. G. Fel'dgandler and G. V. Kazakova, "The effect of sulphur content on pitting corrosion resistance of 03Kh24N6AM3 steel," English, *Protection of Metals*, vol. 30, no. 4, Jul. 1994. [Online]. Available: `https://www.osti.gov/biblio/91219` (visited on 06/06/2023).

[17] T. L. S. L. Wijesinghe and D. J. Blackwood, "Real time pit initiation studies on stainless steels: The effect of sulphide inclusions," en, *Corrosion Science*, vol. 49, no. 4, pp. 1755–1764, Apr. 2007, ISSN: 0010-938X. DOI: `10.1016/j.corsci.2006.10.025`. [Online]. Available: `https://www.sciencedirect.com/science/article/pii/S0010938X06003076` (visited on 05/09/2023).

[18] R. R. Hussain, A. Alhozaimy, A. Al-Negheimish, and D. D. N. Singh, "Role of phosphorus as micro alloying element and its effect on corrosion characteristics of steel rebars in concrete environment," en, *Scientific Reports*, vol. 12, no. 1, p. 12 449, Jul. 2022, Number: 1 Publisher: Nature Publishing Group, ISSN: 2045-2322. DOI: `10.1038/s41598-022-16654-w`. [Online]. Available: `https://www.nature.com/articles/s41598-022-16654-w` (visited on 06/06/2023).

[19] U. Alloys, *What is A Pitting Resistance Equivalent Number (PREN)? - Unified Alloys*. [Online]. Available: `https://www.unifiedalloys.com/blog/pitting-resistance-pren` (visited on 11/07/2022).

[20] C. A. Olsson, "Wet Corrosion of Stainless Steels and Other Chromium-Bearing Alloys," en, in *Encyclopedia of Interfacial Chemistry*, K. Wandelt, Ed., Oxford: Elsevier, Jan. 2018, pp. 535–542, ISBN: 978-0-12-809894-3. DOI: `10.1016/B978-0-12-409547-2.13583-8`. [Online]. Available: `https://www.sciencedirect.com/science/article/pii/B9780124095472135838` (visited on 05/22/2023).

[21] S. Prakash, "10 - Development of advanced alloys with improved resistance to corrosion and stress corrosion cracking (SCC) in power plants," en, in *Structural Alloys for Power Plants*, ser. Woodhead Publishing Series in Energy, A. Shirzadi and S. Jackson, Eds., Woodhead Publishing, Jan. 2014, pp. 294–318, ISBN: 978-0-85709-238-0. DOI: `10.1533/9780857097552.2.294`. [Online]. Available: `https://www.sciencedirect.com/science/article/pii/B9780857092380500103` (visited on 05/22/2023).

[22] V. Kumar, *16 Most Common Stainless Steel Grades [Explained]*, en-US, Apr. 2021. [Online]. Available: `https://www.rankred.com/common-stainless-steel-grades/` (visited on 05/26/2023).

[23] R. Kumar and S. Bharathi, "A Review Study on A-TIG Welding of 316(L) Austenitic Stainless Steel," Mar. 2015.

[24] M. A. A. Mohd Salleh, A. Mustafa, M. M. A. B. Abdullah, A. Abdullah, and H. Kamarudin, "Effects of Seawater (Salt Water) to Aisi 304 Mechanical Properties," *Australian Journal of Basic and Applied Sciences*, vol. 7, pp. 545–554, May 2013.

[25] I. Defrancq, "Corrosion of 316L Stainless Steel in sea water," Jan. 2013.

[26] NORSOK, *M-001*, 2017. [Online]. Available: `https://www.standard.no/pagefiles/1176/m-001.pdf` (visited on 05/14/2023).

[27] R. Francis, G. Byrne, and G. Warburton, "The corrosion of superduplex stainless steel in different types of seawater," *NACE - International Corrosion Conference Series*, Jan. 2011.

[28] J.-y. Jiang, D. Wang, H.-y. Chu, H. Ma, Y. Liu, Y. Gao, J. Shi, and W. Sun, "The Passive Film Growth Mechanism of New Corrosion-Resistant Steel Rebar in Simulated Concrete Pore Solution: Nanometer Structure and Electrochemical Study," *Materials*, vol. 10, no. 4, p. 412, Apr. 2017, ISSN: 1996-1944. DOI: `10.3390/ma10040412`. [Online]. Available: `https://www.ncbi.nlm.nih.gov/pmc/articles/PMC5506972/` (visited on 12/05/2022).

[29] M. J. Pryor, "The Significance of the Flade Potential," en, *Journal of The Electrochemical Society*, vol. 106, no. 7, p. 557, Jul. 1959, Publisher: IOP Publishing, ISSN: 1945-7111. DOI: `10.1149/1.2427437`. [Online]. Available: `https://iopscience.iop.org/article/10.1149/1.2427437/meta` (visited on 05/09/2023).

[30] K. Morshed Behbahani, M. Pakshir, Z. Abbasi, and P. Najafisayar, "Damage mechanism at different transpassive potentials of solution-annealed 316 and 316l stainless steels," en, *International Journal of Minerals, Metallurgy, and Materials*, vol. 22, no. 1, pp. 45–51, Jan. 2015, ISSN: 1869-103X. DOI: `10.1007/s12613-015-1042-x`. [Online]. Available: `https://doi.org/10.1007/s12613-015-1042-x` (visited on 05/09/2023).

[31] S. Pahlavan, M. H. Moayed, and M. Mirjalili, "The Contrast between the Pitting Corrosion of 316 SS in NaCl and NaBr Solutions: Part I. Evolution of Metastable Pitting and Stable Pitting," en, *Journal of The Electrochemical Society*, vol. 166, no. 2, p. C65, Jan. 2019, Publisher: IOP Publishing, ISSN: 1945-7111. DOI: 10.1149/2.0811902jes. [Online]. Available: https://iopscience.iop.org/article/10.1149/2.0811902jes/meta (visited on 05/09/2023).

[32] S. Esmailzadeh, M. Aliofkhazraei, and H. Sarlak, "Interpretation of Cyclic Poten- tiodynamic Polarization Test Results for Study of Corrosion Behavior of Metals: A Review," en, *Protection of Metals and Physical Chemistry of Surfaces*, vol. 54, no. 5, pp. 976–989, Sep. 2018, ISSN: 2070-206X. DOI: 10.1134/S207020511805026X. [Online]. Available: https://doi.org/10.1134/S207020511805026X (visited on 05/23/2023).

[33] N. Sridhar and G. A. Cragnolino, "Applicability of Repassivation Potential for Long-Term Prediction of Localized Corrosion of Alloy 825 and Type 316L Stain- less Steel," en, *CORROSION*, vol. 49, no. 11, pp. 885–894, Nov. 1993, ISSN: 0010-9312, 1938-159X. DOI: 10.5006/1.3316014. [Online]. Available: http://corrosionjournal.org/doi/10.5006/1.3316014 (visited on 05/26/2023).

[34] E. Bardal, *Corrosion and protection*, en. London ; New York: Springer, 2004, ISBN: 978-1-85233-758-2.

[35] Z. Szklarska-Smialowska, "Mechanism of pit nucleation by electrical breakdown of the passive film," en, *Corrosion Science*, vol. 44, no. 5, pp. 1143–1149, May 2002, ISSN: 0010-938X. DOI: 10.1016/S0010-938X(01)00113-5. [Online]. Available: https://www.sciencedirect.com/science/article/pii/S0010938X01001135 (visited on 05/09/2023).

[36] A. Chiba, I. Muto, Y. Sugawara, and N. Hara, "Pit Initiation Mechanism at MnS Inclusions in Stainless Steel: Synergistic Effect of Elemental Sulfur and Chloride Ions," en, *Journal of The Electrochemical Society*, vol. 160, no. 10, p. C511, Aug. 2013, Publisher: IOP Publishing, ISSN: 1945-7111. DOI: 10.1149/2.081310jes. [Online]. Available: https://iopscience.iop.org/article/10.1149/2.081310jes/meta (visited on 05/09/2023).

[37] H. P. Leckie and H. H. Uhlig, "Environmental Factors Affecting the Critical Poten- tial for Pitting in 18–8 Stainless Steel," en, *Journal of The Electrochemical Society*, vol. 113, no. 12, p. 1262, Dec. 1966, Publisher: IOP Publishing, ISSN: 1945-7111. DOI: 10.1149/1.2423801. [Online]. Available: https://iopscience.iop.org/article/10.1149/1.2423801/meta (visited on 05/09/2023).

[38] N. Sridhar, C. S. Brossia, D. S. Dunn, and A. Anderko, "Predicting Localized Corrosion in Seawater," en, *CORROSION*, vol. 60, no. 10, pp. 915–936, Oct. 2004, ISSN: 0010-9312, 1938-159X. DOI: 10.5006/1.3287826. [Online]. Available: http://corrosionjournal.org/doi/10.5006/1.3287826 (visited on 12/15/2022).

[39] R. P. V. Cruz, A. Nishikata, and T. Tsuru, "Pitting corrosion mechanism of stainless steels under wet-dry exposure in chloride-containing environments," en, *Corrosion Science*, vol. 40, no. 1, pp. 125–139, Jan. 1998, ISSN: 0010-938X. DOI: `10.1016/S0010-938X(97)00124-8`. [Online]. Available: `https://www.sciencedirect.com/science/article/pii/S0010938X97001248` (visited on 12/05/2022).

[40] J. Telegdi, A. Shaban, and L. Trif, "8 - Microbiologically influenced corrosion (MIC)," en, in *Trends in Oil and Gas Corrosion Research and Technologies*, ser. Woodhead Publishing Series in Energy, A. M. El-Sherik, Ed., Boston: Woodhead Publishing, Jan. 2017, pp. 191–214, ISBN: 978-0-08-101105-8. DOI: `10.1016/B978-0-08-101105-8.00008-5`. [Online]. Available: `https://www.sciencedirect.com/science/article/pii/B9780081011058000085` (visited on 12/12/2022).

[41] H. A. Videla, "Biofilms and corrosion interactions on stainless steel in seawater," en, *International Biodeterioration & Biodegradation*, Special Issue Marine Biofouling and Corrosion, vol. 34, no. 3, pp. 245–257, Jan. 1994, ISSN: 0964-8305. DOI: `10.1016/0964-8305(94)90086-8`. [Online]. Available: `https://www.sciencedirect.com/science/article/pii/0964830594900868` (visited on 12/12/2022).

[42] R. Johnsen and E. Bardal, "The Effect of a microbiological slime layer on stainless steel in natural sea water," Mar. 1986.

[43] S. Yan, G.-L. Song, Z. Li, H. Wang, D. Zheng, F. Cao, M. Horynová, M. Dargusch, and L. Zhou, "A state-of-the-art review on passivation and biofouling of Ti and its alloys in marine environments," *Journal of Materials Science & Technology*, vol. 34, Nov. 2017. DOI: `10.1016/j.jmst.2017.11.021`.

[44] E. Jones, I. Chierici, M. Skjelvan, K. Y. Norl, H. Børsheim, and K. Lødemel, "Monitoring ocean acidification in Norwegian seas in 2018," Miljødirektoratet, Tech. Rep. M-1417, 2019. [Online]. Available: `https://www.miljodirektoratet.no/globalassets/publikasjoner/m1417/m1417.pdf` (visited on 06/07/2023).

[45] A. Ul-Hamid, H. Saricimen, A. Quddus, A. Mohammed, and L. Al-Hems, "Corrosion study of SS304 and SS316 alloys in atmospheric, underground and seawater splash zone in the Arabian Gulf," *Corrosion Engineering, Science and Technology*, vol. 52, pp. 1–7, Feb. 2017. DOI: `10.1080/1478422X.2016.1213974`.

[46] C. Compere and N. Lebozec, *Behaviour of stainless steel in natural seawater*. Dec. 1997.

[47] B. Wallen, "Critical Pitting Temperature of UNS S31600 in different Sea Waters," in *Marine Corrosion of stainless steels*, 1995.

[48] Alleima, *Exera® SAF 2205™ SH medical wire — Alleima*, May 2022. [Online]. Available: `https://www.alleima.com/se/technical-center/material-datasheets/wire/exera-saf-2205-sh-medical-wire/` (visited on 12/16/2022).

[49] Z. B. Wang and Y. G. Zheng, "Critical flow velocity phenomenon in erosion-corrosion of pipelines: Determination methods, mechanisms and applications," en, *Journal of Pipeline Science and Engineering*, Special Issue on Pipeline Corrosion and Its Management, vol. 1, no. 1, pp. 63–73, Mar. 2021, ISSN: 2667-1433. DOI: `10.1016/j.jpse.2021.01.005`. [Online]. Available: `https://www.sciencedirect.com/science/article/pii/S266714332100007X` (visited on 12/13/2022).

[50] B. Chatterjee, "Science and Industry of Electropolishing," *Jahrbuch Oberflachen technik*, vol. 71, pp. 71–93, Jan. 2015.

[51] H. Dong, Z. Luo, Y. Han, Y.-M. Liu, L. Sun, and W.-Y. Zhai, "The Influence of Pickling Treatment Parameters on the Surface State and Pre-Passivation Behavior of Super 13Cr Martensitic Stainless Steel," en, *Coatings*, vol. 12, no. 2, p. 127, Feb. 2022, Number: 2 Publisher: Multidisciplinary Digital Publishing Institute, ISSN: 2079-6412. DOI: `10.3390/coatings12020127`. [Online]. Available: `https://www.mdpi.com/2079-6412/12/2/127` (visited on 04/17/2023).

[52] S. Trigwell and G. Selvaduray, "Effects of welding on the passive oxide film of electropolished 316L stainless steel," en, *Journal of Materials Processing Technology*, vol. 166, no. 1, pp. 30–43, Jul. 2005, ISSN: 0924-0136. DOI: `10.1016/j.jmatprotec.2004.07.091`. [Online]. Available: `https://www.sciencedirect.com/science/article/pii/S0924013604009938` (visited on 05/29/2023).

[53] *Shielding stainless steel correctly for welding*, en. [Online]. Available: `https://www.canadianmetalworking.com/canadianfabricatingandwelding/article/welding/shielding-stainless-steel-correctly-for-welding` (visited on 05/29/2023).

[54] NORSOK, *M-601*, 2016. [Online]. Available: `https://www.standard.no/no/Nettbutikk/produktkatalogen/Produktpresentasjon/?ProductID=814500` (visited on 05/16/2023).

[55] T. Rogne, J. M. Drugli, and S. Valen, "Testing of Stainless Steel Welds for Various Applications," en, *CORROSION*, vol. 48, no. 10, pp. 864–870, Oct. 1992, ISSN: 0010-9312, 1938-159X. DOI: `10.5006/1.3315886`. [Online]. Available: `http://corrosionjournal.org/doi/10.5006/1.3315886` (visited on 08/25/2022).

[56] N. Larché, D. Thierry, C. Leballeur, and E. Diler, "Crevice Corrosion of High-Grade Stainless Steels in Seawater: A Comparison Between Temperate and Tropical Locations," en, OnePetro, Mar. 2022. [Online]. Available: `https://onepetro.org/amppcorr/proceedings-abstract/AMPP22/4-AMPP22/488801` (visited on 05/15/2023).

[57] C. systems, *Sixteen channel data acquisition monitoring system MS6D | COMET SYSTEM, s.r.o.* 2023. [Online]. Available: `https://www.cometsystem.com/products/sixteen-channel-data-logger-with-alarms/reg-ms6d` (visited on 05/21/2023).

[58] *RS PRO Type K Thermocouple 5m Length, 1/0.2mm Diameter → +260°C | RS*. [Online]. Available: `https://no.rs-online.com/web/p/thermocouples/1236306` (visited on 06/01/2023).

[59] *STELTH 1 » BORIN*, en-US. [Online]. Available: `https://borin.com/products/stelth-1/` (visited on 05/31/2023).

[60] ASTM, *G48 -Standard Test Methods for Pitting and Crevice Corrosion Resistance of Stainless Steels and Related Alloys by Use of Ferric Chloride Solution*, 2013.

[61] S. Swapp, *Scanning Electron Microscopy (SEM)*, en, 2017. [Online]. Available: `https://serc.carleton.edu/research_education/geochemsheets/techniques/SEM.html` (visited on 06/05/2023).

[62] *Scipy.signal.savgol_filter — SciPy v1.10.1 Manual*. [Online]. Available: `https://docs.scipy.org/doc/scipy/reference/generated/scipy.signal.savgol_filter.html` (visited on 05/10/2023).

[63] R. pi, *Raspberry Pi 4 Model B – Raspberry Pi*, 2020. [Online]. Available: `https://www.raspberrypi.com/products/raspberry-pi-4-model-b/` (visited on 05/21/2023).

[64] *Intel® NUC Products*, en, 2023. [Online]. Available: `https://www.intel.com/content/www/us/en/products/details/nuc.html` (visited on 05/21/2023).

[65] USB, *USB 2.0 | USB-IF*. [Online]. Available: `https://www.usb.org/usb2` (visited on 05/04/2023).

[66] Edvard, *4 ways in which noise can enter a signal cable and its control - Part 1*, en, Sep. 2014. [Online]. Available: `https://electrical-engineering-portal.com/4-ways-in-which-noise-can-enter-a-signal-cable-and-its-control-part-1` (visited on 05/10/2023).

[67] AUCS, *Understanding the Reference Cell*, Jun. 2019. [Online]. Available: `https://aucsc.com/downloads/SD_Understanding%20the%20Reference%20Cell_2019.pdf` (visited on 05/10/2023).

Appendix A.

Computer and Electrical Configurations

A.1. Setting Up a Windows Computer to Automatically Start Up as a Server.

A couple of steps are needed, and some thought has to be put into how the data shall be accessed to configure the setup properly. The following description is how it was done at the setup at Senja, after gaining some experience from the setup at Frøya.

A.1.1. Making a Local User Account

To be able to do the following configurations it is advisable to create a local user account on the computer to avoid all domain restrictions imposed by the organization if you utilize an organization-bound PC, like if you get one from the University.

The local account should contain no personal information, as the username and password will later have to be saved on the computer in plain text. Use something generic as "Labuser".

To do this, the steps are already described by Microsoft in this link: `https://support.microsoft.com/en-us/windows/create-a-local-user-or-administrator-account-in-windows-20de74e0-ac7f-3502-a866-32915af2a34d#WindowsVersion=Windows_11`

Ensure that you have administrator rights, or else this step might be impossible. If there is a lack of administrator rights, contact the system administrator and either get administrator rights on your account or have them set up what is needed.

A.1.2. Configure Auto-login

From your administrator account, you can configure the auto-login of a user on the current machine. to do this you need to edit the registry of the computer.

The method used in the setup was "Option Two" in the following tutorial, as "Option One" does not work on organizationally hosted machines. `https://www.tenforums.co`
`m/tutorials/3539-sign-user-account-automatically-windows-10-startup.htm`
`l?fbclid=IwAR2wn0Gp-5yzhnQV7FOANXANVYMmAu0EAhKZOXfIA_HX8km56ImRrLi0SGk`

Follow the instructions but do not perform step six.

A.1.3. Configure Auto-launch of Programs

To ensure that the program for the datalogger is running, it is advisable that this automatically launches.

Download the appropriate program. For the Comet Logger MS6D, this program is found on the manufacturer's website:

`https://www.cometsystem.com/products/sixteen-channel-data-logger-with-a`
`larms/reg-ms6d#software`

Sign in to the local user account that was created. If the previous step is done correctly, this should happen automatically as soon as the PC is turned on.

then follow the steps found here: `https://support.microsoft.com/en-us/window`
`s/add-an-app-to-run-automatically-at-startup-in-windows-10-150da165-dcd`
`9-7230-517b-cf3c295d89dd`

If this step is done correctly, then the computer should log into the local account and open the logger program automatically.

A.1.4. Configure TeamViewer

To be able to control the computer in a remote environment it is advisable to configure TeamViewer on the machine to be able to control it if anything should not work properly.

Create a TeamViewer account and log into it on both your personal computer and the computer you configure. By following the setup wizard, you should have easy access to opening and logging on to the remote computer.

A.1.5. Configure Automatic Boot

To perform this step, the PC needs to be restarted, and as the boot screen is shown, press F2 to enter the BIOS settings. If this does not work, search for "how to enter BIOS" for your particular computer model in your search engine of choice.

Navigate to "Power Management" or "Advanced Setting" and look for an option to "Boot when AC-power is restored". Enable this, and the computer should start up immediately if connected to power.

A.1.6. Internet Connection

If there is a stable WiFi connection at your location, and you are able to connect to this, that will be the easiest option.

If you have a PC without a WiFi antenna, you might need a USB-WiFi adapter to connect to the WiFi.

If there is no WiFi available, the other option is to use a USB 4G modem. To use this, a data-sim connected to a data plan is needed, and this is also plugged into an available USB port on the computer. Follow the setup instructions for the modem and disable the PIN-code for the sim card so it can automatically connect at startup.

A.1.7. USB Power Mode

If a USB modem or WiFi antenna is connected, USB power-saving settings should be turned off, else the computer will disconnect these after a couple of hours.

1. Navigate to Control Panel > Hardware > Power Options > Edit Plan Settings. 2. Select Restore default settings for this plan. 3. Expand the USB Settings drop-down. 4. Expand the USB selective suspend setting drop-down. 5. Select Disabled and Apply/OK the settings.

When this is done, the adapter should stay turned on indefinitely.

A.1.8. Auto-Download Data

In the data loggers' program, there is an option to auto-download the data. Enable this, and choose a suitable time interval to synchronize.

A.1.9. Synchronizing Data to Your Personal Devices

To synchronize the data, there are a couple of options. Drive for desktop was utilized to sync a certain folder on the computer to a personal Google Drive, to be able to access it from anywhere. The folder where the data logger saves the files was chosen. This synchronization occurs every time the folder is updated and makes all data available for download from Google Drive.

This method was chosen instead of One Drive and other options due to potential issues with log-in requirements and credential authentication with two-factor authentication, which is sometimes needed with an organizationally issued licence.

A.2. Wiring

The wiring has to be adapted to the environment in question. The power supply which came with the data logger is suitable if the setup is in a less critical place, or the

circuit is dimensioned for smaller, less current-demanding appliances. Depending on the humidity level and the placement of the electronics box, it might be viable to route 230V AC power directly to the electronics box, and put the power supply inside, as was the case with the first prototype of the test setup.

If the environment is more humid and there is a risk of a potential shortage of 230V, the power supply should be located in a dry, enclosed environment, where it is not exposed to these kinds of risks. The same goes for the location of the computer. In this test setup, the computer and power supply were placed either on a separate floor, or in a separate room, with only an Ethernet cable for communication, and a power cable from the 24V supply was drawn between these locations. A grounding wire was also drawn, to mitigate the risks in case a ground fault should occur.

These solutions have to be adapted to each location, depending on the local layout of the testing grounds. If the cable distance between the computer and the datalogger is less than 5 meters, a USB cable might be a viable option for communication between the two.

The data cables into the logger should be shielded, especially if 230V mains power is present in the near vicinity.

Appendix B.
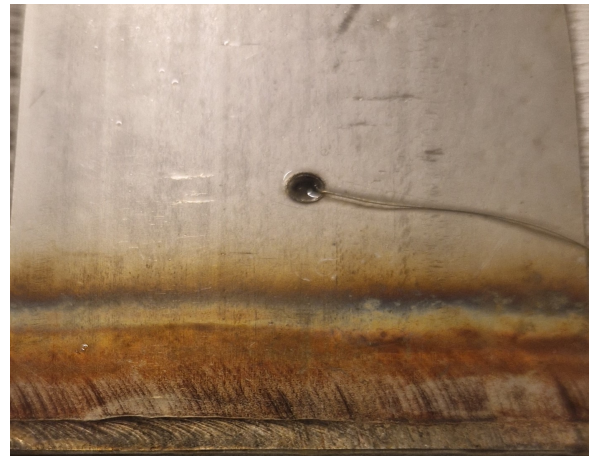
Result Images and Graphs

B.1. OCP - Corrosion Lab

(a) Bad Weld Inside.

(b) Bad Weld Outside.

(c) Pitted Weld Inside.

(d) Pitted Weld Outside.

Figure B.1.: Welded samples from OCP setup at the Corrosion Lab.

B.2. Potentiostatic Tests

(a) 2°C, 400 mV.

(b) 2°C, 300 mV.

(c) 5°C, 300 mV.

(d) 10°C, 100 mV.

Figure B.2.: 304L Crevice samples.

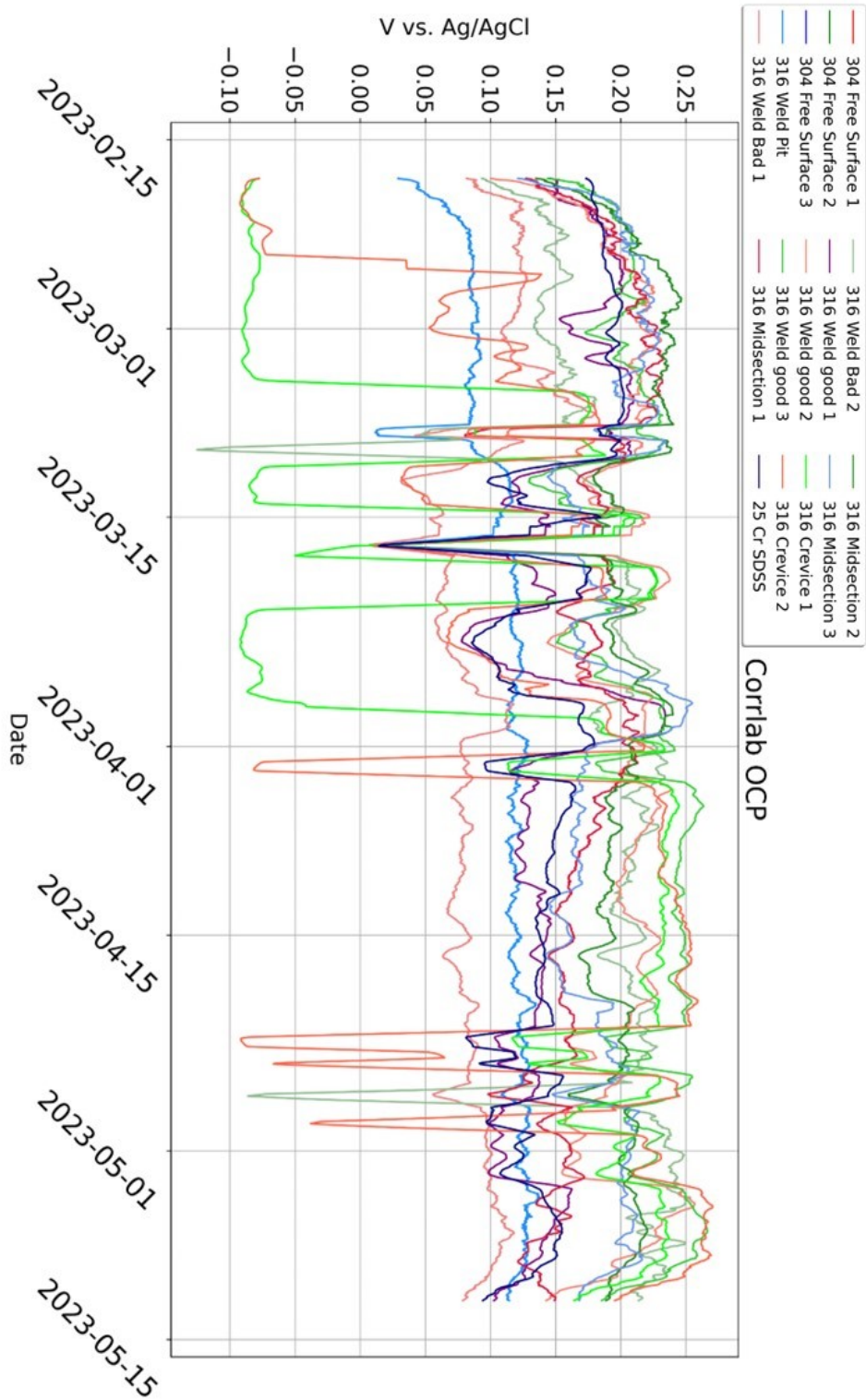(a) Front before exposure.

(b) Back before exposure.

(c) Front after exposure.

(d) Back after exposure.

Figure B.3.: Pitted AISI 316L weld samples, 300mV at 2°C.

B.3. OCP Graphs

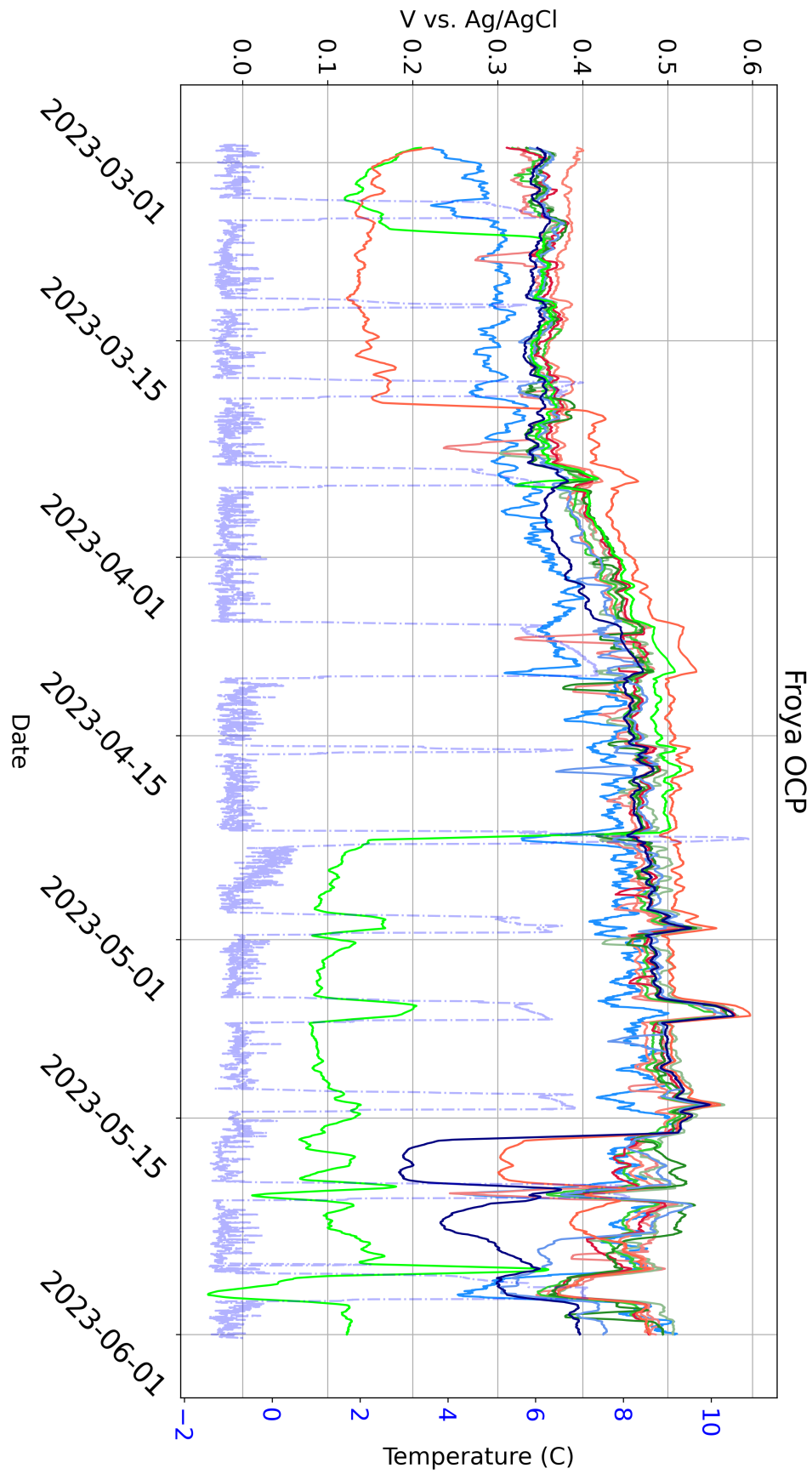**Figure B.4.:** OCP values from the Corrosion lab plotted together. The legend is applicable for all OCP plots.

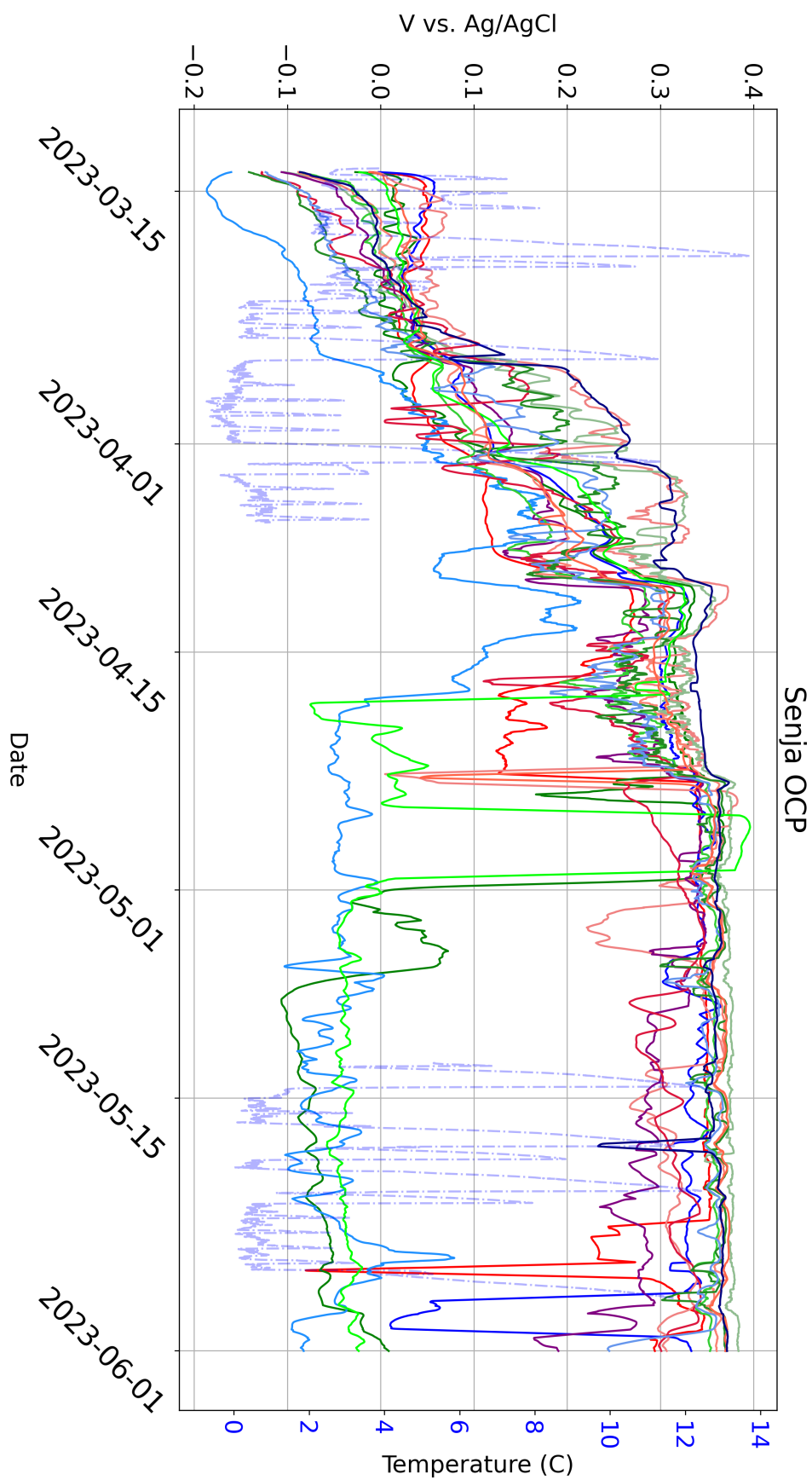**Figure B.5.:** OCP values from the HEMOS at InnovaMar - Frøya plotted together.

Figure B.6.: OCP values from the HEMOS at InnovaNor - Senja plotted together.
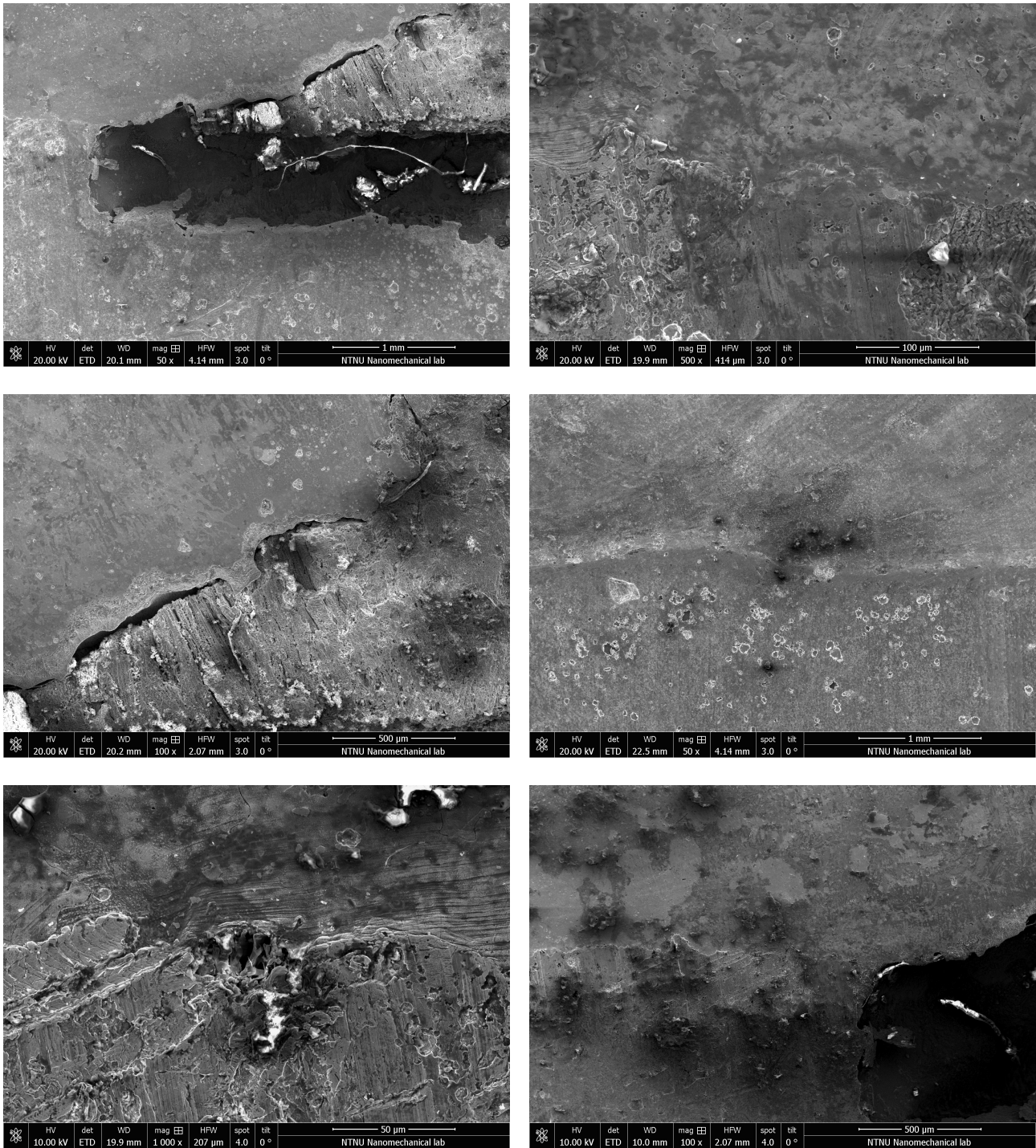
B.4. SEM Imaging
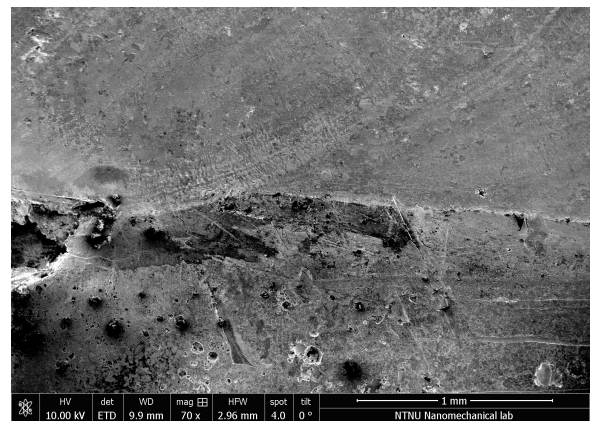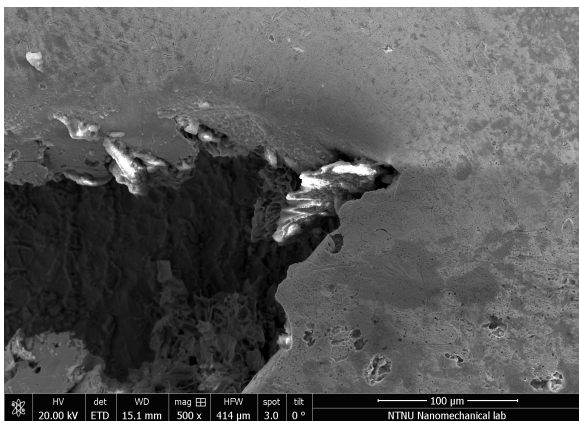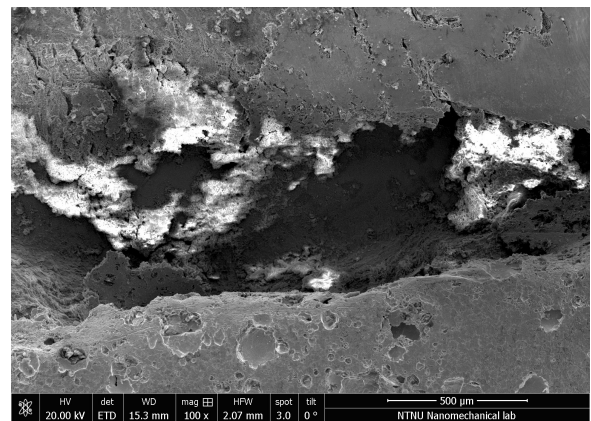

Figure B.7.: SEM imaging of 400mV 2°C sample.
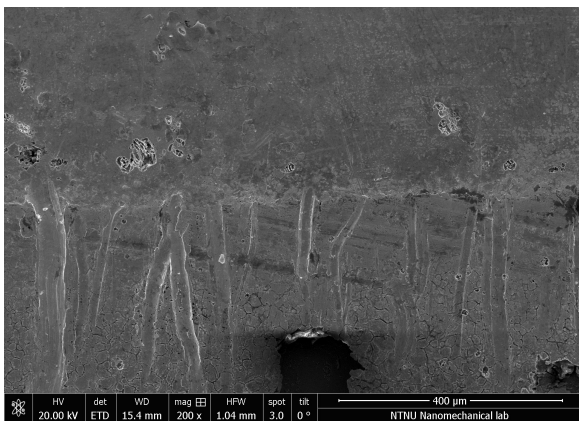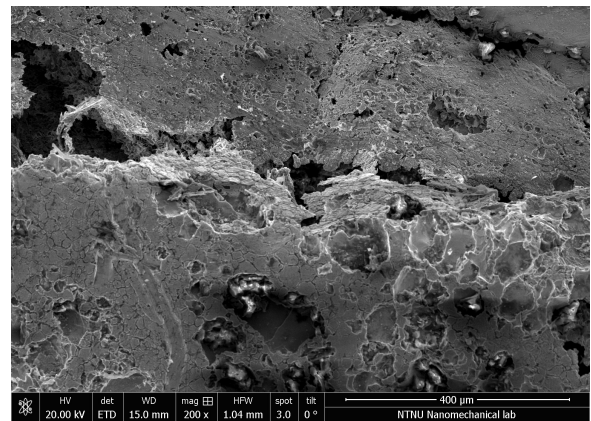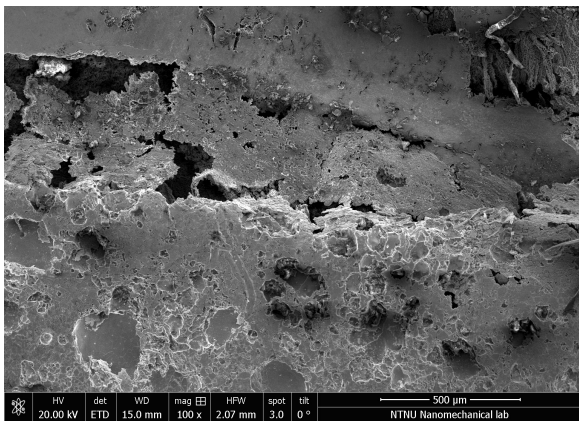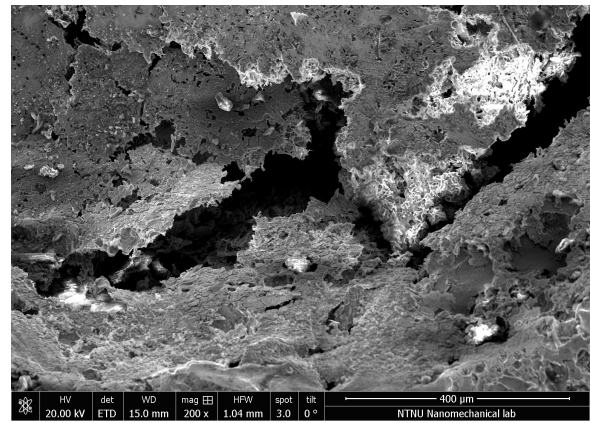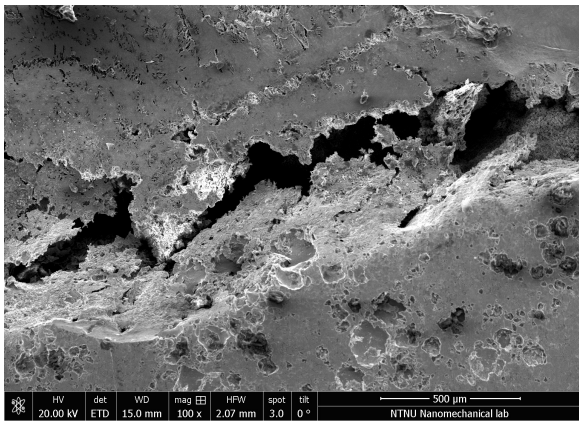
Figure B.8.: SEM imaging of 300mV 5°C sample.

Appendix C.

Code

C.1. File Preperation

Code to gather all data files with OCP data into .xlsx files suitable for plotting.

C.1.1. HEMOS Data

```python
# import required module
import os
import pandas as pd
# assign directory

def createCombinedFile(place):

    directory = "INSERT DIRECTORY OF CHOICE"+place #change this to the
    directory where the files are located

    dfs = []

    if place=="Froya":
        skip=[1,2,3]
    else:
        skip=[1,2,3,4]

    # iterate over files in that directory
    for filename in os.listdir(directory):
        f = os.path.join(directory, filename)
        # checking if it is a file
        if os.path.isfile(f):
            if f[-1]=="s":
                print(f)
                read_file = pd.read_excel(f,skiprows=skip) #4 for
    senja, 3 for froya
                dfs.append(read_file)
                #df=pd.concat((df,read_file))

    # Concatenate all the dataframes into a single dataframe
    combined_df = pd.concat(dfs)
```

```python
30      combined_df['DATE'] = pd.to_datetime(combined_df['DATE'])
31
32      # Round the datetime column to the nearest hour
33      combined_df['DATE'] = combined_df['DATE'].dt.round('T')
34      # Check for duplicate datetime elements
35      duplicates = combined_df.duplicated(subset='DATE', keep='first')
36      #duplicated_rows = combined_df[duplicates]
37
38      # Remove duplicate rows
39      combined_df = combined_df.drop_duplicates(subset='DATE', keep='first')
40
41      combined_df.to_excel (place+".xlsx",
42                      index = None,
43                      header=True)
44
45  createCombinedFile("Froya")
46  createCombinedFile("Senja")
```

C.1.2. Corrosion Lab Data

Reading values from .txt files.

```python
1   import pandas as pd
2
3
4   def readfile(filename):
5       # defining neccecary variables
6       xval=[]
7       yval=[]
8       yval2=[]
9       channelNames=""
10      yvalChan=""
11      yval2Chan=""
12      # opening file and reading lines
13      f=open(filename,'r')
14      lines = f.readlines()[9:]
15      for line in lines:
16          #checking if it is preliminary lines
17          if line == lines[0]:
18              #extracting channel names
19              channelNames=line.split()
20              yvalChan=int(channelNames[2][:-1])
21              yval2Chan=int(channelNames[5])
22              continue
23          if line == lines[1] or line == lines[2]:
24              #skipping next lines in the txt file
25              continue
26          #reading the values from consecutive lines
27          string=line.replace(',','.')
28          values=string.split()
29          xtempvals=values[0]+' '+values[1]
30          xtempvals=pd.to_datetime(xtempvals,format="%d.%m.%Y %H:%M:%S")
31          xval.append(xtempvals)
```

```python
32            try:
33                if float(values[2])<0.38 and float(values[2])>-0.2: #
     filtering out bad values
34                    yval.append(float(values[2]))
35                else:
36                    yval.append(0)
37            except:
38                yval.append(0)
39            try:
40                if float(values[3])<0.38 and float(values[3])>-0.2: #
     filtering out bad values
41                    yval2.append(float(values[3]))
42                else:
43                    yval2.append(0)
44            except:
45                yval2.append(0)
46        f.close()
47
48        return xval,[yvalChan,yval],[yval2Chan,yval2]
49
50 def prepareData(filenames):
51        xvalues=[] # list of time and date
52        yvalues=[] #list of name and values
53        for filename in filenames:
54            xtemp,ytemp,y2temp=readfile(filename)
55            if xvalues==[]:
56                xvalues=xtemp
57            yvalues.append(ytemp)
58            yvalues.append(y2temp)
59        return xvalues,yvalues
```

Preparing .xlsx files.

```python
1 from Corrlab_bib import *
2
3 filenames=[
4     "TEST0006.txt",
5     "TEST0007.txt",
6     "TEST0008.txt",
7     "TEST0009.txt",
8     "TEST0010.txt",
9     "TEST0011.txt"
10     ]
11
12 rolling_average_size=350
13 measurements_per_hour=20
14
15 def makeCSVfromPreparedData():
16     headers=["DATE","Weld Good 1","Weld Good 2","Weld Good 3","SDSS",
17             "316 Crev 1","316 Crev 2","Weld Pit","Weld Bad 1","Weld
     Bad 2",
18             "316 Mid 1","316 Mid 2","316 Mid 3"]
19     xValues,yValues=prepareData(filenames)
20     #pandas dataframe with xvalues as first coloumn, and yvalues as
```

```
     the rest
21   df=pd.DataFrame(xValues)
22   for element in yValues:
23       df=pd.concat([df,pd.DataFrame(element[1])],axis=1)
24   df.columns=headers
25   df["304 1"]=[0]*len(df)
26   df["304 2"]=[0]*len(df)
27   df["304 3"]=[0]*len(df)
28   df=df[['DATE','304 1','304 2','304 3','Weld Pit','Weld Bad 1','
     Weld Bad 2',
29         'Weld Good 1','Weld Good 2','Weld Good 3','316 Mid 1','316
     Mid 2',
30         '316 Mid 3','316 Crev 1','316 Crev 2','SDSS']]
31   df.to_excel("Corrlab.xlsx",index=False,header=True)
32
33 makeCSVfromPreparedData()
```

C.2. Plotting Graphs

Code for plotting a graph from the previously constructed .xlsx sheet, and the potentiostatic data from the lab.

C.2.1. Plotting Library

```
1 import numpy as np
2 import matplotlib.pyplot as plt
3 import pandas as pd
4 from scipy.signal import savgol_filter
5
6
7 def fix_xaxis(x_values):
8     for element in x_values:
9         element=pd.Timestamp.to_pydatetime(element)
10    return x_values
11
12 def makeColorMap(dataLabels): #with element from dataLabels as key and
     color as value
13    colorMap={}
14    i=0
15    for element in dataLabels:
16        colorMap[element]=graphColors[i]
17        i+=1
18    return colorMap
19
20 def makeLabelMap(dataLabels): #with element from dataLabels as key,
    and name as value
21    labelMap={}
22    i=0
23    for element in dataLabels:
24        labelMap[element]=nameDict[i]
```

```python
25          i+=1
26      return labelMap
27
28 graphColors={
29      0:"red",
30      1:"green",
31      2:"blue",
32      3:"DodgerBlue",
33      4:"lightcoral",
34      5:"Darkseagreen",
35      6:"purple",
36      7:"salmon",
37      8:"limegreen",
38      9:"Crimson",
39      10:"forestgreen",
40      11:"cornflowerblue",
41      12:"lime",
42      13:"Tomato",
43      14:"navy"
44 }
45 nameDict={
46
47      0: "304 Free Surface 1",
48      1: "304 Free Surface 2",
49      2: "304 Free Surface 3",
50      3:"316 Weld Pit",
51      4:"316 Weld Bad 1",
52      5:"316 Weld Bad 2",
53      6:"316 Weld good 1",
54      7:"316 Weld good 2",
55      8:"316 Weld good 3",
56      9:"316 Midsection 1",
57      10:"316 Midsection 2",
58      11:"316 Midsection 3",
59      12:"316 Crevice 1",
60      13:"316 Crevice 2",
61      14:"25 Cr SDSS",
62      15:"Temperature",
63      16:"alarm"
64 }
65
66 def extractValues(var,labels):
67      corrdata=[]
68      for element in labels:
69          corrdata.append(list(var[element]))
70      return corrdata
71
72 def prepareGraphs(data,xvalues,dataLabels): #expects data as a list of
      data, and xvalues as a set dataset.
73      for i in range(len(data)):
74          plt.plot(xvalues,data[i],label=dataLabels[i],color=graphColors
      [i])
75
76 def avgData(sampleSize,corrdata):
```

```
77     corr2data=[]
78     stdData=[]
79     for element in corrdata:
80         data=pd.Series(element)
81         corr2data.append(data.rolling(sampleSize).mean().shift(-int(
    sampleSize/2)))
82         #corr2data.append(savgol_filter(element, sampleSize, 2))
83         stdData.append(element)
84     return corr2data,stdData
85
86 def avgTemp(sampleSize,var,temperatureLabel):
87     temperaturevals=[]
88     data=pd.Series(var[temperatureLabel])
89     temperaturevals.append(data.rolling(sampleSize).mean())
90     return temperaturevals
```

C.2.2. Plotting Code

```
1 import pandas as pd
2 import matplotlib.pyplot as plt
3 from filplotbib import *
4 from datetime import datetime
5
6 plt.rcParams.update({'font.size': 18})
7 def plotLocationGraph(location,index_start=0,index_stop=11,
8                       showTrue=False,showAvg=True,showTrueDev=True,
    plotVerticalRedLine=False):
9                       #index_start and index_stop are the columns
    you want to plot
10     place=location
11     smoothingfactor=400 #change this to the smoothing factor you want
    to use
12     var= pd.read_excel(place+".xlsx") #reads the excel file
13     dataLabels=list(var.columns.values.tolist()) #creates a list of
    the column names
14     dataLabels.remove("DATE") #removes the date column
15     if place !="Corrlab":
16         dataLabels.remove("INTERRUPT") #removes the interrupt column
17
18     temperatureLabel="Temperature"
19     colorMap=makeColorMap(dataLabels) #creates a dictionary with the
    column names as keys and colors as values
20     labelMap=makeLabelMap(dataLabels) #creates a dictionary with the
    column names as keys and names as values
21     if place=="Senja":
22         temperatureLabel="Thermometer"
23         dataLabels.pop(-1) #removes the last column
24         dataLabels.remove(temperatureLabel) #removes the temperature
    column
25
26     if place == "Froya": #removes the columns that are not needed
27         for i in range (3):
28             dataLabels.pop(0)
29         dataLabels.remove("316 -weld_good-1")
```

```python
30            dataLabels.remove(temperatureLabel)
31
32      if place == "Corrlab": #removes the columns that are not needed
33          for i in range (3):
34              dataLabels.pop(0)
35
36      x_val=list(var["DATE"]) #creates a list of the dates
37      if place!="Corrlab":
38          x_val=fix_xaxis(x_val) #fixes the dates so they are readable
39
40      fig, ax1 = plt.subplots(figsize=(16,9)) #creates a subplot
41
42      corrdata=extractValues(var,dataLabels) #extracts the values from
    the excel file
43      corrdata,stdData=avgData(smoothingfactor,corrdata) #averages the
    data
44
45      for i in range(index_start,index_stop): #plots the ocp data
46              if showAvg: #plots the average data
47                  ax1.plot(x_val,corrdata[i],label=labelMap[dataLabels[i
    ]],color=colorMap[dataLabels[i]])
48              if showTrueDev: #plots the true deviation
49                  ax1.fill_between(x_val,stdData[i], corrdata[i], alpha
    =0.2, color=colorMap[dataLabels[i]])
50              if showTrue: #plots the true data
51                  ax1.plot(x_val,stdData[i],label=labelMap[dataLabels[i
    ]],color=colorMap[dataLabels[i]])
52              if plotVerticalRedLine:
53                  date_time = datetime(2023, 5, 16, 10, 24)
54                  ax1.axvline(x=date_time, color='r', linestyle='--',
    alpha=0.5)
55
56      ax1.set_xlabel("Date") #sets the labels and titles and grid
57      ax1.set_ylabel("V vs. Ag/AgCl")
58      ax1.set_title(place+" OCP")
59      ax1.legend(loc='upper center', bbox_to_anchor=(0.5,2),ncol=3,
    fancybox=True, shadow=True) #sets the legend
60      ax1.grid(True)
61      ax1.tick_params(axis='x',labelsize='large',labelrotation=45) #
    rotates the x axis labels
62
63
64      if place !="Corrlab":
65          ax2=ax1.twinx() #creates a second y axis
66          temperature=avgTemp(20,var,temperatureLabel) #averages the
    temperature data
67
68          color = "blue" #color of the temperature line
69          ax2.plot(x_val,temperature[0],label=temperatureLabel,color=
    color,linestyle="-.",alpha=0.3) #plots the temperature data
70
71          ax2.set_ylabel("Temperature (C)") #sets the labels and titles
    and grid
72          ax2.tick_params(axis='y', labelcolor=color)
```

```python
73          ax2.legend(loc=4)
74
75    fig.tight_layout() #makes sure the labels are not cut off
76
77    plt.savefig("INSERT REQUIRED DIRECTORY"+place+str(index_start)+".
      png",dpi=300) #saves the plot as a png file to the directory you
      want
78
79    plt.show() #shows the plot
80    print("Done with "+place+str(index_start)+".png")
```